AD-A124 680 A REVIEW AND COMPARISON OF LIGHTNING RETURN STROKE MODELS USING EXPERIMENTAL DATA(U) AIR FORCE INST OF TECH WRIGHT-PATTERSON AFB OH SCHOOL OF ENGI.. 1/2

UNCLASSIFIED S M HANIF DEC 82 AFIT/GE/EE/82D-61 F/G 12/1 NL

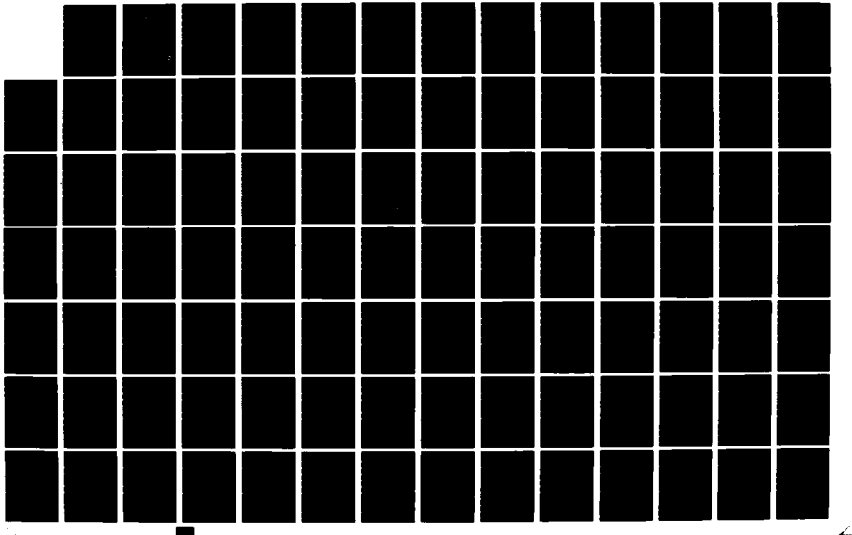

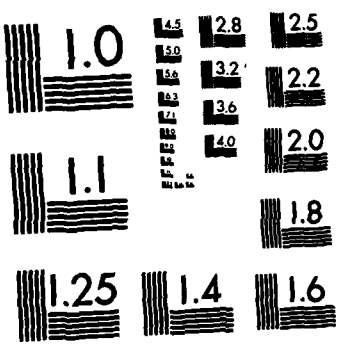

DEPARTMENT OF THE AIR FORCE

AIR UNIVERSITY (ATC)

AIR FORCE INSTITUTE OF TECHNOLOGY

Wright-Patterson Air Force Base, Ohio

AFIT/GE/EE/82D-61

A REVIEW AND COMPARISON OF LIGHTNING RETURN STROKE MODELS USING EXPERIMENTAL DATA

Thesis

Shad M. Hanif
AFIT/GE/EE/82D-61 Sqn Ldr PAF

AFIT/GE/EE/82D-61

A REVIEW AND COMPARISON OF LIGHTNING RETURN STROKE MODELS USING EXPERIMENTAL DATA

THESIS

Presented to

the Faculty of the School of Engineering
of the
Air Force Institute of Technology
Air University

in Partial Fulfillment of the
Requirements for the Degree of
Master of Science

by

Shad M. Hanif, M.A., B.S.E.E.
Sqn Ldr PAF

Approved for public release; distribution unlimited.

Preface

Lightning effect on modern airborne electronics is of immense importance because of the changing aircraft technology. I took up this investigation because of the sound and deep professional knowledge of Dr. Pedro L. Rustan in this field. I wish to thank him for contagious enthusiasm, continued assistance, and above all, unlimited patience throughout all phases of this study. My special thanks are due to M.J. Master from the University of Florida for permission to use the computer program for his lightning return stroke model. I also would like to thank Mrs. Jean Reazer of Technology Scientific Incorporated for providing valuable data and assistance.

Rebecca Brumlow, who typed this thesis, is a lady of great patience. I am thankful to her particularly because she typed this thesis on a short notice.

Finally, I wish to express my thanks to Iffat and my daughters for sharing with me the famous AFIT studies' stress.

Shad M. Hanif

Contents

List of Figures

List of Tables

Abstract

A detailed review of the seven lightning return stroke models is presented. These models were proposed by Bruce and Golde (1964), Dennis and Pierce (1964), Little (1978), Y.T. Lin et al. (1980), R.L. Gardner (1980), Strawe et al. (1980), and Master et al. (1981). For the better understanding of the subject, a review of lightning return stroke process is also included. The equations to compute the electric and magnetic fields in space due to a vertical channel are also derived. The last part of the thesis is related to the comparison of these models. The predicted fields due to Master et al. were plotted and compared with the empirical results. Also, Master et al. model (1981) was modified for the channel current pulse propagation velocity and the channel current wave form. The plots due to these modifications are included and compared with the experimental data.

A REVIEW AND COMPARISON OF LIGHTNING RETURN STROKE MODELS USING EXPERIMENTAL DATA

I. Introduction

Over the last three decades many lightning return stroke models have been proposed to predict the current pulse of the return stroke as it propagates in the channel. These models were mainly proposed by trying to solve the inverse problem of suggesting the current in the channel which will give the experimental measurement of the electromagnetic (EM) fields on the ground. Due to the lack of airborne data, the validity of these models as a function of height have not been verified. In this thesis we provide a discussion of all the significant return stroke models and their credibility as a function of height by comparing their EM fields with recent acquired airborne lightning data (Rustan et al., 1982).

Prior to 1970, the main concern about the lightning phenomena was due to its effect on transmission lines. However, from 1970 to 1981 seven USAF aircraft were lost due to confirmed lightning related incidents and more than 150 serious lightning related mishaps were recorded (Corbin: IEEE Trans 1982). These numerous incidents coupled with recent changes of the aircraft structure to composite materials alarmed the electromagnetic interference community

of the ever present lightning hazards. Additional testing of the aircraft to the airborne lightning environments was required. The new fiber-reinforced plastics and other non-metallic materials, which have replaced the conventional aluminum structure, are more susceptible/vulnerable to lightning damage because these are usually incapable of withstanding high voltage stresses created by lightning and thus causing dielectric breakdown (J.A. Plumer & J.D. Robb, 1982). Although the use of composite materials in aircraft technology has resulted in lower cost, lighter weight and lower radar return signatures, it has also caused undesirable external EM energy coupling into the aircraft. Particularly, the external EM radiation at high frequency is a serious hazard for modern electronic devices, which are more responsive at higher frequencies and can be destroyed at lower voltages than their predecessors (Corbin, 1979). Electromagnetic transients produced by lightning currents have frequency spectrum from near DC to GHz range (Uman et al:1980). These transients when coupled inside the aircraft produce resonance effects, particularly in the range of 1 MHZ to 10 MHZ. This in turn critically affects the performance of wideband digital systems which are not shielded properly. In summary, return stroke EM radiation may jeopardize the aircraft safety by causing data and software error in the onboard computers (Baum:1980).

To determine the EM coupling to the aircraft for direct and nearby lightning, one must have an accurate model

of the lightning process. By doing so one can determine the level of interference and what phase of the lightning discharge is likely to produce induced electromagnetic pulses. This will help in designing the aircraft structure and shielding for the modern digital electronics systems inside the aircraft.

In order to determine the needed protection and to learn more about the physical properties of the lighting discharge, many researchers have developed lightning return stroke models which describe different aspects of this natural phenomena. Within the scope of this thesis, the author has chosen to review the most significant work in this area. The return stroke models to be included in our discussions are the ones proposed by

(a) C.E.R. Bruce and R.H. Golde (1941)

(b) A.S. Dennis and E.T. Pierce (1964)

(c) P.F. Little (1978)

(d) Y.T. Lin, M.A. Uman and R.B. Strandler (1980)

(e) R.L. Gardner (1980)

(f) P.F. Strawe et al (1980)

Lightning return stroke models derived by the above mentioned authors predict EM field at ground level. However, M.J. Master et al (1981) proposed a model to predict EM fields at altitudes. This model, in fact, is a slightly modified version of Lin's model, which he presented in his Ph.D. thesis.

Problem

The problem of this thesis is three-fold. First of all, the most significant lightning return stroke models found in the literature are reviewed and critically analyzed. Secondly, the results from the Master's model are analyzed and compared with the flight data obtained near active thunderstorms at the same altitudes and distances. This will enable us to determine whether or not the proposed model reproduces the surface fields measured on an aircraft during airborne tests. Finally, we will modify the Master's model in the form of variations in certain parameters to establish relationship between lightning currents and the resultant EM fields. Since most of the previous models use data measured at ground level for their analysis, we will determine which one of these models best reproduces the electromagnetic fields as a function of height.

Scope

The scope of this thesis is to collect and fully analyze the information contained in different lightning return stroke models in concise and compact form. This will enable the researcher interested in lightning phenomena to have quick access to some of the important models presented over the last few decades. The analysis and comparison part of this thesis will enable the reader to select a model for further studies and modifications. In selecting the return stroke lightning models which appear most significant, we have

taken equal contributions of the linear and the nonlinear approaches into model development.

Lin et al (1980) model, with modification by Master et al (1981), is presently the only model which derives EM fields as a function of height and distances. This model is studied in detail in this thesis. The comparison of their results with the data collected by the Air Force Flight Dynamic Laboratory will show how well this model can predict the fields produced by a lightning return stroke.

The Masters et al. computer model, used to predict the fields produced by a lightning current as a function of height and distances is based on the statistical averages of the model parameters described by Lin et al (1980). Additional variations in the channel current parameters are introduced to calculate the fields. By comparing the results of these variations with the experimental data we can determine the refinements required in this model. Due to the time constraint in this study it was not possible for the author to explore all the possible variations and adjustments in this model.

Presentation

In Chapter II the lightning flash mechanism is described. A study of return stroke model essentially requires the understanding of this chapter. Relevant terminologies used in lightning literature are also defined here. Chapters III and IV describe the linear and the nonlinear models, respectively. Equations for the calculation of EM field at a point

in space are derived in Chapter V. These derivations will provide an analytic insight to the Master et al. model. Master et al. model (1982) and modification to it are discussed in Chapter VI and Chapter VII discusses the validity of experimental data. Comparison of models is presented in Chapter VIII. Finally, Chapter IX summarizes the conclusions and recommendations based on this research.

II. Lightning Mechanism

Cloud-to-Ground Lightning

Lightning is a transient, high current electric discharge, which has a path length extended over several kilometers (Uman, 1969). It is commonly initiated by thunderclouds, which range from one or two km diameter to giant electrical storms as shown in Fig 2.1 (Vonnegut, 1965). Most of the lightning flashes that occur around the world are intracloud discharges (70 to 80% of all lightning in Florida), but the type of lightning flashes which are of most concern to us are cloud-to-ground and these are the only ones studied.

Generally, cloud-to-ground lightning is referred to as streaked or forked lightning. An entire discharge to ground lasts typically .2 to .25 seconds and is called a flash (Bruce Gold, 1941; Uman, 1969). The flash is composed of individual discharges called strokes, each stroke lasts for a few milliseconds with a time between strokes of tens of milliseconds. There are typically three or four strokes per flash, the minimum being one, the maximum measured 26. Fig 2.2 shows a distribution of the number of strokes in a flash in different parts of the world. Thomson (1980) reports that there is no significant correlation between the average number of strokes per flash and the average interstroke time interval. There are varying parameters which affect the lightning

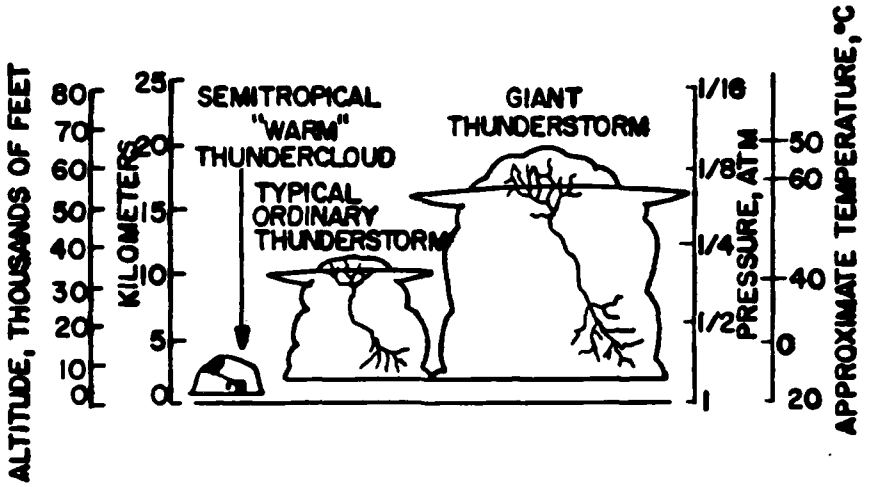

Fig 2.1 Comparison of Various Sizes of Convective Clouds that Produce Lightning Discharge (adapted from Vannegut, 1965).

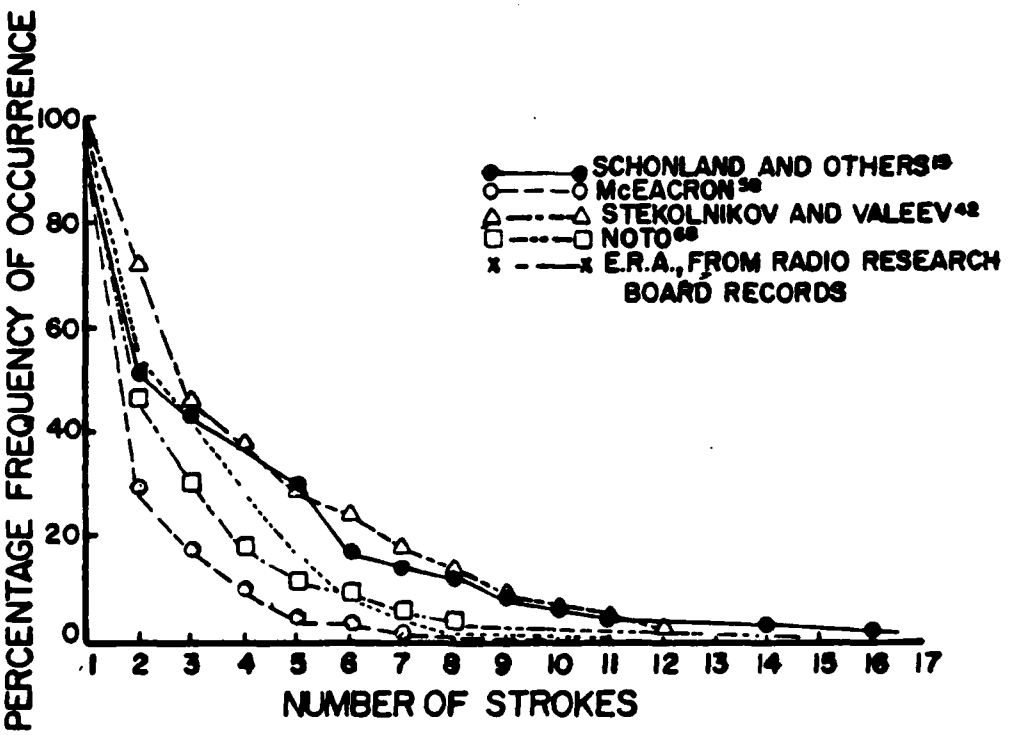

Fig 2.2 Number of Successive Strokes in Lightning Flashes (Adapted from Bruce & Golde, 1941).

characteristics. Frontal storms, for example, produce a higher flash rate and more strokes in a flash than local convective storms (Uman, 1982). Similarly, the relative height of the terrain affects the channel length.

In 1930 Schonland et al., using photographic techniques, determined that lightning flashes were initiated by the stepped leaders in the channel. To explain this phenomena a simple model for the charge structure of a thunderstorm was made from ground-based measurements of the cloud electric fields and lightning field changes. Fig 2.3 shows such a model, in which the major region of positive charge build-up occurs at the top of the cloud (P). Below this positive charge distribution there is a strong negative charge distribution (N). The bottom of the cloud has a weak positive charge distribution (p). Although the actual process by which stepped leader propagate is unknown, the local electrical breakdown between the N and p region of the thundercloud is considered to cause this phenomena. Streak-camera photographs as shown in Fig 2.4 indicate that the stepped leader has a strongly luminous step. There is a silent period between steps and each new step has a faintly luminous channel in the clouds. Thus, the stepped leader is a cloud-to-ground predischarge preceding the first return stroke.

The average length of a stepped leader is 50 meters with pause time of 50 microseconds (μsec) between steps. The average velocity of steps towards the ground is nearly 1.5×10^5 meters/sec. However, Baum et al (1980) suggested that

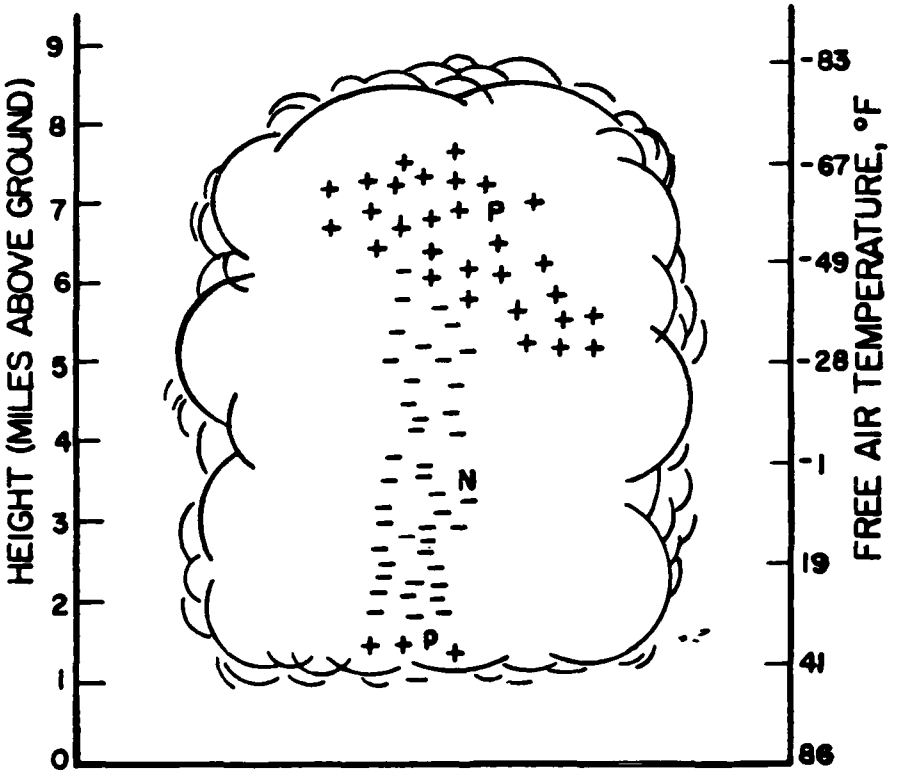

Fig 2.3 A Typical Charge Distribution in a South African Cloud According to Malan (1952,1963). From Electric Field Measurements It Appears P = +40 Coul, N = -40 Coul, and p = +10 Coul (Uman, 1969).

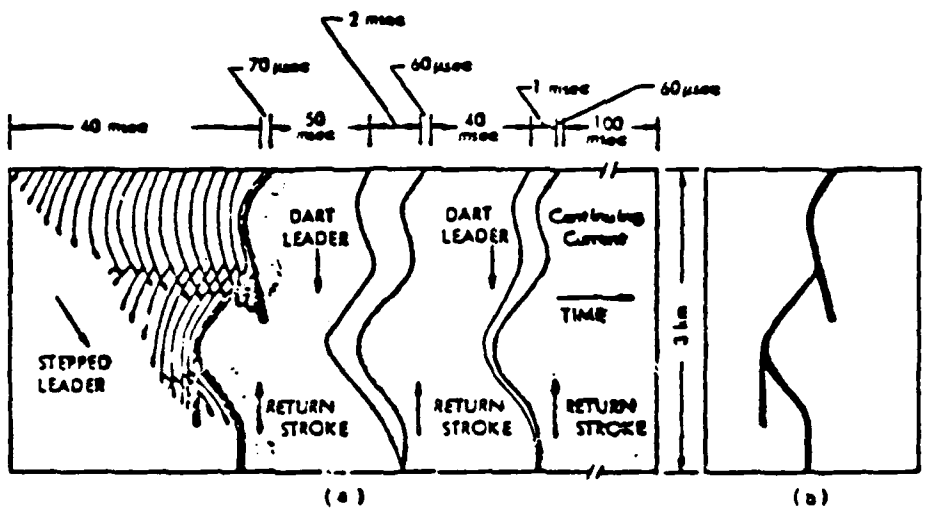

Fig 2.4 (a) Streak Camera Photograph of Stepped Leader Process, Scale of Drawing is Distorted for Illustrative Purpose.

(b) Ordinary Camera Picture of a Lightning Flash. (Adapted from Uman, 1969).

stepped leaders may form in shorter than 10 m steps and faster than the velocity calculated by earlier authors. When stepped leaders propagate down towards earth they lower a negative potential of the order of -10^8 volts and on the average they distribute negative charge of 5 coulombs along their path.

When the stepped leader nears the ground, the electric field there is sufficient to cause streamers to be initiated and propagate upward to meet the leader tip. At the junction of the downward-moving leader and the upward moving streamer the "return stroke" wavefront forms and thereafter propagates upwards carrying ground potential into the cloud. The return stroke is responsible for ground and channel currents of typically 20 kA rising to peak value in about one microsecond. However, risetime to peak current of hundreds of nanoseconds has also been reported in the literature (Berger et al. 1975). The above measurements are at the base of the channel, measurements of the channel current above the ground are lacking (Price & Pierce 1977).

The upward velocity of the return stroke is of the order of 1×10^8 meter/sec and the trip between ground and cloud base is completed in approximately 70 μsec. Bruce and Golde (1941) suggested that the velocity of the return stroke decreases as it proceeds upwards and it can be represented as

$$v = v_o e^{-\gamma t} \qquad (2.1)$$

where $v_o \simeq .8 \times 10^8$ meters/sec and $\gamma \simeq 3 \times 10^4$. (If t = 70 μsec then according to this relation the velocity of the return stroke at the bottom of the cloud is 9.796×10^6 m/sec.) Lin (1978) also reports that the return stroke velocity near the ground is 1×10^8 meters/sec and at the top of the channel is of the order of 4×10^7 meters/sec. Boyle and Orville (1976) suggested that this velocity is of the order of .05 - .5 of the speed of light. This variation in velocity with height indicates that there is possible dispersion and dissipation of the return stroke pulse along the channel.

As the charge in the channel is depleted, the stroke current ceases to flow ending the flash. However, if the channel is replenished with charge (from the N region in clouds) within about 100 microseconds, a continuous or "dart leader" may start moving down the previous return stroke channel. The downward velocity of the dart leader is almost uniform (of the order of 2×10^8 m/sec) and greater than that of the stepped leader. The return stroke caused by the dart leader is termed as "a subsequent return stroke."

Sometimes the lower part of the stroke channel disappears due to long interstroke periods or high wind velocities shear and disintegrate the channel. In such cases the dart leader on its downward trip changes its role to a stepped leader form. This kind of leader is named as "dart stepped leader" and it initiates the first return stroke.

Subsequent return stroke field changes, though of smaller magnitude, are similar to but faster than those of the first return stroke. Also the subsequent return stroke has faster current risetime and similar maximum rate of change of current. Consecutive return strokes in the same channel are usually separated by 40 to 80 microseconds; however, this interval may exceed 100 msec provided a continuous current keeps on flowing in the channel (Uman & Krider, 1981).

We have briefly described the characteristics of a return stroke which lowers negative potential and negative charge from the cloud towards ground. The return stroke models discussed in this thesis are of this form. Occasionally, stepped leaders lower positive charge. Return strokes caused by this type of leader have slow rate of rise of current and large charge transfer. Positive discharge flashes are rarely composed of more than one stroke. Another kind of stepped leader is that which moves upward towards the cloud and may carry either positive or negative charge. A detailed description of this form of stroke is given by Uman (1969).

Return Stroke Current Waveforms

In the modeling of return strokes, the current waveform has a key role. As said earlier, the direct current measurements have always been done at the ground level. The most common device to measure the amount of current and its waveform is the magnetic link. This device is preferred because it can measure peak currents regardless of their duration and

relative variations. However, the fast risetime to peak currents or fast variations in the current waveform are limited by the system response.

In the early works on lightning, the peak value of the first return stroke current was measured as 15-20 kA. (McCann, 1944; Lewis & Foster, 1945). The accuracy of their measurements was questioned by Anderson and Hegenguth (1959) and Szpor (1969). Szpor (1969) suggested that these values were low by a factor of two and thus peak current value is approximately 30 kA at 50% distribution level. Similar values for peak currents were calculated by Berger et al.,(1975) and Garbagnati et al.,(1974). The average peak value in subsequent return strokes is almost half of that in the first return stroke.

Bruce and Golde (1941) suggested that the return stroke waveform could be represented as

$$I(t) = I_o \left(e^{-\alpha t} - e^{-\beta t}\right) \qquad (2.2)$$

where $\alpha = 4.4 \times 10^4$, $\beta = 4.6 \times 10^5$, $I_o = 30$ kA and $I(t)$ is the current at the base of the return stroke at time t. These values give average time to crest and to half value of about 6 μsec and 23.5 μsec, respectively. Current waveforms observed by different authors differ by various parameters and such waveforms are shown in Fig 2.5. Parameters, which are compared to these waveforms, are risetime to peak current, time to half value of peak current, and charge transferred. The

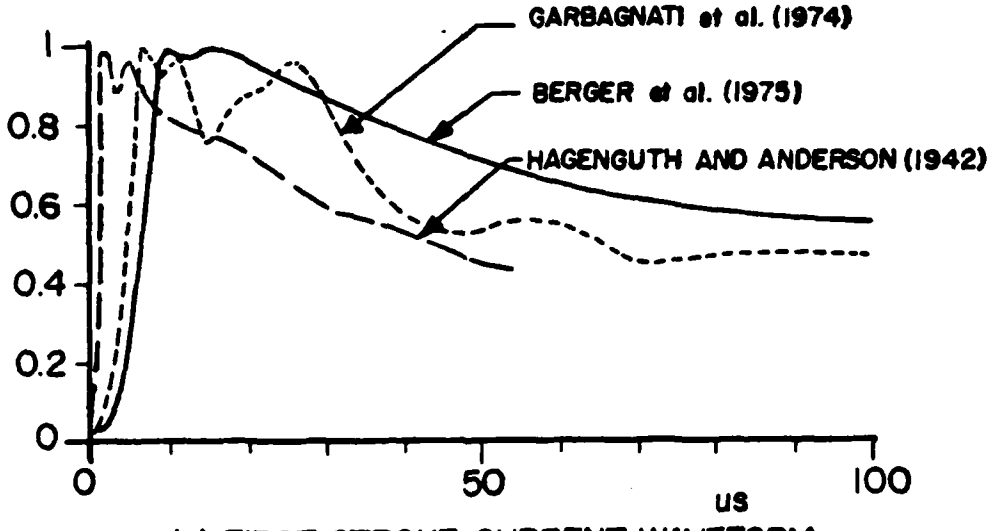

(a) FIRST STROKE CURRENT WAVEFORM

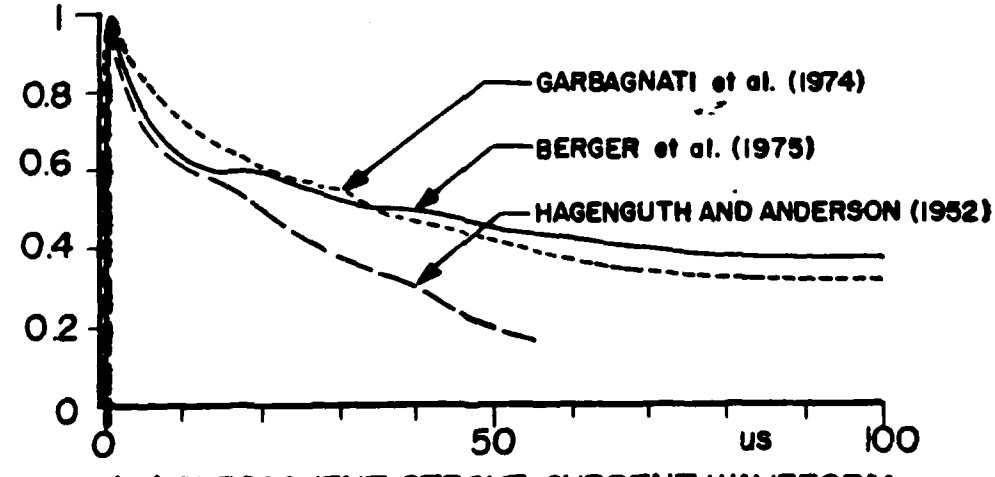

(b) SUBSEQUENT STROKE CURRENT WAVEFORM

Fig 2.5 Typical First and Subsequent Return Stroke Current Waveforms: Averaged Current by Berger et al. (1975). Typical Currents by Hagenguth et al. (1952) and Garbagnatic et al. (1974). (Adapted from Lin, 1978).

current waveform of a lightning return stroke at the base of the channel has been suggested by Uman (1969) as

$$I = I_o \left(e^{-\alpha t} - e^{-\beta t}\right) + I_1 e^{-\gamma t} \qquad (2.3)$$

This waveform differs from that of the Bruce & Golde (1941) by the quantity $I_1 e^{-\gamma t}$, which is considered as intermediate current. For the first return stroke, values of I_o, α and β are 30 kA, $2.0 \times 10^4 sec^{-1}$ and $2.0 \times 10^5 sec^{-1}$, respectively. In a subsequent return stroke these values are 10 kA, $1.4 \times 10^4 sec^{-1}$ and $6.0 \times 10^4 sec^{-1}$. The intermediate current has been specified as I_1 = 2.5 kA and $\gamma = 1.0 \times 10^3 sec^{-1}$.

From Fig 2.4 and data listed above, it is apparent that the first return stroke has longer risetime, higher peak current, longer half-value time for current waveform and larger amount of charge transferred than the subsequent return strokes. There are other parameters in the first return stroke which differ from the subsequent return stroke, such as channel tortuousity and velocity of propagation. In this thesis the channel will be considered as straight and vertical whereas velocity parameter will be discussed in one of the next chapters.

III. Linear Models

This chapter analyzes the linear return-stroke models proposed by Bruce & Golde (1941), Dennis & Pierce (1964) and Y.T. Lin et al., (1980). These models provide a relationship between return-stroke EM fields and the corresponding channel current. These models attempt to solve the inverse problem of estimating the current in the channel based on the measurements of the EM fields a certain distance away from the channel. If the estimated current in the channel satisfies other measurements of the EM fields as a function of distance we claim the model is adequate. Each one of these three authors pursued this same objective and kept making improvements over previous models.

Bruce and Golde Model (1941)

In this model the return stroke current at any given time is assumed to be uniform with height below the return stroke wave front and zero above it. Thus, the current at the base of the channel and below the wave front are identical, that is

$$i(z,t) = i(o,t) \qquad z \leq 1 \qquad (3.1)$$

and

$$i(z,t) = o \qquad z \geq 1 \qquad (3.2)$$

where

$$i(z,t) = I_o\left[\exp(-\alpha t) - \exp(-\beta t)\right] \qquad (3.3)$$

is the current wave form at the ground, and 'l' is the height of the channel. Also, Bruce and Golde (BG) assumed from the photographic data of Schonland (1956) that for the first return stroke the propagation velocity decreases with time and is given by

$$v_t = v_o \exp(-\gamma t) \qquad (3.4)$$

(Values of γ and v_o are given in Chapter II.).

However, for the subsequent return stroke this velocity was assumed to be constant. An illustration of Bruce-Golde model is given in Fig 3.1.

To calculate fields from the above current wave form Bruce-Golde used the "charge moment" equations (Lejay, 1926; Ratcliffe et al., 1932). According to these equations the electric and magnetic field strength at a distance R from a dipole of moment M are given by

$$E_z(R,t) = \frac{-1}{2\pi\varepsilon_o}\left[\frac{M}{R^3} + \frac{1}{cR^2}\frac{dM}{dt} + \frac{1}{c^2R}\frac{d^2M}{dt^2}\right] \qquad (3.5)$$

$$B(R,t) = \frac{\mu_o}{2\pi}\left[\frac{1}{cR^2}\frac{dM}{dt} + \frac{1}{c^2R}\frac{d^2M}{dt^2}\right] \qquad (3.6)$$

where "c" is the velocity of light, ε_o is the permittivity of the medium and μ_o is the permeability of the medium.

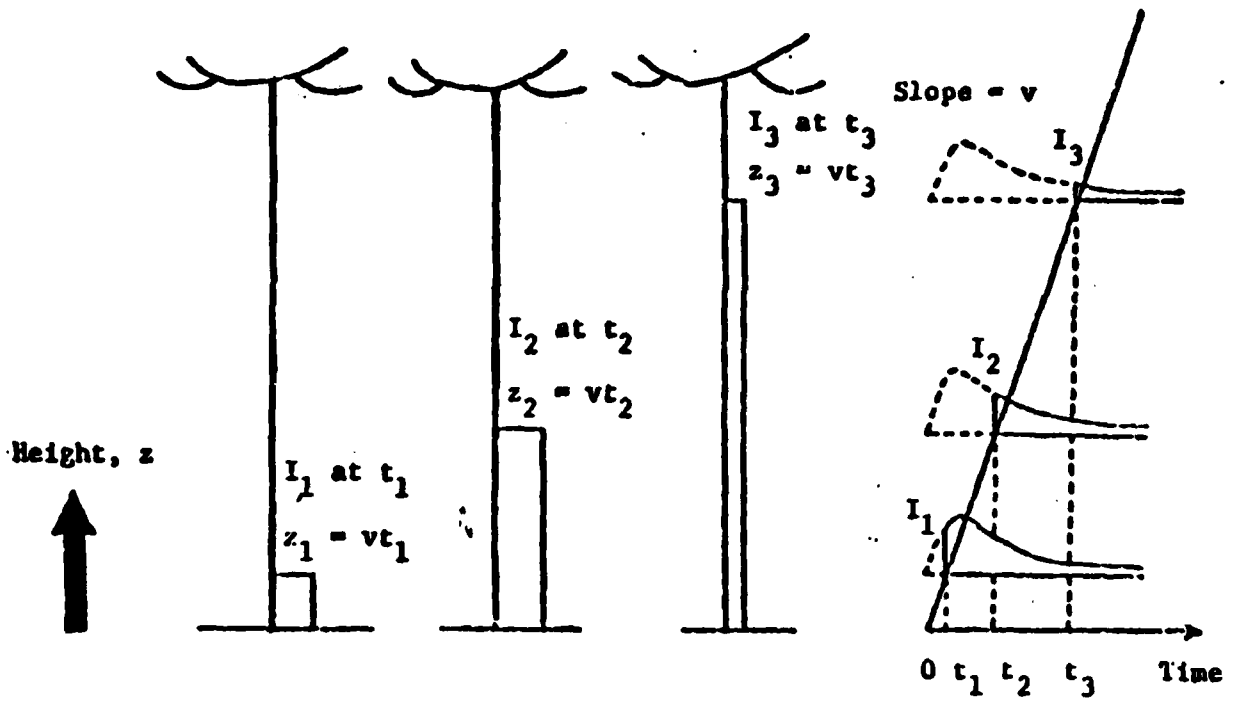

Fig 3.1 Current Distribution in Bruce & Golde Model (1941)
(Adapted from Lin, 1978)

In equation (3.5) the first term is the electrostatic field, the second term is the induced field, and the last term is the radiated field. The time rate of change of electric moment is given by

$$\frac{dM}{dt} = 2i(t) \int_0^t v_t \, dt \tag{3.7}$$

The factor 2 allows for image charges. Substituting equations (3.3) and (3.4) in equation (3.7), yields

$$\frac{dM}{dt} = 2 \frac{I_o v_o}{\gamma} \left[\exp(-\alpha t) - \exp(-\beta t) \right] \left[1 - \exp(-\gamma t) \right] \tag{3.8}$$

Fields derived from equations (3.5) and (3.6) in conjunction with equation (3.8) agreed relatively well with the measured values (Lin, 1978).

However, there are two obvious deficiencies in this model. First of all, since it is assumed that the current distribution along the channel is uniform, the charge and the magnitude of the current at the tip of the channel are required to be instantaneously transferred from the base of the channel, that is, infinite velocity. This phenomena contradicts physical laws because the travel velocity cannot exceed the speed of light. Secondly, there is always a current discontinuity at the wave front. This causes an infinite rate of change of current for zero time. The second problem can be solved by considering the finite rate of change of the current and then taking the limit which converges; however, the first problem

cannot be physically justified. In order to correct the infinite speed problem, Dennis & Pierce (1964) modified the Bruce-Golde model, which will be discussed in the following section.

Dennis and Pierce Model (1964)

From equation (3.4) the channel length z at time 't' is given by

$$z = \int_0^t v_t \, dt \tag{3.9}$$

To remove the discrepancy in the BG model, Dennis & Pierce modified equation (3.3) so that

$$i(z,t) = i(t-z/u) \tag{3.10}$$

where 'u' is the assumed constant velocity of current waveform behind the return-stroke wavefront, and the quantity z/u provides the delay time in getting the information. This model becomes the BG model if 'u' is set equal to infinity. Dennis & Pierce considered values of u of 8×10^7, 3×10^8 and infinite meter/sec in their computations. However, the value of u in their final model was equal to the speed of light.

Dennis & Pierce used charge deposit equations, which will be defined next, to calculate the electric moment M and its derivatives. To derive charge equation, consider that at any time 't' the charge at the tip of the channel is "frozen" or deposited there to neutralize the opposite charge stored

earlier at that point by the stepped leader. Let the channel at any time, t, has a flowing charge density ρ per unit length and deposited charge density ρ' per unit length; then the total charge per unit length will be $(\rho+\rho')$. Assuming that ρ is a function of the channel height, h, and time, t, and that the current waveshape proposed by BG in equation (3.3) is adequate, then the charge deposit can be computed by the equation

$$\rho = \frac{I_o}{\mu}\left[\exp\left[-\alpha(t-\frac{h}{\mu})\right] - \exp\left[-\beta(t-\frac{h}{\mu})\right]\right]. \qquad (3.11)$$

If ρ_t is the charge density at the channel tip of height z, then the charge deposited at the tip of the channel in a unit time is $\rho_t(u-v_t)$ whereas the charge density deposited in a unit length is

$$\rho'_t = \rho_t\left(\frac{u-v_t}{v_t}\right) \qquad (3.12)$$

where

$$\rho_t = \frac{I_o}{\mu}\left\{\exp\left[-\alpha(t-z/u)\right] - \exp\left[-\beta(t-z/u)\right]\right\} \qquad (3.13)$$

From equation (3.9) in general

$$h = \int_o^t v_t\, dt \quad \text{then} \quad \frac{dh}{dt} = v_t$$

Substituting these values in equation (3.7) gives

$$dM = 2\, i_t \frac{h}{v_t}\, dh$$

But $\frac{i_t}{v_t}$ is the total charge $(\rho+\rho')$ in the channel of unit length as defined earliers. Hence

$$\frac{dM}{dm} = 2\,(\rho+\rho')\,h$$

Electric moment M due to the total charge in channel length of height z is obtained by integrating the above equation. Thus

$$M = 2 \int_0^z (\rho + \rho')\, h\, dh \qquad (3.14)$$

Since ρ' is not a function of time and ρ, ρ' are zero at $z = 0$, by differentiating the above equation using Leibnitz's Rule, we obtained

$$\frac{dM}{dt} = 2 \int_0^z \frac{\partial \rho}{\partial t}\, hdh + 2 \int_0^z (\rho+\rho') \frac{\partial h}{\partial t}\, dh + 2\,(\rho_t+\rho'_t)\, z\frac{dz}{dt} \qquad (3.15)$$

In addition, as the channel height, h, is not a function of time, and the second term in (3.15) is zero, the result is

$$\frac{dM}{dt} = 2\int_o^z \frac{\partial \rho}{\partial t}\, h\, dh + 2(\rho_t + \rho'_t)\, z\, \frac{dz}{dt} \qquad (3.16)$$

Derivatives of equations (3.9) and (3.11) once substituted in equation (3.16) give

$$\frac{dM}{dt} = \frac{2I_o u}{\alpha} \exp(-\alpha t)\left[\exp\left(\frac{\alpha z}{u}\right) - 1\right] - \frac{2I_o \mu}{\beta} \exp(-\beta t)$$

$$\left[\exp\left(\frac{\beta z}{u}\right) - 1\right] \qquad (3.17)$$

Further differentiation of equation (3.17) yields

$$\frac{d^2M}{dt^2} = 2I_o u \exp(-\alpha t)\left[1-\exp\left(\frac{\alpha z}{u}\right)\right] + 2I_o v_o \exp(-\gamma t) \exp$$

$$\left[-\alpha\left(t-\frac{z}{u}\right)\right] - 2I_o u \exp(-\beta t)\left[1-\exp\left(\frac{\beta z}{u}\right)\right] - 2I_o v_o \exp$$

$$(-\gamma t) \exp\left[-\beta\left(t-\frac{z}{u}\right)\right] \qquad (3.18)$$

Radiated field calculated from equation (3.18) at a distance of 100 km is shown in Fig (3.2), and is compared with the BG model in which $u = \infty$. The values of α, β, γ and I_o used for computation are 4.5×10^{-4} sec^{-1}, 4.5×10^{5} sec^{-1}, 3×10^{4} sec^{-1} and 30 kA, respectively.

Fig 3.2 shows that the peak radiation field intensity decreases with decrease in velocity, u, and also the peak value is delayed in time. However, the radiation fields become almost identical after 100 μsec.

Since the maximum length of a return stroke channel is

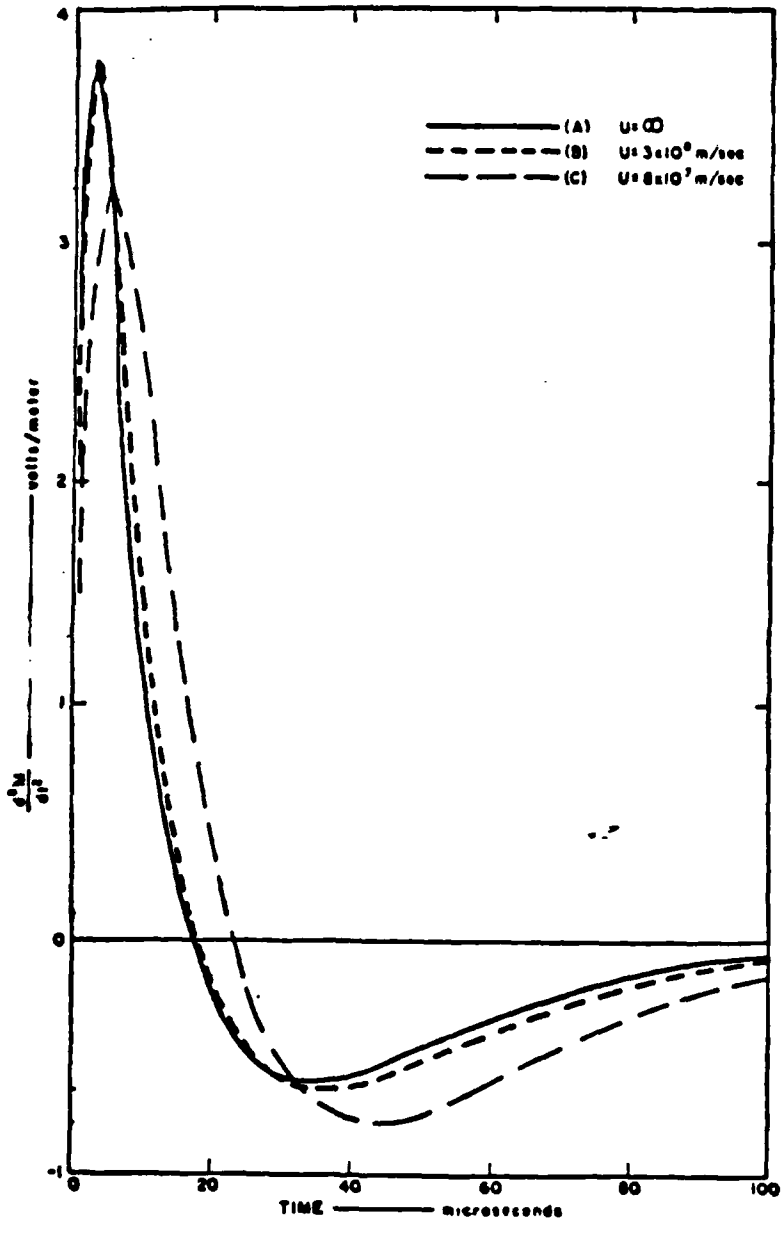

Fig 3.2 Radiated Field at 100 km Distance and Calculated from Equation 3.18 (Adapted from Dennis & Pierce, 1964).

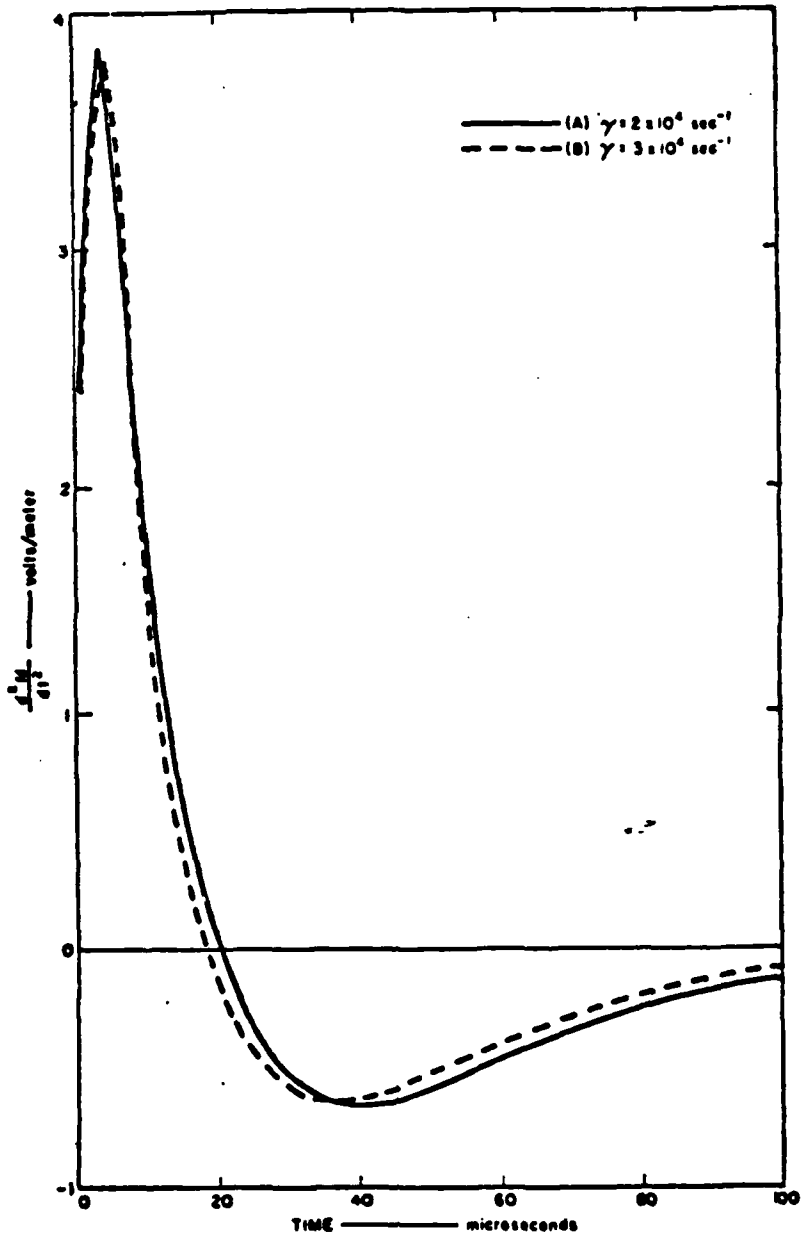

Fig 3.3 Effect of γ Variation on Radiated Field at 100 km (Adapted from Dennis & Pierce, 1964)

$\frac{v_o}{\gamma}$, to increase the length either v_o has to be increased keeping γ constant or γ is to be decreased keeping v_o constant. Dennis & Pierce chose the latter option (third possibility of varying v_o and γ simultaneously not considered). Fig 3.3 shows that no appreciable effect in the radiated field occurs due to variations in the channel height. The value of γ is restricted by equation (3.4).

The Dennis & Pierce (DP) model has also zero current above the wavefront and thus a discontinuity which was considered a shortcoming in the BG model. Therefore the basic physical limitations of the BG model are not solved by the DP model. In order to remove this problem Uman and McLain (1969) proposed a return stroke model, which is known as "Transmission Line Model" in the literature. Since this transmission line model is the basis for Lin's model (1978), it will be briefly discussed here.

Transmission Line Model

In this model the channel current takes the form

$$i(z,t) = I_o\left[\exp\left[-\alpha(t-\frac{z}{v})\right] - \exp\left[-\beta(t-\frac{z}{v})\right]\right] \qquad (3.19)$$

where equation (3.19) is of the same form as equation (3.10). The difference between the two current waveform lies in the velocity of propagation of the wavefront. In equation (3.19) the wavefront travels along the channel with a velocity, v, as it would along a suitable transmission line. Uman and McLain (1969) used arbitrary current waveshapes in their model but in this thesis it will be the same as suggested by BG.

Although the transmission line model is physically reasonable and provides easy analytical computation of EM fields, the current in this model does not lower the charge stored in the corona sheath. Instead, the model represents impulse-like current due to the atmospheric breakdown between the end of the leader and start of the return stroke. Fig 3.1 illustrates the current in this model, whereas Fig 3.4 provides the geometry used to derive the field equations.

Radiation fields at a distance D (D>50 kM) from the bottom of a straight vertical channel are proportional to the product of the return-stroke velocity and its current wave-shape (Uman & McLain 1969; and Uman and McLain 1971) for any time 't' such that t<H/v, where H is the height of channel. This yields

$$\vec{E}(R,t) = \frac{1}{2\pi\varepsilon_o} \frac{\sin^2\theta}{c^2 R} v I_o \left\{ \exp\left[-\alpha(t-R/C)\right] - \exp\left[-\beta (t- R/C)\right] \right\} \vec{a}_z \qquad (3.20)$$

$$\vec{B}(R,t) = \frac{\mu o}{2\pi} \frac{\sin\theta}{cR} v I_o \left\{ \exp\left[-\alpha(t-R/C)\right] - \exp\left[-\beta(t-R/C)\right] \right\} \vec{a}_\phi \qquad (3.21)$$

These equations are only useful to find the channel current waveform when the distant radiated field is known. However, the exact electric and magnetic fields due to the return-stroke current in a straight vertical channel above a

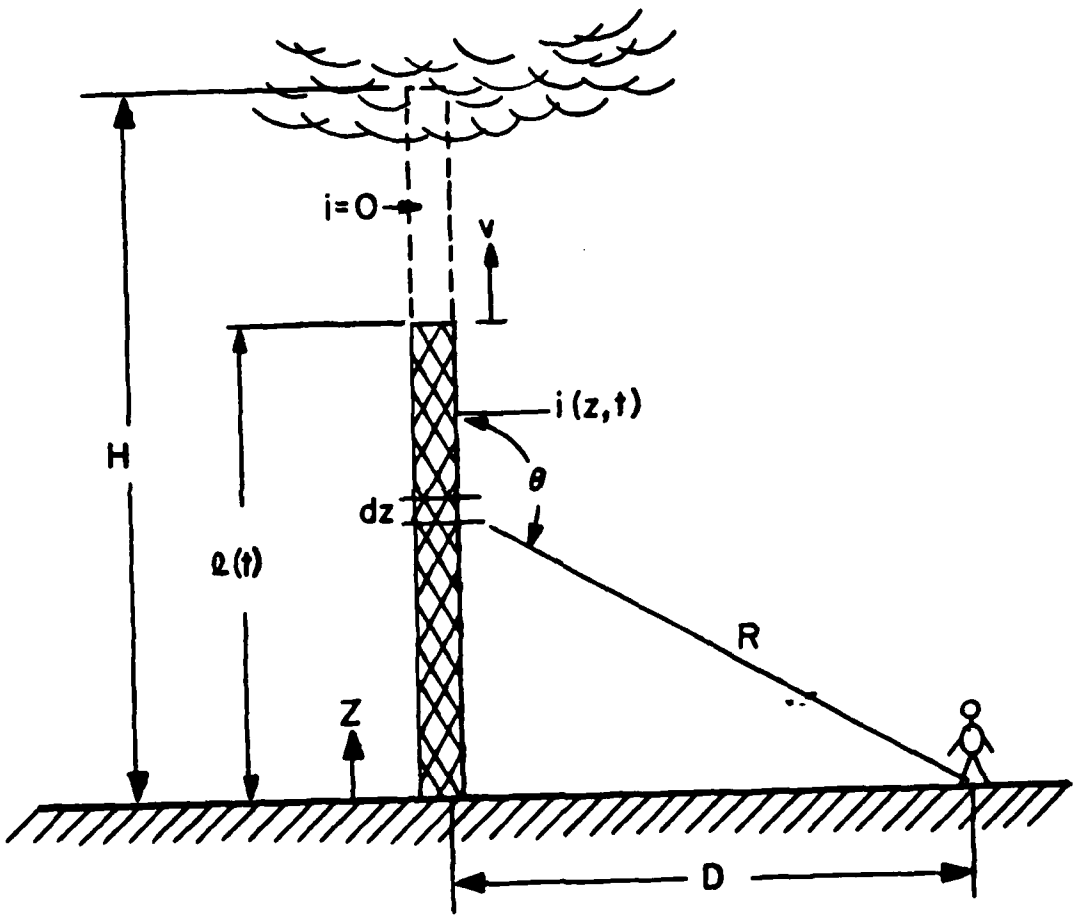

Fig 3.4 Geometrical and Physical Parameter Used in Transmission Line Return Stroke Modeling (Adapted from Lin et al., 1980)

perfect conducting plane earth cannot be computed at any distance by the use of these equations. For return-stroke current i(z,t) the fields at any distance can be calculated from the equations derived by Uman & McLain (1969 & 1971).

$$E_z(D,t) = \frac{1}{2\pi\bar{\epsilon}_o}\left\{\int_o^H\int_o^t \frac{2-3\mathrm{Sin}^2\theta}{R^3}\, i\,(z,\,-R/c)d\tau \;\; dz \right.$$

$$\left. + \int_o^H \frac{2-3\mathrm{Sin}^2\theta}{cR^2}\, i\,(z,\,t-R/c)\,dz \right\}$$

$$- \int_o^H \frac{\mathrm{Sin}\theta}{c^2R}\,\frac{\partial i}{\partial t}\,(z,t-R/c)\,dz \qquad (3.22)$$

$$B_\phi(D,t) = \frac{\mu o}{2\pi}\left\{\int_o^H \frac{\mathrm{Sin}\theta}{R^2}\, i\,(z,t-r/c)\,dz + \right.$$

$$\left. \int_o^H \frac{\mathrm{Sin}\theta}{cR}\,\frac{\partial}{\partial t}\, i\,(t,t-R/c)\,dz \right\} \qquad (3.23)$$

since by virtue of equation (3.4)

$$z = \int_o^t v_t\, dt$$

Therefore, variable velocity of propagation can be incorporated in these equations. Detailed derivations of equations (3.22) and (3.23) are given by Uman et al. (1975).

Lin's Model (1980)

To remove the shortcomings of the Bruce Golde, Dennis and Pierce and Transmission Line models, a new model was proposed by Lin et al. (1980). The channel current in the new model is composed of three separate components: (1) a short-duration upward propagating break down current pulse of constant magnitude and waveshape. This pulse is responsible for the return stroke peak current and the risetime. This pulse is assumed to propagate up at a constant velocity; (2) a uniform current which may already be flowing (leader current) or it may start to flow soon after the return stroke begins; (3) a corona current caused by the downward movement of charge initially stored in the corona sheath around the leader channel.

The current contribution due to the three components is illustrated in Fig 3.5. The geometry of the channel is the same as for the transmission line model shown in Fig 3.4.

The channel current at any instant time 't' at altitude z and due to source at z' of length $\Delta z'$ is represented by

$$i(z,z',t) = i_b+I_u+I_o\left[\exp(-\frac{z'}{\lambda})\left(\exp(-\alpha(t-t')\right.\right.$$
$$\left.\left.-\exp(-\beta(t-t')\right)\right]\Delta z' \qquad (3.24)$$

for $t \geq t'$ and $z' \geq z$ where i_b is the current in the breakdown pulse. The time t' is defined by the relation

$$t' = \frac{z'}{u} + t_{on} + \frac{(z'-z)}{c} + \frac{R(z)}{c} \qquad (3.25)$$

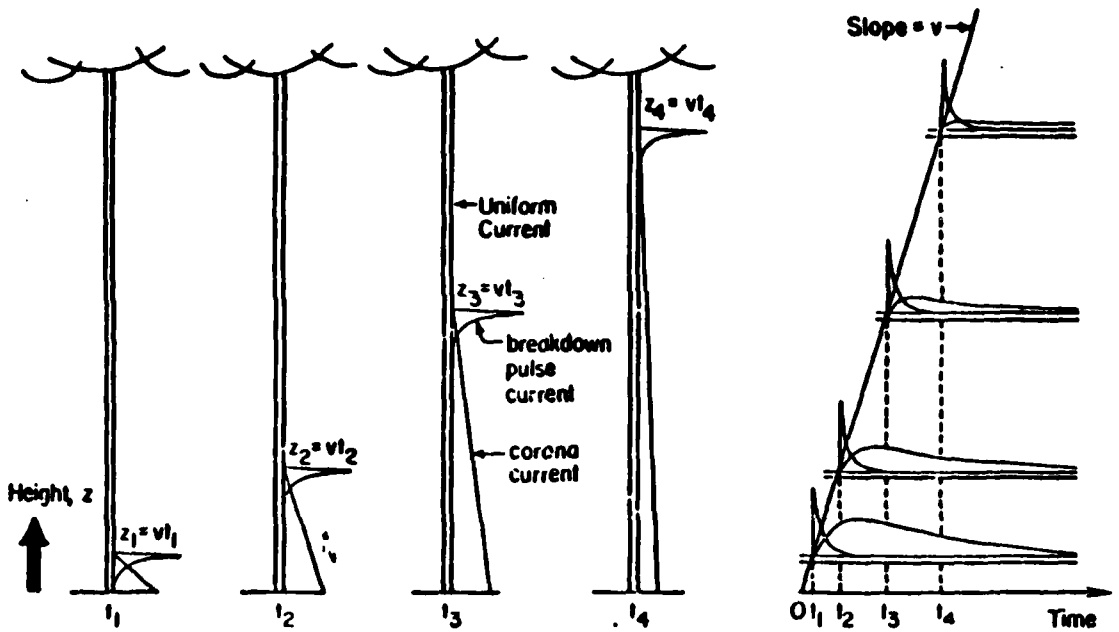

Fig 3.5 Current Distribution in Lin et al., Model (1980)
(Adapted from Lin et al., 1980)

where t_{on} is the time in which the pulse current i_b attains its maximum value. The constant I_o in Equation (3.24) has typical values of 10-50 A/meter. Values of α and β are arbitrarily set equal to 10^5 sec^{-1} and $3x10^6$ sec^{-1} respectively, and the scale factor λ is assumed to have value of 1200.

In this mode the value of I_u, the uniform current, is determined from the slope $\frac{dE}{dt}$ of the electric field near the lightning during the linear ramp region from the following equation:

$$|I_u| = 2\pi\epsilon_o \left| \frac{(H^2+D^2)^{3/2}}{H} \frac{dE}{dt} \right| \qquad (3.26)$$

The above equation should be used with some reservation to calculate I_u. Uniform current field and electrostatic field are both distance dependent. At a distant station the electric field at 100 μsec due to I_u becomes very small and thus the ramp of the field is difficult to detect. A calculation of I_u from such a field becomes highly erratic and overestimated in magnitude. Also, if the field is measured much closer to the lightning channel (distance < 2 kM) then the ramp is more effected by the corona current. Measurement in such a condition will also be inaccurate and overestimated.

The corona current waveshape is assumed to be identical at all heights but its magnitude decreases exponentially with height. Corona current in the channel flows towards the ground at the speed of light. A fast turn on time corona current is considered the best for this model. A good agreement between

predicted and measured fields is obtained when the corona current reaches its peak value in 1 μsec after being turned on by the breakdown pulse and decays exponentially with a 10 μsec time constant. It may be noted that the corona current waveform at any altitude along the channel is the B.G. current waveform which decreases exponentially in amplitude with height. Analytically, this waveform is represented by the last part of equation (3.24) with the values of α and β mentioned on page 34.

Once the current in the vertical lightning channel is established then the associated fields can be computed from Equations (3.22) and (3.23). However, the corona current at altitude z, due to the charge sources above it, can be computed by integrating Equation (3.24) with respect to z' from z to H. A simplified procedure in this respect is proposed by Lin et al. (1980).

This model provides an insight to the channel losses which are not considered in lossless transmission line model. The EM fields predicted in this model are much closer to the experimental data than those predicted using the previous models.

IV. Nonlinear Models

The linear models which were presented in the last chapter did not account for certain important aspects of the lightning phenomena. For example, most of the lightning channels are tortuous and tortuosity in a channel is a random factor. There are not straightforward techniques that can be used to approximate the tortuosity in the channel. However, the effect of tortuosity on the radiated EM fields can be estimated. Also, in the previous models earth was considered as perfect conductor whereas it has finite amount of conductivity. Radiation in the earth ionosphere environment is yet another factor which has not been considered in linear models. Robert L. Gardner (1980) considers all these parameters in a nonlinear lightning channel model consisting of arbitrarily connected and oriented line segments.

To account for time varying parameters in a return stroke channel, P.F. Little (1978) describes a nonuniform transmission line model using a lumped-parameter network. In his paper he describes methods to calculate such parameters. These calculations will be presented in brief form during the description of this model. Variation in the current pulse during return stroke propagation is also reviewed in his paper.

The third nonlinear transmission line model reviewed in this thesis was presented by Strawe et al. (1980). The

authors of this model predict the return stroke current rise rate and velocity of propagation on the basis of non-linear breakdown physics of the channel arc. The current waveform, as in other models, is not based upon experimental data. In fact, the current waveform in this model is the solution of energy balance equations, which are the result of physical phenomena occurring in an arc channel. In this model, it is claimed that current rise rate decays rapidly with propagation distance from the point of return stroke initiation.

For the ease of understanding, the first model reviewed in this chapter is by P.F. Little (1978), the next model is of R.L. Gardner (1980) and finally, the model presented by Strawe et al. will be reviewed.

Little's Model (1978)

In this model, the lightning channel is formed of resistive and inductive elements in a series RLC circuit as shown in Fig 4.1. The switch SW shown in this figure connects the channel to ground where the final stepped leader meets the short return leader propagating upward from the ground level. Thus, a charged transmission line is terminated in a resistance, and the channel charge is allowed to flow towards the ground. It is assumed that the inductance in this connecting path is negligible and hence, a fast-rising current pulse is produced. However,

the magnitude of current peak reduces as the channel height increases above the ground.

Since the transmission line presented in Fig 4.1 consists of nonuniform lumped RLC elements, the shape of the current pulse will change with height.

To find the voltage and current at the ith element of the RLC network shown in Fig 4.1, consider the transmission line equations:

$$\frac{\partial V_i}{\partial z} = - RI_i - L \frac{\partial I_i}{\partial t} \tag{4.1}$$

and

$$\frac{\partial I_i}{\partial z} = - C \frac{\partial V_i}{\partial t} \tag{4.2}$$

Differentiating equation (4.1) and substituting (4.2) yields

$$\frac{\partial^2 V_i}{\partial z^2} = RC \frac{\partial V_i}{\partial t} + LC \frac{\partial^2 V_i}{\partial t^2} \tag{4.3}$$

and

$$\frac{\partial^2 I_i}{\partial z^2} = RC \frac{\partial I_i}{\partial t} + LC \frac{\partial^2 I_i}{\partial t^2} \tag{4.4}$$

The solutions to equations (4.3) and (4.4) determine the value of voltage and current in the transmission line at height z and time t.

P.F. Little uses uniform transmission line segments. In that case, if V is the input voltage at the base of the channel, which is terminated in its characteristic impedance, the current at the ground rises to its maximum

value depending on R. Since the transmission line is uniform, the subscript 'i' in equation (4.3) can be dropped and it takes the form

$$\frac{\partial^2 V}{\partial z^2} = RC \frac{\partial V}{\partial t} + LC \frac{\partial^2 V}{\partial t} \qquad (4.5)$$

The RLC parameters are derived from physical arguments rather than from analytic treatment. To determine the capacitance element, consider the vertical channel as a charged conductor of small radius and having the same potential all along the channel. Depending upon the size of the clouds and its height above the ground, the channel can be modeled as shown in Fig 4.2. The electrostatic field distribution is determined by numerical method and the results are shown in Fig 4.3.

By determining the electrostatic E-field around a cylindrical channel at a distance r, the charge on the channel per unit length λ becomes

$$\lambda = 2\pi r \varepsilon_o E \qquad (4.6)$$

and the capacitance per meter, C^*, is calculated from the relation

$$C^* = \frac{\lambda}{V} \qquad (4.7)$$

The tip nearest the ground can be considered spherical shape containing the charge

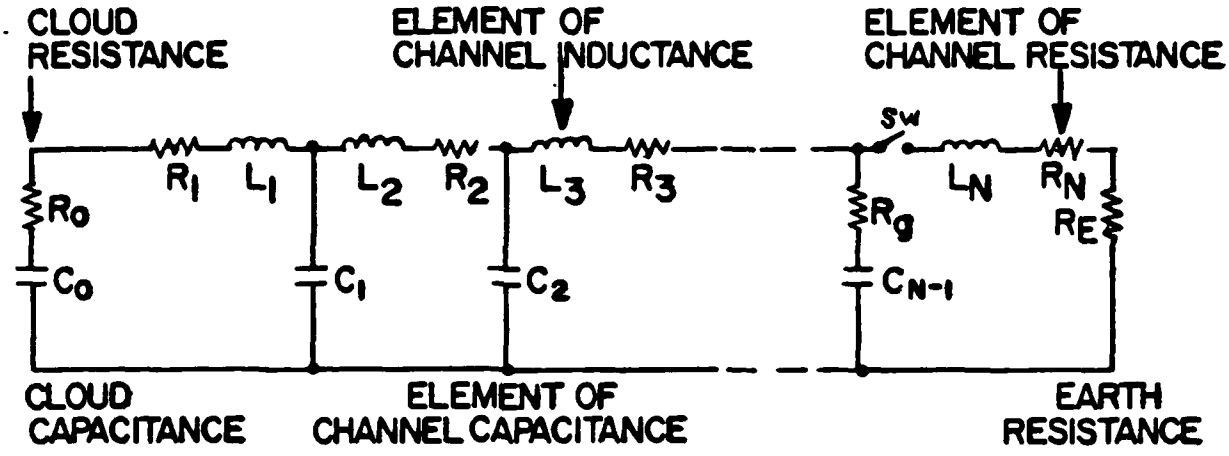

Fig 4.1 Lumped Parameter Transmission Line as a Representative of a Lightning Return Stroke in Little's Model (1978).

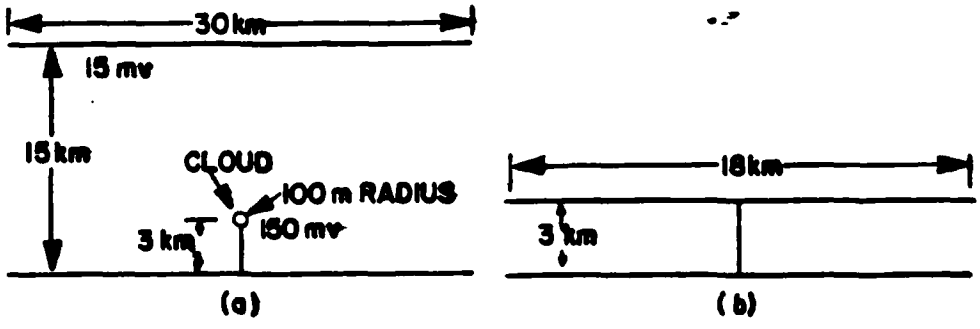

Fig 4.2 Lightning Channel Models for Small and Large Clouds (a) Spherical Cloud Model (b) Plane Cloud Model (Adapted from Little, 1978).

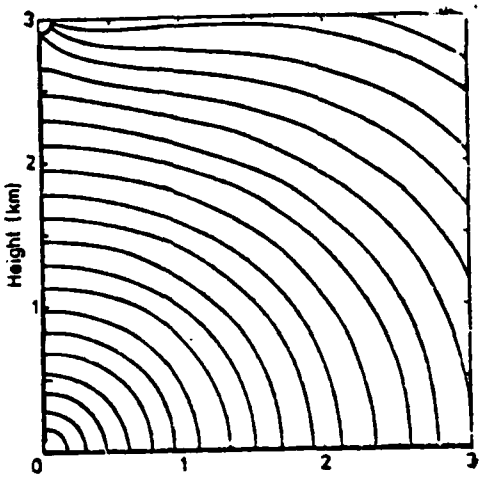

Radius km
(a)

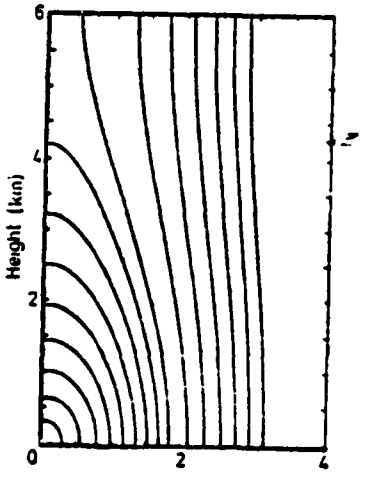

Radius km
(b)

Fig 4.3 Electrostatic Field Lines Around the Lightning Channel of Fig 4.2 (a) Spherical Cloud (b) Plane Cloud (Little, 1978)

$$Q = 2\pi\, r^2\, \varepsilon_o E \qquad (4.8)$$

It is to be noted that the charge distribution should affect the length of the gap to be covered by the last stepped leader due to the height of gap above the ground and the dimensions and height of the cloud. Typical charge distributions in the channel are shown in Fig 4.4a and Fig 4.5b.

Once C^* is found then for any channel segment the associated C_n can be calculated by multiplying C^* with the length of the segment. However, the value of C_n changes with time. This is because the C_n value is associated with the beginning of the return stroke as the field distribution changes, the value of C_n also changes in each segment. This argument puts this model in the category of nonlinear models. However, P.F. Little has preferred to use the constant values of C_n during the channel discharge.

The displacement current between the ground and the line segments of the model provides a closed loop path for the segment current. Assuming that the field distribution is stationary then the displacement current I_d is given by

$$I_d = \varepsilon_o \frac{\partial E}{\partial t} \qquad (4.9)$$

Now the inductance L_n associated with this current flow in the nth segment is determined by the area under the

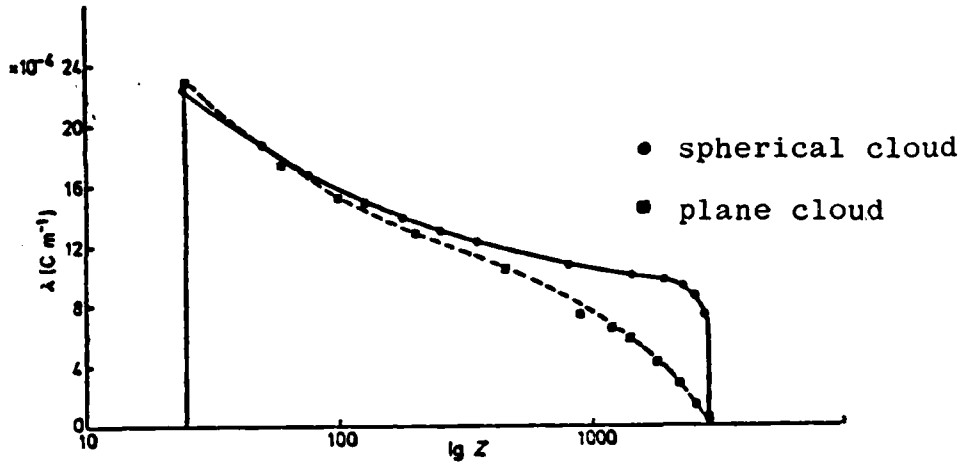

Fig 4.4a Distribution of Linear Charge Density λ Along 3 km Lightning Channel for Two Clouds Model (Little, 1978).

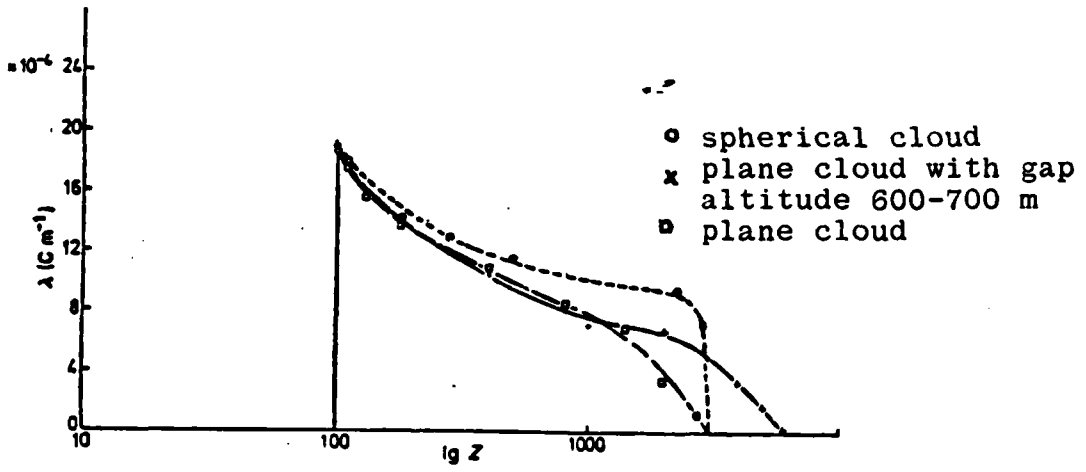

Fig 4.4b Distribution of Charge Density λ Along 3 km and 6 km Lightning Channels with Gap Length of 100 m at an Altitude of 100 m (Little, 1978).

field lines. The inductance for closed path is given by

$$L = \frac{1}{I_d} \int_S \bar{B}.d\bar{s}.$$

where I_d is considered as constant. Assuming that the channel radius is very small as compared to the segment length, the area S can be approximated by an arc of radius equal to the segment length as shown in Fig 4.5. The shaded and dotted zones in Fig 4.5 determine S for the nth element at the beginning of the return stroke. Inductance due to (n+1)th element is calculated in the same manner and associated area is the dotted region of Fig 4.5. The difference between the two areas, shown as hatched portion in Fig 4.5a then determines the flux due to nth element. Circular or rectangular approximation within the same limits as shown in Fig 4.5a, b give essentially the same value of L_n. The inductance of line segment L_n is then determined by considering the channel as coaxial line, whose outer radius is equal to the length of the segment. P.F. Little (1978) approximates the radius of the channel equal to 2 cm and assuming that field lines are circular, he suggests that inductance per unit length is roughly 2 μH/m.

The resistance element in the channel is difficult to calculate because it is a complex function of time and height. R^*, the resistance per meter, is estimated in such a manner that the current remains unidirectional but its oscillations are not completely dampened. A value of R^* of 1 ohm per meter is assumed in this model. In the switch

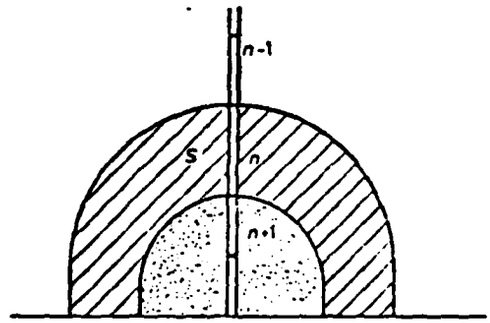

(a)

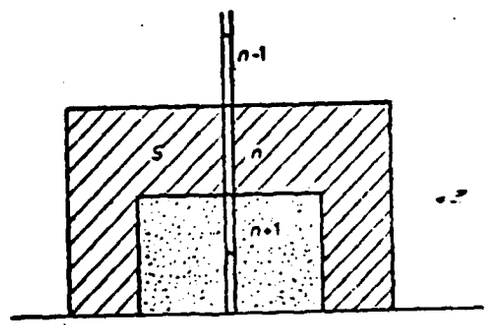

(b)

Fig 4.5 Areas Determining Inductance of Lightning Channel (a) Actual Field Lines (Diagrametic) (b) Approximate Rectangular Presentation (Little, 1978)

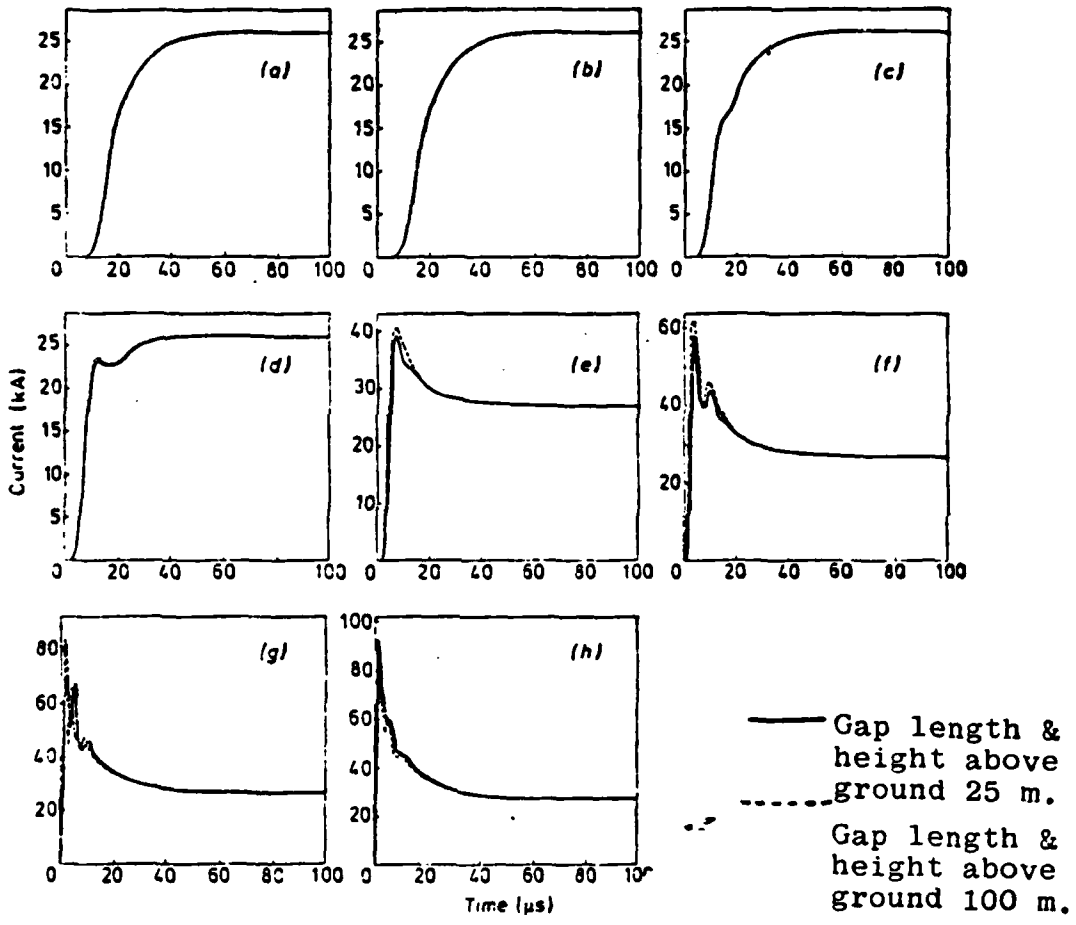

Fig 4.6a Current Waveforms in a 3 km Lightning Channel for Small Cloud. Height Above Ground (m): 9 (a) 2950, (b) 2550, (c) 1950, (d) 1450, (e) 900, (f) 450, (g) 225, (h) 75. (Little, 1978)

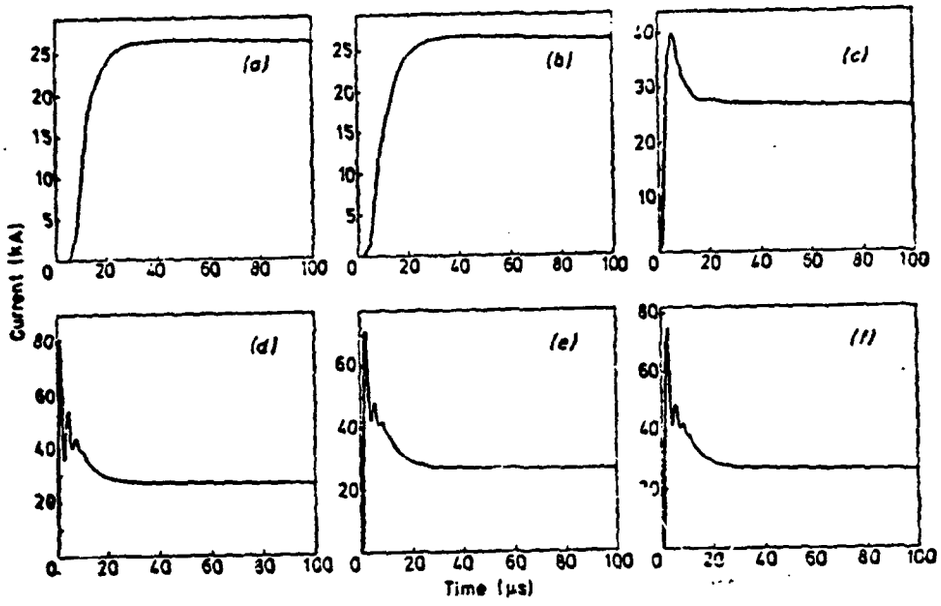

Fig 4.6b Current Waveforms in a 3 km Lightning Channel for a Plane Cloud Model. Height Above Ground (m): (a) 2950, (b) 1950, (c) 900, (d) 450, (e) 225, (f) 75. Gap length 100 m and 200-300 m Above Ground (Little, 1978).

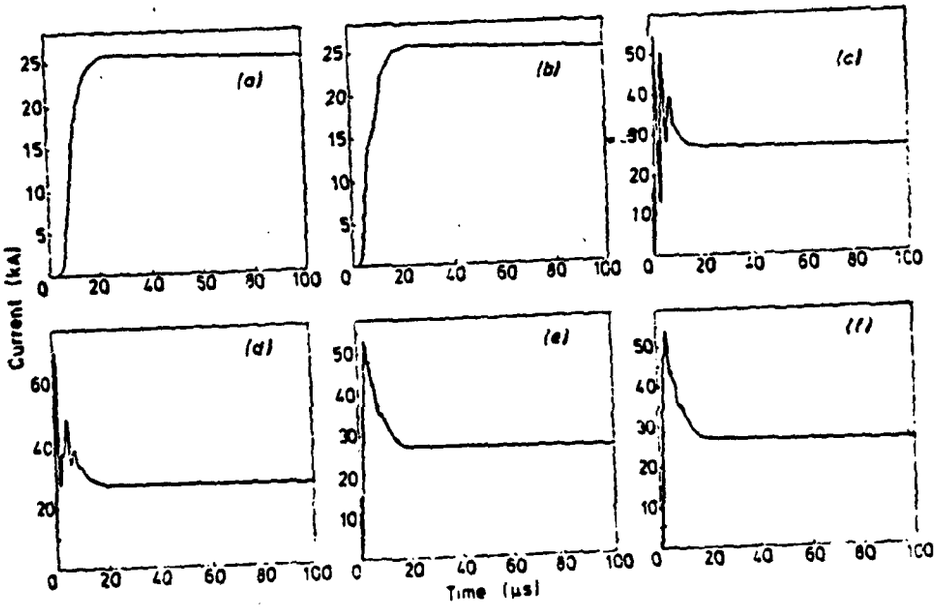

Fig 4.6c Current Waveforms in 3 km Lightning Channel for a Plane Cloud Model. Gap Length of 100 m and 600-700 m Above Ground. Height Above Ground (m): (a) 2950, (b) 1950, (c) 825, (d) 675, (e) 450, (f) 150. (Little, 1978).

loop the resistance R_n is approximated as 600 ohm. This value represents the energy loss in the breakdown process.

Finally, the terminating resistance R_E is given by

$$R_E = 8.9 \left(\frac{I\rho}{I_{max}}\right)^{\frac{1}{2}} \qquad (4.10)$$

where ρ is the specific resistivity of the ground.

Equation (4.10) gives a value of $R_E = 100$ for $I_{max} = -100$ kA. The cloud capacitance C_o is assumed to be 1 μF.

Even though the parameter values predicted by the above model are not correct, they are fairly close to the values observed on the ground. Considering this aspect of the model, the current pulse shape of the channel current can be approximated at all altitudes. The computed current waveforms at different heights are shown in Fig 4.6a, b & c.

Gardner's Model (1980)

This model considers the lightning channel as a number of arbitrarily oriented line segments connected together. Contrary to other models which consider the earth as a perfect conductor, this model accounts for the finite conductivity of the earth. Also, the EM fields radiation in the earth ionosphere waveguide are included in this model. The current in the channel is treated as a pulse when a precharged transmission line is subjected to a discharge. The current pulse parameters are the same as described in equation (2.3). The geometry of a point charge on the

channel is shown in Fig 4.7.

In order to calculate the $\overline{E}$ and $\overline{B}$ fields due to a line segment, the three orthogonal components L_x, L_y, and L_z are calculated where L_x, L_y and L_z represents the length of the segment component in x, y, and z direction. The current pulse is assumed to travel along these orthogonal components at the appropriate component velocity.

Since L_z constitutes a vertical dipole over a conducting half space, the fields from this dipole can be calculated using the Sommerfeld integral technique (Wait 1970, Baños, 1966). The Hertz potential in frequency domain due to a dipole of length L_z is given by

$$\pi_z(\omega) = \frac{f(\omega)L_z}{j4\pi\omega\epsilon_o} \left[\frac{e^{-jk_2R_2}}{R_2} \right] \tag{4.11}$$

where $R_2 = \rho^2 + (z-h)^{2\,½}$ from Fig 4.7, $f(\omega)$ is the Fourier transform of the current in the channel (Equation 2.3) given by

$$f(\omega) = I_o \left[\frac{1}{\alpha+j\omega} - \frac{1}{\beta+j\omega} + \frac{I_1}{\gamma+j\omega} \right] \tag{4.12}$$

and the value of k_2 is given by

$$k_2 = \omega\sqrt{\mu_2\epsilon_2} \tag{4/13}$$

Using the Sommerfeld integral form, equation (4.11) can be written as

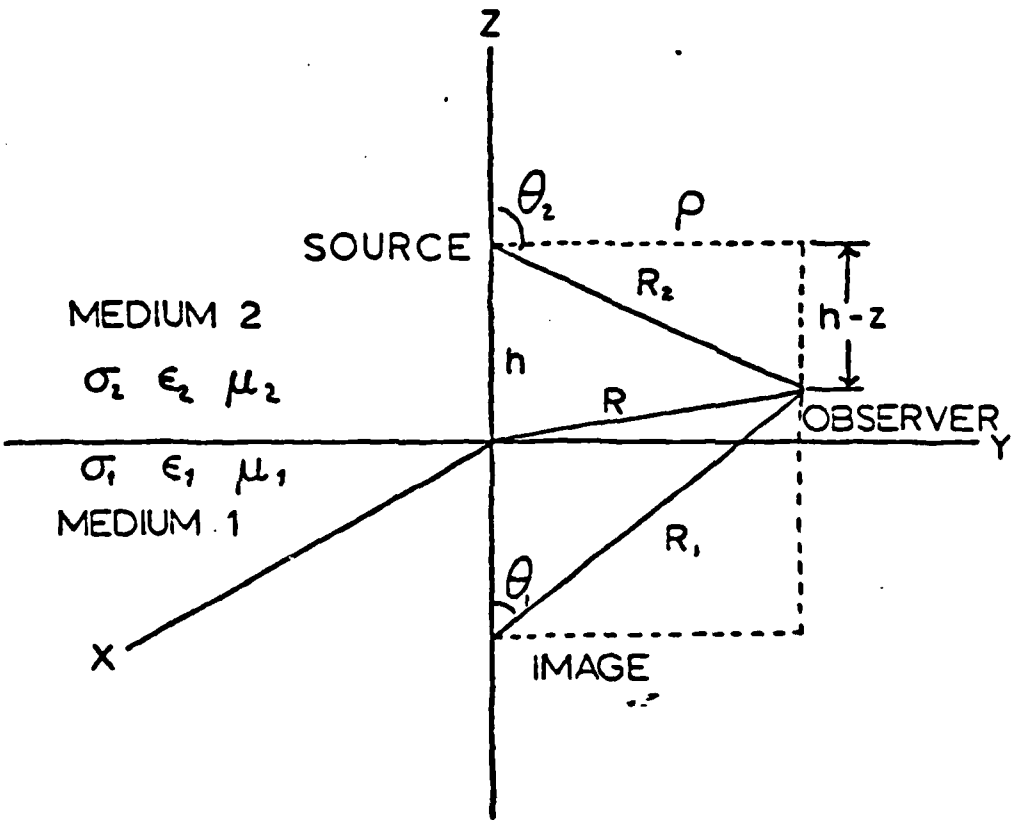

Fig 4.7 Geometry of a POint Charge Source When Earth is Imperfect Conductor (Gardner, 1980)

$$\pi_z(\omega) = \frac{f(\omega)L_z}{4j\pi\omega\epsilon_o}\left[\frac{e^{-jk_2R_2}}{R_2} + \frac{e^{-jk_2R_1}}{R_1} - 2P\right] \qquad (4.14)$$

where

$$P = \int_o^\infty \frac{k_2U_1}{k_1^2U_2+k_2^2U_1^2}\, e^{-U_2(z+h)}\, \frac{\lambda}{U_2}\, J_o(\lambda\rho)\, d\lambda \qquad (4.15)$$

$$U_m = (\lambda^2 - k_m^2)^{\frac{1}{2}} \quad , m = 1,2 \qquad (4.16)$$

$$k_1 = \left[\omega^2\mu_1\epsilon_1 - j\,\omega\mu_1\sigma_1\right]^{\frac{1}{2}} \qquad (4.17)$$

and $J_o(\lambda\rho)$ is Bessel function of the first kind. The term 2P in equation (4.14) is a correction used to make the earth a perfectly conducting surface.

Wait (1970) approximated the value of the integral given by equation (4.15) and obtained

$$P = (\pi p)^{\frac{1}{2}}\, e^{-\omega}\, \mathrm{erfc}(j\omega^{\frac{1}{2}})\, \frac{e^{-jk_2R_1}}{R_1} \qquad (4.18)$$

where

$$p = \frac{-jk_2R_1}{2}\,\Delta^2 \quad \text{and} \quad \omega = p\left(1+\frac{h+z}{\Delta R_1}\right)^2$$

Δ is given by the relation

$$= \frac{Z_1}{\eta_o} = \frac{u_1}{(\sigma_1 + j\omega\epsilon_1)} \tag{4.19}$$

Here η_o is the free space impedance and Z_1 represents the wave impedance of the ground surface. The quantity p defined above is also known as the Sommerfeld Numerical Distance.

The electric field can be calculated from the Hertz vector $\bar{\pi}(\omega) = \left[0, 0, \pi_z(\omega)\right]$ by the equation

$$\bar{E}(\omega) = \nabla\nabla.\bar{\pi}(\omega) + \bar{k}_2^2\, \bar{\pi}(\omega) \tag{4.20}$$

Before computing the field, let $R = |\bar{r} - \bar{r}_c|$ where R is the distance from the observer to the source (R is either R_1 or R_2 in Fig 4.7). If $R_c = |\bar{r}_c|$ represents the distance of observer from the center of the source and also the dipole length is much smaller than R_c, i.e.

$$\frac{k_2 L_z^2}{P_c} << 1$$

then R can be written to first approximation as,

$$R = R_c + |\bar{r}_c - \bar{r}| \cos\phi \tag{4.21}$$

Assumed that source filament is electrically small or $k_2 L_z << 1$

Now to find the field due to a finite length segment a source integration technique given by LeVine and Meneghini (1978) is followed. The field components from a vertical dipole are found as

$$E_r(\omega) = \frac{j\omega f(\omega) L_z \mu_o}{4\pi k_2^2} \left\{ \text{sinc}\left[\tfrac{1}{2} k_2 L_z (\eta_z - (\nabla R_c)_z) \right] \frac{\partial^2}{\partial r \partial z} \frac{e^{-jk_2 R_2}}{R_2} \right.$$

$$+ \text{sinc}\left[\tfrac{1}{2} k_2 L_z (\eta_z - (\nabla R_c')_z) \right] \frac{\partial^2}{\partial r \partial z}$$

$$\left. \left[\frac{e^{-jk_2 R_1}}{R_1} - 2P \right] \right\} \qquad (4.22)$$

and

$$E_z(\omega) = \frac{j\omega f(\omega) L_z \mu_o}{4\pi k_2^2} \left[\text{sinc}\left(\tfrac{1}{2} k_2 L_z (\eta_z - (\nabla R_c)_z) \right) \left(\frac{\partial^2}{\partial z^2} + k_2^2 \right) \frac{e^{-jk_2 R_2}}{R_2} \right.$$

$$+ \text{sinc}\left(\tfrac{1}{2} k_2 L_z (\eta_z - (\nabla R_c')_z) \right) \left(\frac{\partial^2}{\partial z^2} + k_2^2 \right)$$

$$\left. \left(\frac{e^{-jk_2 R_1}}{R_1} + 2P \right) \right] \qquad (4.23)$$

R_c' is the same as R_c but for the filament image. η_z is the ratio of speed of light to the z component of the

pulse propagation velocity v_z. Thus

$$\eta_z = \frac{c}{v_z} \tag{4.24}$$

Similarly, we can derive the field due to the horizontal component of the line segment, by using the components of the Hertz vector $\bar{\pi}$ $(\pi_x, 0, \pi_z)$. The details of this computation are given in Gardner (1978). The electric field components due to x component of the line segment are given by

$$E_r(\omega) = -\frac{j\omega f(\omega) L_x \mu o}{4\pi k_2^2} \cos\phi \left[\left(\frac{\partial^2}{\partial r^2} + k_2^2\right) \frac{e^{-jk_2R_2}}{R_2} \operatorname{sinc}\left(\tfrac{1}{2}k_2 L_x(\eta_x - (\nabla R_c)_x)\right) - \left(\left[\frac{\partial^2}{\partial r^2} + k_2^2\right] \frac{e^{-jk_2R_1}}{R_1} - k_2^2 \frac{\partial^2}{\partial r^2} V - k_2^2 U\right) \operatorname{sinc}\left(\tfrac{1}{2}k_2 L_x(\eta_x - (\nabla R_c')_x)\right)\right] \tag{4.25}$$

$$E_\phi(\omega) = -\frac{j\omega f(\omega) L_x \mu_o}{4\pi k_2^2} \sin\phi \left\{\left[\frac{1}{r}\frac{\partial}{\partial r} + k_2^2\right] \frac{e^{-jk_2R_2}}{R_2} \operatorname{sinc}\left[\tfrac{1}{2}k_2 L_x(\eta_x - (\nabla R_c)_x)\right] - \left(\left[\frac{1}{r}\frac{\partial}{\partial r} + k_2^2\right] \frac{e^{-jk_2R_1}}{R_1} - k_2^2 \frac{1}{r}\frac{\partial}{\partial r} V - k_2^2 U\right) \operatorname{sinc}\left[\tfrac{1}{2}k_2 L_x(\eta_x - (\nabla R_c')_x)\right]\right\} \tag{4.26}$$

and

$$E_z(\omega) = -\frac{j\omega f(\omega) L_x \mu o}{4\pi k_2^2} \cos\phi \left[\frac{\partial^2}{\partial r \partial z}\left(\frac{e^{-jk_2R_2}}{R_2}\right)\right.$$

$$\operatorname{sinc}\left[\tfrac{1}{2}K_2L_x(\eta_x - (\nabla R_c)_x)\right]$$

$$+\left(\frac{\partial^2}{\partial r \partial z}\left[\frac{e^{-jk_2R_1}}{R_1} - k_1^2 V\right] \operatorname{sinc}\left(\tfrac{1}{2}K_2L_x(\eta_x\right.\right.$$

$$\left.\left.\left. - (\nabla R_c')_x)\right)\right)\right] \qquad (4.27)$$

where ϕ is the angle made by $\bar{r}_c$ with the x-axis and the quantity U is defined as

$$U = \frac{2\left[1+jk_1(z+h)\right]}{k_1^2} \frac{1}{r}\frac{\partial}{\partial r}\left[\frac{e^{-jk_2r}}{r}\right] \qquad (4.28)$$

The value of V can be found from the equation

$$2P = 2 - k_1^2 V \qquad (4.29)$$

where P has already been defined in equation (4.18).

The field components due to line segment L_y can be obtained from equations (4.25) to (4.27) by rotating the observer location parallel to the ground. Thus, when the field components are known then their vector sum provides the electric field at a point $\bar{R}$ in space.

The second part of this model is about the calculation

of reflected fields from ionosphere. Only single bounce approximation is considered because the subsequent bounces contribute very little to the total field. Fig 4.8 illustrates the rays contributing to the single bounce reflection model.

Wait (1962b) has calculated reflection coefficients for incident wave on ionospheric layer using quasi longtitudinal approximation. Ground reflection coefficients are also described there. According to these calculations and as shown in Fig 4.9 and 4.10 the ionosphere effect is only applicable up to 100 KHZ and the anisotropy effect begins near 800 HZ and is maximum near 100 KHZ.

To estimate the sky wave fields simple optical ground reflection technique is used for fields due to each line segment. In order to determine the extra travel time and attenuation due to increased distance, a new separation vector from the segment midpoint to a new observation point $\bar{R}_I$ is defined as

$$\bar{R}_I = (R_x, R_y, R_z + 2D) - \bar{R}_c \qquad (4.30)$$

where D is the height of the ionosphere above the ground.

The transmitted field $\bar{E}_D$ measured at the new observation point due to a vertical segment is given as

$$\bar{E}^D(\bar{R}_I) = \left(\frac{\mu_o}{\epsilon_o}\right)^{\frac{1}{2}} L_z \left[\exp(jkR_I)/R_I \right.$$

$$\left\{ \left(1 - \frac{j}{k_2 R_I} - \frac{1}{k_2^2 R_I^2}\right) \hat{l} \right.$$

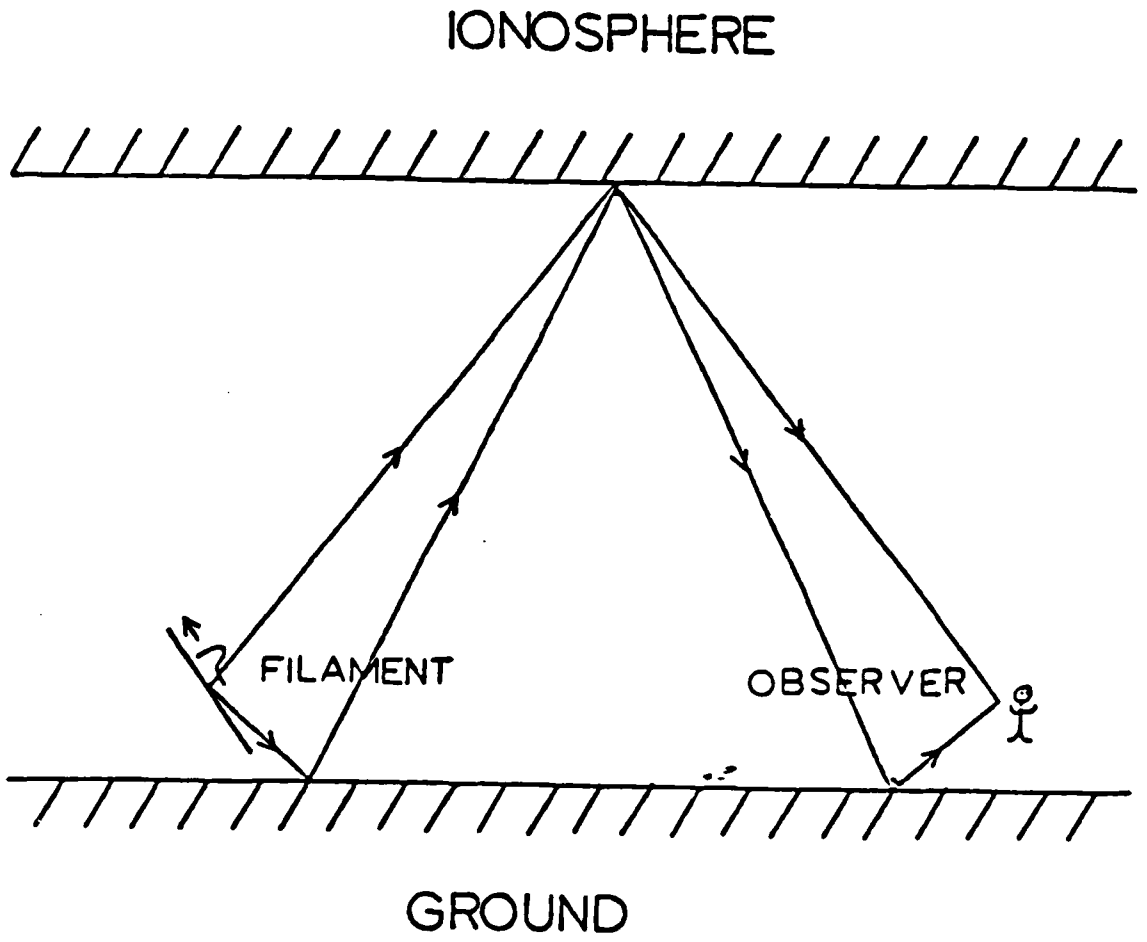

Fig 4.8 Geometry of Rays Showing Single Bounce Reflection Model (Gardner, 1980)

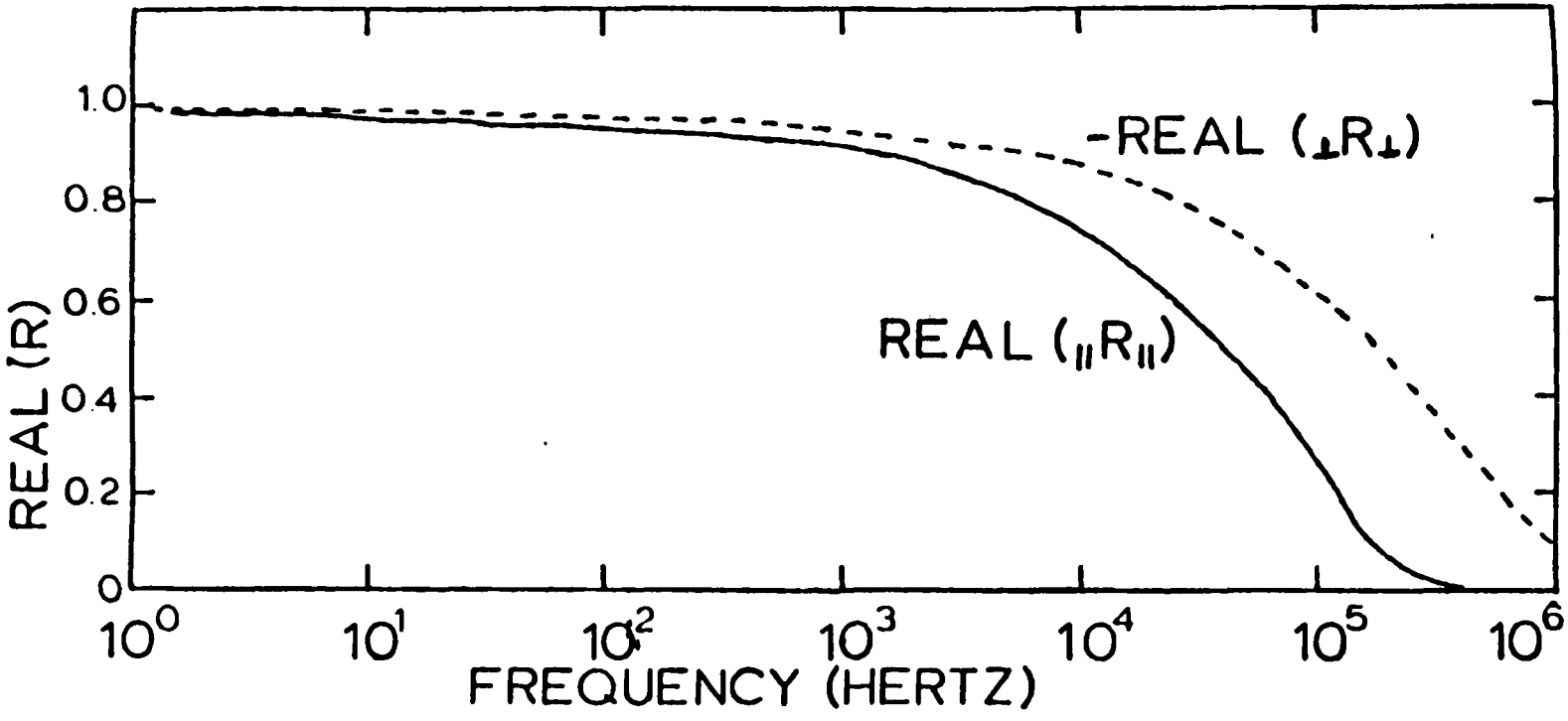

Fig 4.9 Frequency vs Reflection Coefficient for Preserved Polarization When Waves Reflected from Ionosphere (Gardner, 1980)

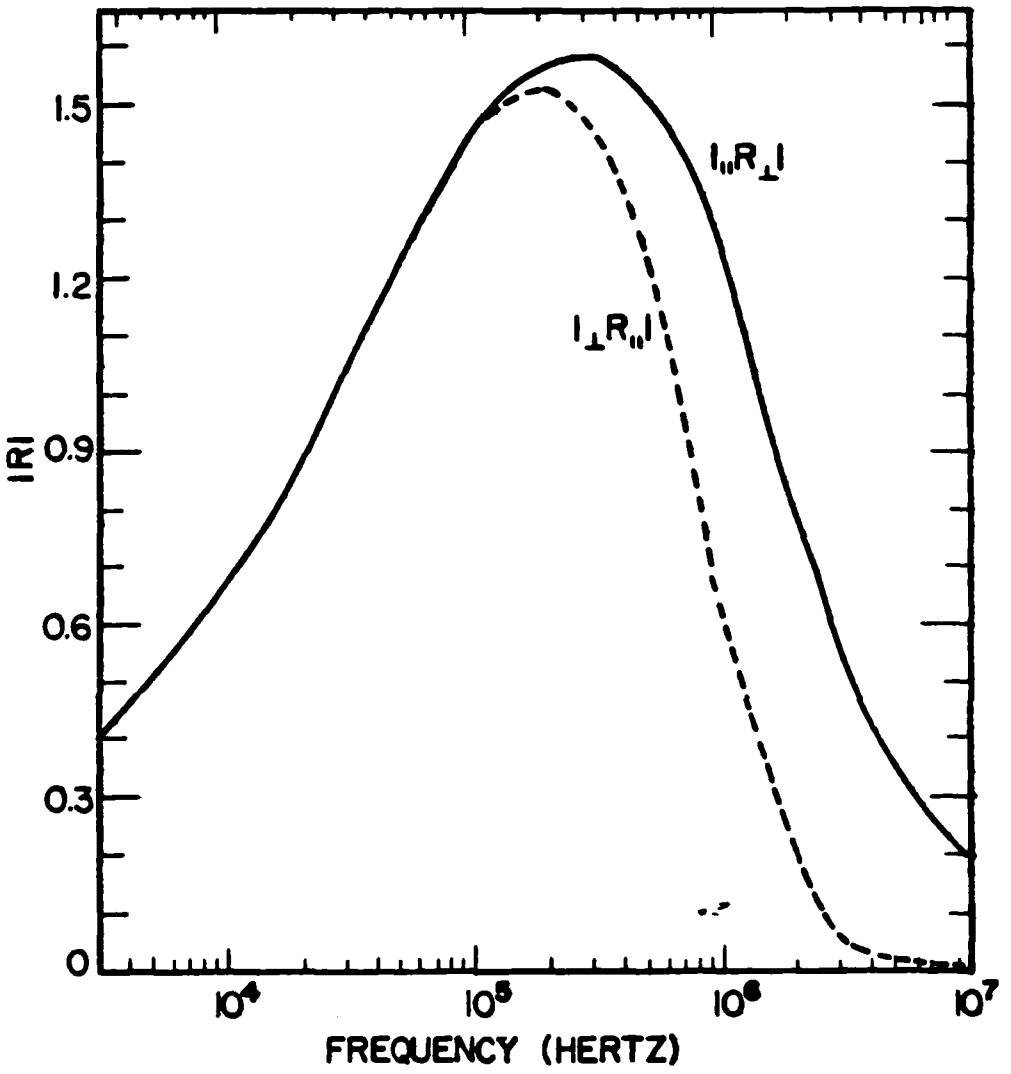

Fig 4.10 Cross Polarization Reflection Co-Efficient from Ionosphere as a Function of Frequency (Gardner, 1980)

$$-\left(1 + \frac{3j}{k_2 R_I} - \frac{3}{k_2^2 R_I^2}\right)(\hat{1}-\nabla R_I)\nabla R_I\Big\}$$

$$x\ \mathrm{sinc}\left[\frac{k_2 L_z}{2}\ (\eta_z-(\nabla R_I)_z)\right]\Big]$$

$$-\frac{R_g}{R_I'}\exp(jk_2 R_I')\left[\left(1+\frac{j}{k_2 R_I'} - \frac{1}{k_2^2 R_I'^2}\right)\hat{1}'\right.$$

$$-\left(1 - \frac{3j}{k_2 R_I'} - \frac{3}{k_2^2 R_I'^2}\right)$$

$$\left.(\hat{1}'.\nabla R_I')\nabla R_I'\right] x\ \mathrm{sinc}\left(\frac{k_2 L_z}{2}\ (\eta_z-(\nabla R_I')_z)\right) \qquad (4.31)$$

where $\hat{1}$ and $\hat{1}'$ are unit vectors along the filament and its image, respectively. R_g denotes the reflection coefficient due to the ground. Quantitites having superscript (') are due to the image. In equation (4.31) the sinc function is due to the phase change along the filament. From the transmitted field $\bar{E}^D$, the sky wave field $\bar{E}^S$'s on the ground are given by the equations.

$$E_x^S(\omega) = \left[\ ||R||\ E_x^D(\omega) + \perp R||\ E_y^D(\omega)\ \sin\theta\right] x$$

$$\left[1 + R_g||\right] \qquad (4.32)$$

$$E_y^S(\omega) = \Big[||R\perp\ E_x^D(\omega) + \perp R\perp E_y^D(\omega)$$

$$+ ||R\perp E_z^D(\bar{\omega})\Big]\left[1+R_g\perp\right] \qquad (4.33)$$

$$E_z^s(\omega) = \left[\perp R||\ \ E_y^D(\omega) + ||R||\ E_z^D(\omega)\ \ \cos\theta\right]$$

$$\left[1 + R_g||\right] \qquad (4.34)$$

Here θ is the angle between the wave and the vertical and symbol $||R$ indicates the reflection coefficient for the incident wave with polarization parallel to the plane of incidence to the reflected wave with polarization perpendicular to the plane of incidence.

From the foregoing discussion and Fig 4.9, it is obsious that radiations up to 1000 HZ can be treated as propagation in the earth ionosphere waveguide. The geometry of such a waveguide configuration is shown in Fig 4.11. Wait (1970) developed this model using three layer Sommerfeld integrals. Using vertical line sigment, this model gives

$$\pi_z(\omega) = \frac{j\pi M}{D} \sum_{n=\infty}^{\infty} H_o^{(2)} (k_2 S_n \rho)\ f_n(h) f_n(z)_n(c) \delta_n(c) \qquad (4.35)$$

where

$$M(\omega) = \frac{f(\omega)\ L_z}{j_4 \pi \omega \varepsilon_o}$$

and

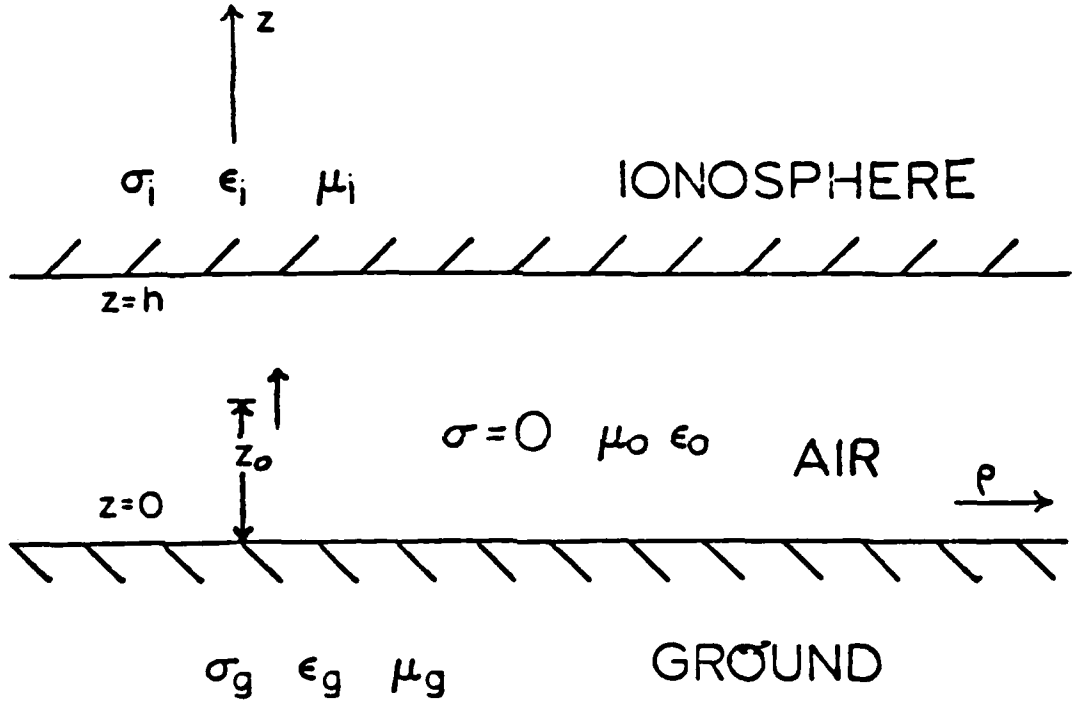

Fig 4.11 Geometry for Waveguide Model (Gardner, 1980)

$$\delta_n(c) = \left[1+j\frac{\frac{\partial}{\partial c}\left[R_i(c)R_g(c)\right]}{2k_2 D R_i(c)R_g(c)}\right]^{-1}\Bigg|_{c = c_n}$$

R_i are the reflection coefficients from the ionosphere layer due to parallel polarization and c_n's are the solutions to

$$R_g(c)\ R_i(c)\ \exp\ (jk_2 cD) = 1 \qquad (4.36)$$

$H_o(2)$ is Hankel function.

Equation (4.35) provides relationship between the ionosphere reflection coefficients and the ground reflection coefficients. Quantity $f_n(z)$ mentioned in equation (4.35) is defined as

$$f_n(z) = \frac{\exp(jk_2 c_n z) + R_g(c_n)\ \exp(-jk_2 c_n z)}{\left[2\ R_g(c_n)\right]^{\frac{1}{2}}} \qquad (4.37)$$

From the Hertz potential of equation (4.35) the electrical field due to a vertical filament is calculated using equation (4.20). Therefore

$$E_z(\omega) = \left(\frac{\partial^2}{\partial z^2} + k_2^2\right)\ \pi_z(\omega) = \frac{j\pi M k_2^2}{D}\sum_{n=\infty}^{\infty} s_n^2$$

$$H_o^2(k_2 S_n \rho) f_n(h) f_n(z) \delta_n(c) \qquad (4.38)$$

Also the field from the horizontal filament can be derived from equation (4.38) by using the reciprocity theorem (Wait 1960). Since the fields due to $E_x(\omega)$ and $E_y(\omega)$ are negligible when the observation point is near ground, the net field due to $E_z(\omega)$ is given by

$$\bar{E}_z(\omega) = \frac{-\partial}{\partial x}\left[\frac{k_o f(\omega) L_x}{j4\omega\varepsilon_o h} \sum_n H_o^{(2)}(k_2 S_n \rho)\, g_n(z_o) f_n(z)\, \delta_n(c)\right] \qquad (4.38)$$

Here f_n and c_n are the same as defined by equations (4.36) and (4.37). However, $g_n(z)$ is the solution to

$$k_o g_n(z_o) = -j \frac{\partial}{\partial z_o} f_n(h) \qquad (4.39)$$

z_o mean the value of z in free space. In fact, the suffix 0 wherever it appears refers to free space quantities. (See Fig 4.11). From equations (4.31), (4.35) and (4.38) it is apparent that the frequency spectrum, and thus the value of radiated field, depends upon (a) finite size of the channel, (b) velocity of propagation of current pulse, (c) channel tortuosity and (d) ground conductivity. A lightning return stroke model which is not based upon these four important parameters will not predict EM fields accurately. The ionospheric reflection discussed in this model is only important for times exceeding 500 μsec or so, otherwise this parameter may be neglected.

The results of this model are compared to Lin's (1978) data in Fig 4.12.

Strawe et al. Model (1979)

This is a nonlinear transmission line model which accounts for consistent return stroke current and channel resistance as a function of time. The model is based on the idea that the return stroke channel diameter increases by several orders of magnitude in about the first 100 microseconds. Thus, due to this time varying parameter, the other parameters during a return stroke also vary with time. Particularly the channel resistance drops to a great extent and as a consequence the current increases in the same order. In fact, not only the channel diameter changes with time but parameters like pressure, temperature and particle density also change with time. All these parameters interact during the return stroke process and affect the size and shape of the current pulse.

The current calculations in this model are based on time varying resistance per unit length. Although inductance and capacitance per unit length also vary with time due to corresponding changing channel parameters, such changes are considered weak functions of time and are not considered (Strawe 1979, 80). However, capacitance variance is compensated by considering large channel radius instead of sub-centimeter current carrying core. The channel tortuosity

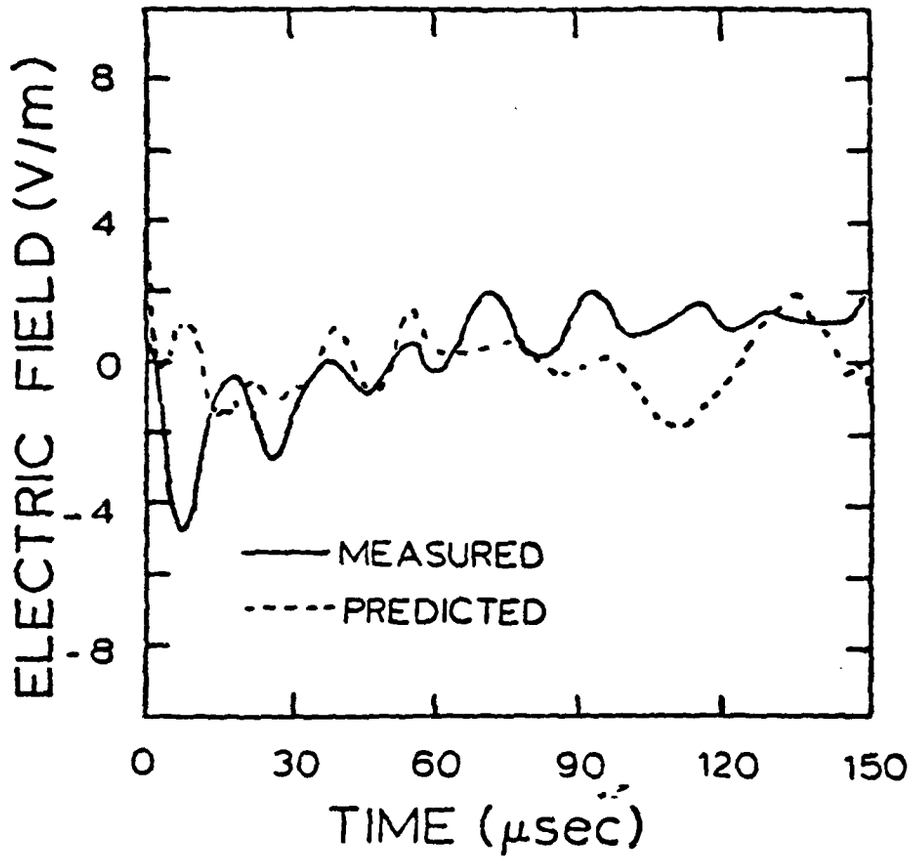

Fig 4.12 Comparison of Distant Measured Transient Waveform from Gardner's Model (1980) to Lin's Data (1978) Gardner (1980)

and corona sheath charge storage effects are accomplished by modification to the hot channel velocity factor (v_f), characteristic impedance (Z_o) and by increasing the resistance per unit length, R (Strawe et al. 1980).

The model representation is divided in two different forms. The first form consists of uniform transmission line segments as shown in Fig 4.13. Here the channel height is 2 kilometers (Strawe 1979). The switch shown in the channel closes when the stepped leader merges with the upward positive leader from the ground. The channel resistance is measured for each segment using Braginsikii's (1958) theory of the development of a spark channel. This process involves the past current time history.

According to Braginsikii's theory the return stroke channel carries the current in a narrow path formed of a high temperature gas. As the Joule heat (i^2R) is released, the pressure in the channel increases and so does the channel radius. This inflated part of the channel in turn acts as a piston on the remaining gas which expands with supersonic speed. This gas then causes a shock wave in the channel. The temperature of the gas near the shock wave is much higher than the temperature of the still gas, whereas below the shock wave the temperature is many times higher. This phenomena causes low gas density in the channel and defines the piston boundaries. With increased temperature and resulting ionization in the channel, the electrical conductivity, which is proportional to $T^{3/2}$, increases (Braginsikii

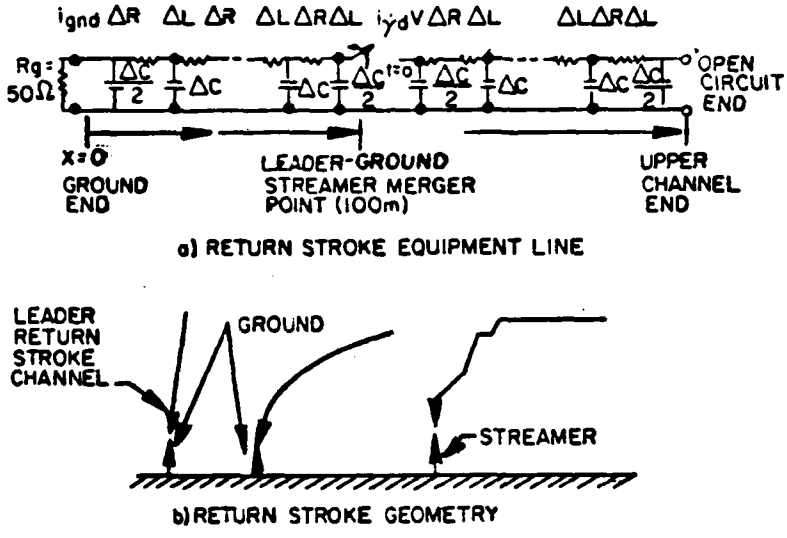

Fig 4.13 Return Stroke Channel as a Transmission Line and Its Geometry in Strawe's Model. (Strawe, 1978)

1958).

The channel resistance per unit length is measured from its conductivity and the arc radius. For time dependent conductivity $\sigma(t)$ and arc radius $a(t)$ the channel resistance per unit length $R(t)$ can be obtained from the following equations

$$a^2(t) = a_o^2 + \beta \int_o^t \left[\frac{i^2(t')}{\sigma(t')} \right]^{1/3} dt \qquad (4.40)$$

$$\frac{1}{R(t)} = \pi \sigma(t) a^2(t) \qquad (4.41)$$

In equation (4.40) the quantity a_o defines the initial condition of the current path radius. Equation (4.40) is a solution of Braginsikii's arc model, which will be presented in the following paragraphs. Equation (4.41) is a form of ohm's law.

In arc model, the channel geometry is assumed locally of cylindrical symmetry. The energy deposit in the channel is given by current local time history (i^2R). Typical arc channel radial profile is shown in Fig (4.14a). The idealized relation between temperature T and arc radius assumed by Braginsikiiis shown in Fig (4.14b). In fact, Braginsikiiassumes three radial regions in the channel. The central "channel" region is the hottest region with low density plasma. The entire shock system internal energy is contained here except for the kinetic energy of translation.

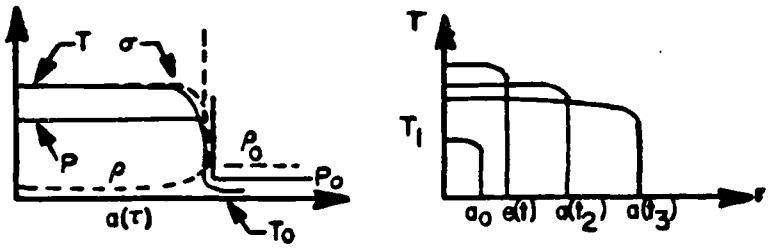

a) TYPICAL ARC CHANNEL RADIAL PROFILES

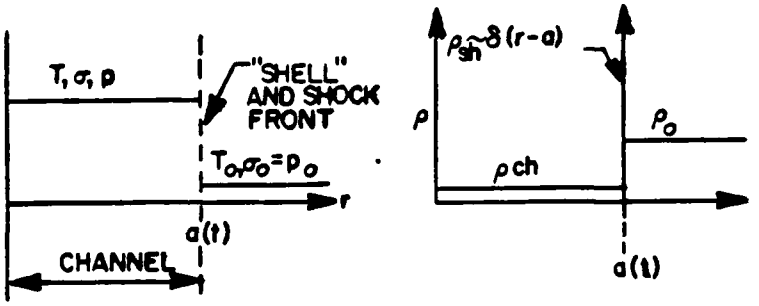

b) BRAGINSKII'S MODEL IDEALIZATION

T	TEMPERATURE	ρ	MASS DENSITY
p	PRESSURE	a	CHANNEL OR SHOCK RADIUS
σ	ELECTRICAL CONDUCTIVITY	r	CYLINDRICAL RADIAL DIMENSION

Fig 4.14 Arc Channel Radial Geometry (Strawe, 1979)

Outside this region is the "shell" region where most of the gas expelled from the main arc is trapped. Although this region is of negligible thickness, almost all the kinetic energy of the shock is contained here. The outermost region is known as "ambient region" and it is beyond the shock or shell radius a(t). This region does not contribute to or take energy from the channel. In fact, all the energy is conserved by the shock and shell region as assumed by Braginsikii. The relative positions of these regions are shown in Fig (4.15).

From piston approximation, as mentioned earlier, if ρ_o is the ambient air mass density, then in general, the channel pressure p is calculated from

$$(p-p_o) = k_p \rho_o \dot{a}^2 \qquad (4.42)$$

where p_o is the ambient pressure and k_p is the efficiency factor ($k_p<1$). Now, if p is much larger than p_o then equation (4.42) reduces to

$$p = k_p \rho_o \dot{a}^2 \qquad (4.43)$$

The above equation provides pressure-velocity relation and the momentum of the system is conserved.

To describe the channel development, the energy conservation equation, the thermal and caloric equations are formed. The energy balance equations are

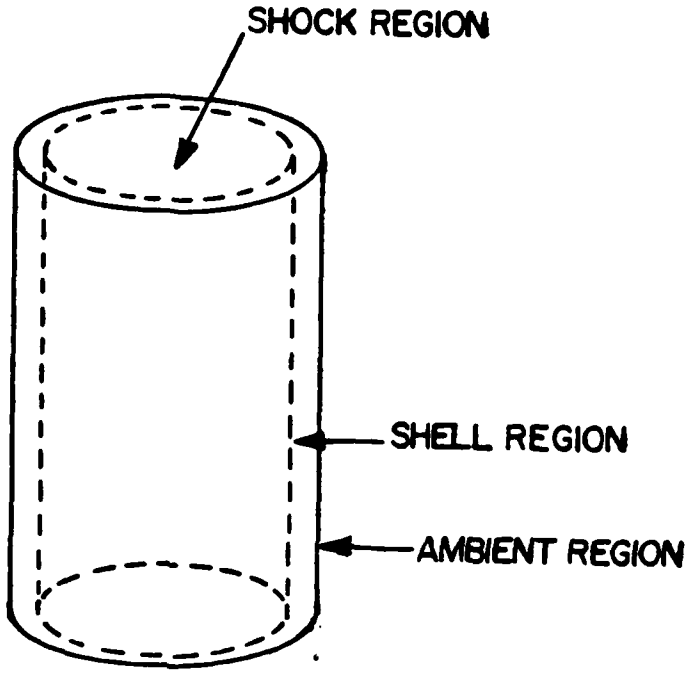

Fig 4.15 Radial Regions in Braginsikii's Arc Channel Model

$$\frac{dWc}{dt} + p \frac{d}{dt} \left[\pi a^2(t)\right] = i^2(t) \quad R \tag{4.44}$$

$$\varepsilon \frac{dM}{dt} = Q_t + Q_r \tag{4.45}$$

where W_c, M and ε are internal energy, channel mass ($\pi a^2 \rho$) and internal energy per unit mass, respectively. Q_t and Q_r represent rates of heat conduction and heat radiation from the lightning channel to the outer shell (Fig 4.15). Equation (4.45) elucidates the phenomena of mass transfer with heating of the channel.

Thermal and caloric equations from thermal physics are

$$p = \frac{(Z+1)\rho kT}{m_{av}} \tag{4.46}$$

$$\varepsilon = \frac{3p}{\rho} + \frac{1}{m_{av}} = \frac{p}{(\gamma-1)p} \tag{4.47}$$

Here Z is the average ionic charge, whereas ρ, k, T, and m_{av} are channel mass density, Boptzmann's constant, channel temperature in degree kelvins and average atomic mass (kg), respectively. Here γ is the effective ratio of specific heats. Braginsikii assumes second form of equation (4.47) with constant value of γ He also assumes that σ is independent of time and temperature and is a constant quantity (assumed $\sigma = 2.22 \times 10^4$ mhos/meter). Thus, under

these assumptions the channel resistance per unit length becomes the function of a(t).

Since

$$W_c = \epsilon M = (\pi \rho_o a^2) \tag{4.48}$$

Substituting equations (4.43) and (4.47) gives

$$W_c = \frac{k_p \rho_o \dot{a}^2}{(\gamma - 1)} \pi a^2 \tag{4.49}$$

After another substitution of equation (4.44) with equations (4.41), (4.43) and (4.49), the result becomes

$$\frac{d}{dt}\left[\frac{\pi k_p \rho_o}{(\gamma-1)} a^2 \dot{a}^2\right] + \pi k_p \rho_o \dot{a}^2 \frac{d}{dt}(a^2) = \frac{i^2}{\pi \sigma_a 2} \tag{4.50}$$

or

$$\frac{i^2}{\sigma} = \pi^2 k_p \rho_o \left[\frac{a^2}{(\gamma-1)} \frac{d}{dt} a^2 \dot{a}^2 + a^2 \dot{a}^2 \frac{d}{dt}(a^2)\right]$$

or

$$\frac{i^2}{\sigma} = 2\pi^2 k_p \rho_o \left[a^3 \dot{a}^3 + \frac{a^3 \dot{a}}{2(\gamma-1)} \ddot{a}\right]$$

or

$$\frac{i^2}{\sigma} = 2\pi^2 k_p \rho_o a^3 \dot{a}^3 \left[1 + \frac{\ddot{a}^2}{2(\gamma-2)\dot{a}^2}\right] \tag{4.51}$$

$$\text{Let } E = 1 + \frac{\ddot{a}^2}{2(\gamma-1)\dot{a}^2} \tag{4.52}$$

Apparently E is a function of time. But it is assumed by Braginskii that E is constant due to power law and hence equation (4.51) becomes

$$\frac{i^2}{\sigma} = 2\pi^2 E\, \rho_o k_p\, (a\,\dot{a})^3 \tag{4.53}$$

or

$$a\,\dot{a} = \frac{1}{\sqrt[3]{2\pi^2 E \rho_o i_p}}\, \left(\frac{i^2}{\sigma}\right)^{1/3} \tag{4.54}$$

Integration of equation (4.54) gives

$$a^2 = a_o^2 + \beta \int_o^t \left(\frac{i^2}{\sigma}\right)^{1/3} dt \tag{4.55}$$

where

$$\beta = \frac{2}{\sqrt[3]{2\pi^2 k_p \rho_o E}}$$

Obsiously equation (4.40) and equation (4.55) are identical.

Since the channel radius is a funciton of time (assumed a simple power form) therefore

$$a \sim t^k \tag{4.56}$$

Also channel current depends on resistance per unit length and some function of time,therefore 'i' can be expressed as

$$i = Rt^n \tag{4.57}$$

From equations (4.52) and (4.56) the result after simplification becomes

$$E = 1 + \frac{(2 - 1/k)}{(\gamma - 1)} \tag{4.58}$$

Substitution of the values from equations (4.57) and (4.58) in equation (4.53) after comparing the powers of t results in

$$k = \frac{2n+3}{6} \tag{4.59}$$

Braginskii assumed that the value of a_o is very small as compared to a(t). Substitution of equation (4.57) in equation (4.55) yields

$$a^2 = \beta \int_o^t \left(\frac{R^2 t^{2n}}{\sigma} \right)^{1/3} dt$$

The solution of this integral gives a result of the form

$$a_n = \alpha_n \, i^{1/3} \, t^{1/2} \tag{4.60}$$

where

$$\alpha_n^2 = \frac{3\beta}{(2n+3)\sqrt[3]{\sigma}}$$

This is Braginskii analytic solution for the arc model of lightning channel. However, as suggested by Strawe (1979) the numerical solution of equation (4.40) is convenient and he has used this equation in his first model.

The second model suggested by Strawe (1979) is a refined version of the first model. This last model accounts for the effective energy. Also σ is no longer considered as constant. Instead values of σ are computed as a function of channel temperature and pressure. Equation (4.42) is re-written by applying Newton's Second law to the shell with ambient and shell pressures working in opposite direction. Thus

$$(p-p_o)\, 2\pi a = \text{Time rate of change of momentum}$$

$$= \frac{d}{dt}\left[\text{shell mass x } \dot{a}\right]$$

$$= \frac{d}{dt}\left[\, k_p \rho_o\, \pi(a^2-a_o^2)\, \dot{a}\right] \qquad (4.61)$$

Since the shell does not exist before the arrival of the shock wave, therefore, initial mass of the shell is considered to be zero. Equation (4.45) provides a relation between energy and mass transfer. Q_r is considered as

as ultraviolet radiation from the channel which is absorbed by the shell to produce plasma in the channel. Evidently, all the ultraviolet radiation is not absorbed, and some of it is wasted. Taking this into account, Q_r can be represented as

$$Q_r = Q_{total} \quad f_a$$

where Q_{total} is the total radiation and f_a is the absorption factor. Therefore, equation (4.44) can be modified as:

$$\frac{dW_c}{dt} + p \frac{d}{dt} \quad \pi a^2(t) \quad = i^2 R - Q_{total}(1-f_a) \quad (4.62)$$

It is assumed in this model that the total radiated power is the transparent radiation and proportional to the radiation factor and channel mass. Thus,

$$Q_{total} = pa^2 F_r(t) \quad (4.63)$$

where $F_r(t)$ is the radiation factor of the arc channel. The heat conduction term Q_t has the value given by

$$Q_t = 2\pi mK_T \quad (4.64)$$

where m has value 2 or 3 and it changes with a(t). K_T is a function of T and p and it is related by the Weedmann-franz law for values of T exceeding 15,000 K (F. Reif, 65).

The values of $\sigma(p,T)$ and K_T used in second model are a curve fits to the results calculated by Plooster (1971)

$$\sigma(p,T) = \frac{1.52\text{x}10^{4}\ p^{-22}}{\left(1+\frac{13.4}{T_k}\right)^{6}\ p^{-54}} \tag{4.65}$$

$$K_T\ (p,T) = \left[\frac{T_k}{10} + \frac{(\sigma T\text{x}10^{-4})^2}{29.1}\right]^{\frac{1}{2}} + \frac{4}{1+10^{3}\left(1-\frac{T_k}{6}\right)^{4}} \tag{4.66}$$

The current waveform used in this model is similar to Bruce-Golde model waveform with peak value of 20 kA at 1.5 μsec and a half value fall time of 40 μsec. The resulting temperature, pressure and radius of the channel due to this current are shown in Fig 4.16.

Em fields from the current are calculated in time domain with the assumption that earth is plane and perfect conductor.

The comparison of models presented in Chapter III, and IV will be discussed in Chapter VIII.

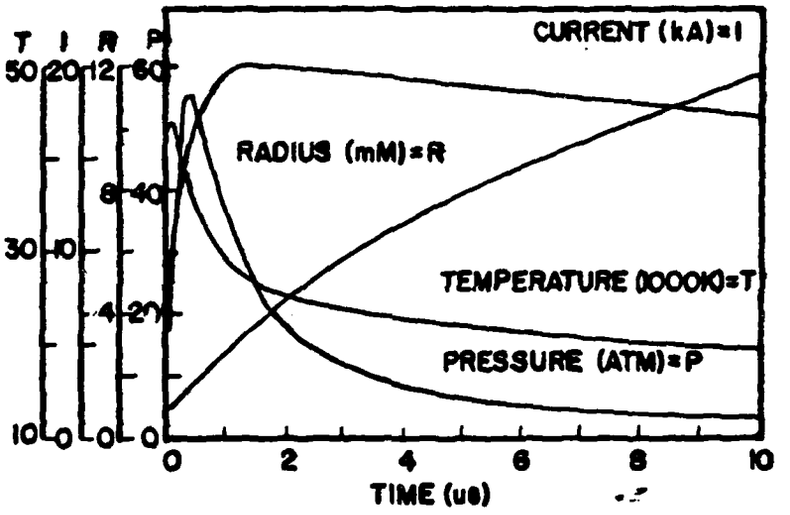

Fig 4.16 Temperature, Pressure, and Channel Radius Variation with Time in Strawe's Model (1978)

V. Electromagnetic Fields Due to Verticle Channel of Variable Height and Having Arbitrary Current Flow

Most of the models presented in the last two chapters predicted EM fields at ground level due to a vertical channel having arbitrary current flow i(z',t). Master et al. (1981) have introduced a lightning return stroke model in which the return stroke electric and magnetic field measured above the ground level can be reproduced. The equations which predict EM fields in space have not been derived in their presentation (Master et al. (1981). However in this chapter we will derive these equations of electromagnetic fields to have an analytic insight of the model and it is hoped that these derivations will enable the reader to understand better the modifications made by the author in the original Master et al. model. The model and the modifications will be discussed in the next chapter.

The geometry of a straight vertical channel of height H above a perfect conducting ground plane is shown in Fig 5.1. In the figure the observation point $P(r,\phi,z)$ is at attitude z and a vertical dipole of length dz' is at height z'. Equations for EM fields will be derived using the method similar to Uman et al. (1975). From electromagnetic field theory, we know that

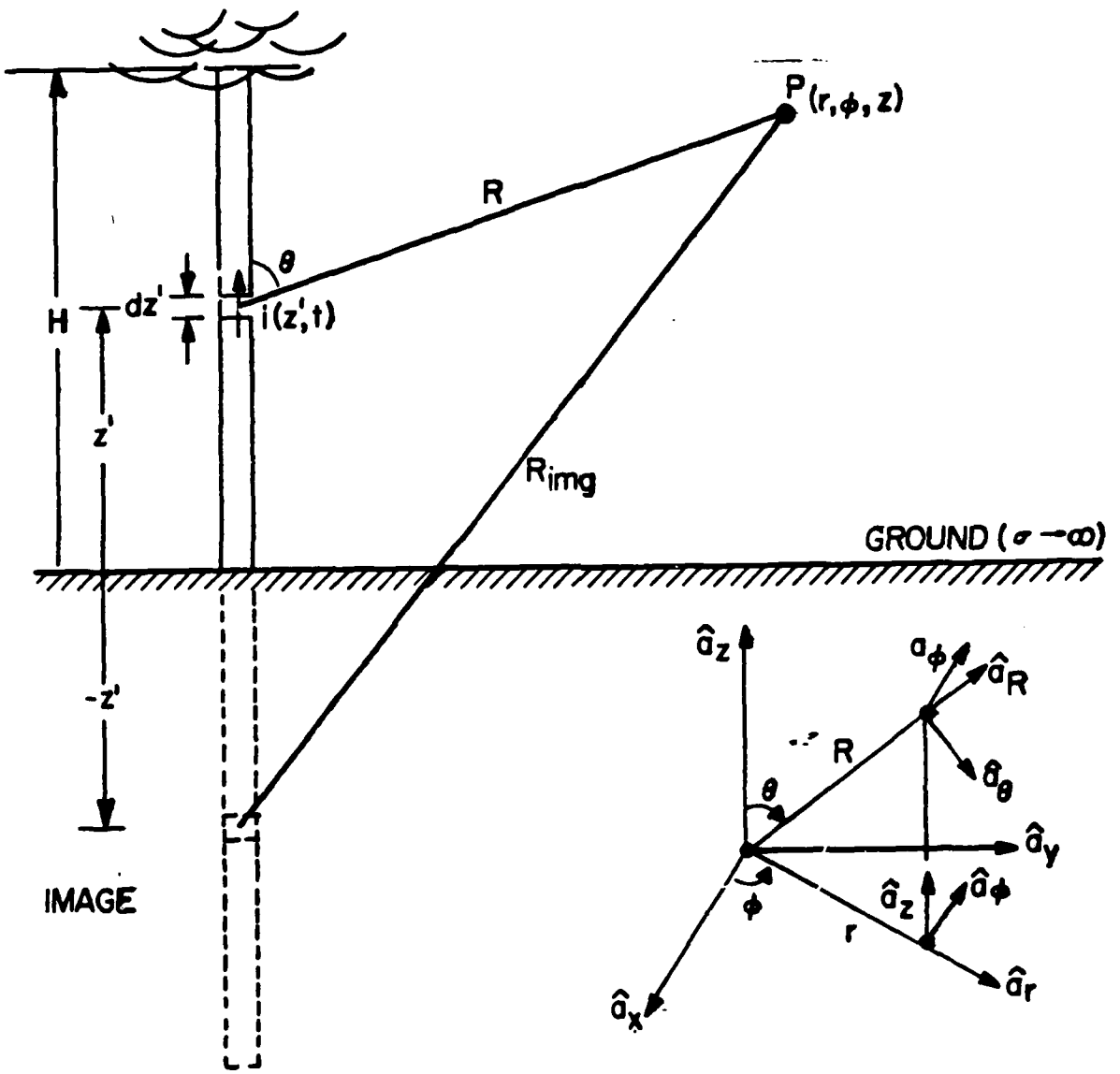

Fig 5.1 The Geometry a Verticle Lightning Return Stroke Channel (Master et al., 1951)

$$\overline{B} = \nabla x \overline{A} \tag{5.1}$$

and

$$\nabla x (\overline{E} + \frac{\partial \overline{A}}{\partial t}) = 0 \tag{5.2}$$

where $\overline{A}$ is the vector potential, Equation (5.2) holds when

$$\overline{E} + \frac{\partial \overline{A}}{\partial t} = -\nabla \phi \tag{5.3}$$

Equations (5.1) and (5.3) can predict time dependent fields provided value of $\overline{A}$ is known for the point in space. The Lorentz condition

$$\nabla \cdot \overline{A} = -\mu_o \, \varepsilon_o \, \frac{\partial \phi}{\partial t} \tag{5.4}$$

in conjunction with Maxwell's equations lead us to a result

$$\nabla^2 \overline{A} - \mu_o \, \varepsilon_o \, \frac{\partial^2 \overline{A}}{\partial t^2} = -\mu_o \overline{I} \tag{5.5}$$

The solution of the inhomogeneous wave equation (5.5) is very similar to the solution of Poisson's equation (Plonsey and Collin, 1961). Note that the resultant value of vector potential in free space is only dependent on the current density $\overline{I}$. Thus, if current information in the lightning channel is known, then the value of $\overline{A}$ is

AD-A124 680 A REVIEW AND COMPARISON OF LIGHTNING RETURN STROKE MODELS USING EXPERIMENTAL DATA(U) AIR FORCE INST OF TECH WRIGHT-PATTERSON AFB OH SCHOOL OF ENGI. 2/2

UNCLASSIFIED S M HANIF DEC 82 AFIT/GE/EE/82D-61 F/G 12/1 NL

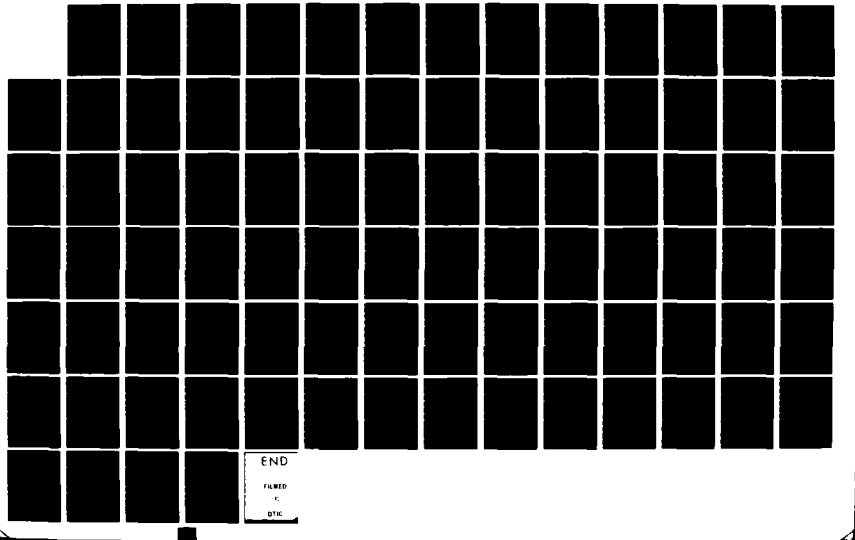

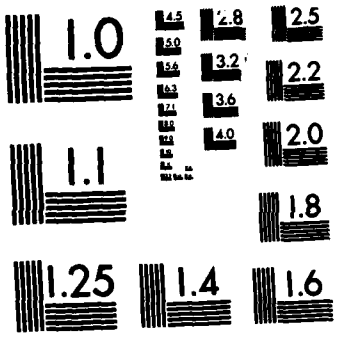

$$\bar{A} = \mu_o \int_V \frac{\bar{I}(t-R/c)}{4\ R}\ dV \qquad (5.6)$$

where $C = 1/\sqrt{\mu_o \epsilon_o}$ and dV is infinitesimal volume having current density $\bar{I}$. Fig 5.2 illustrates the geometry in the computation of retarded potentials given by the equation (5.6).

To implement these results in the case of a vertical channel as shown in Fig 5.1 and meet the boundary conditions an imaginary current of equal amount must exist vertically below the channel.

Now consider a dipole of length dz' along the vertical channel at height z' (Fig 5.1). Using equation (5.6), the differential vector potential at point P due to dz' is

$$d\bar{A}(r,\phi,z) = \frac{\mu o}{4\pi}\frac{1}{R}\ i\ (z',t-R/c)\ \hat{a}_z\ dz' \qquad (5.7)$$

In spherical coordinates

$$\hat{a}_z = \hat{a}_R \cos\theta - \hat{a}_\theta \sin\theta$$

Hence, equation (5.7) becomes

$$d\bar{A} = \frac{\mu o}{4\pi}\frac{1}{R}\ i(z',t-R/c)\left[\hat{a}_R\cos\theta - \hat{a}_\theta\sin\theta\right] dz' \qquad (5.8)$$

But from equation (5.1)

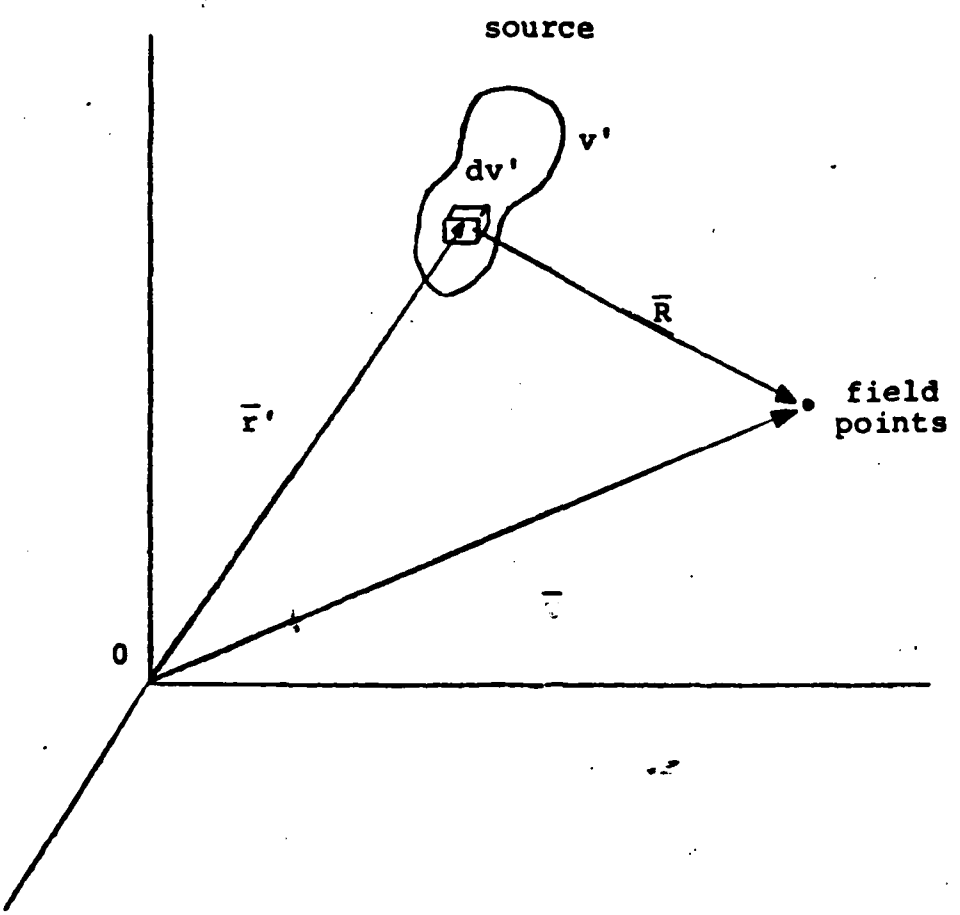

Fig 5.2 Geometry for the Calculation of Retarded Potential at Field Point Due to Charge Location in Volume v' (Uman et al., 1969)

$$d\bar{B} = \nabla x d\bar{A} \tag{5.9}$$

In polar coordinates the curl of $\bar{A}$ is

$$\nabla x \bar{A} = \frac{1}{r\sin\theta}\left[\frac{\partial}{\partial\theta}(A_\phi \sin\theta) - \frac{\partial A_\theta}{\partial\phi}\right]\hat{a}_r + \frac{1}{r}\left[\frac{1}{\sin\theta}\frac{\partial Ar}{\partial\phi} - \frac{\partial}{\partial r}(rA_\phi)\right]\hat{a}_\theta + \frac{1}{r}\left[\frac{\partial}{\partial r}(rA_\theta) - \frac{\partial Ar}{\partial\theta}\right]a_\phi \tag{5.10}$$

Equations (5.8), (5.9) and (5.10) yield

$$d\bar{B} = \frac{\mu o}{4\pi}\left[-\frac{1}{R}\sin\theta\frac{\partial}{\partial R}\, i(z', t-\frac{R}{c}) + \frac{1}{R^2}\sin\theta\, i(R, t-\frac{R}{c})\right]\hat{a}_\phi dz'$$

but

$$\frac{\partial}{\partial R}\, i(z', t-\frac{R}{c}) = -\frac{1}{c}\frac{\partial}{\partial t}\, i(z', t-\frac{R}{c})$$

Therefore,

$$d\bar{B} = \frac{\mu o \sin\theta}{4\pi}\left[\frac{1}{cR}\frac{\partial}{\partial t}\, i(z', t-\frac{R}{c}) + \frac{1}{R^2}\, i(z', t-\frac{R}{c})\right]\hat{a}_\phi\, dz' \tag{5.11}$$

Since the image element ($-\hat{a}_z dz'$) has the current $i(z', t)$ in the $\hat{a}_z$ direction, the resultant magnetic field $d\bar{B}$ at Point P is dependent on vector distance R_m (subscript m indicates

quantities due to imaginary element). Using the result from equation (5.11), we get

$$d\bar{B}_m = \frac{\mu_o \sin\theta_m}{4\pi}\left[\frac{1}{cR_m}\frac{\partial i}{\partial t} i(z', t-\frac{R_m}{c}) + \frac{1}{R_m^2} i(z', t-\frac{R_m}{c})\right]\hat{a}_\phi dz' \qquad (5.12)$$

where θ_m is the angle made by R_m with z-axis.

The resultant magnetic field $d\bar{B}$ at point P is given by the vector sum of equations (5.11) and 5.12), therefore,

$$d\bar{B}_{total} = d\bar{B} + d\bar{B}_m$$

$$= \frac{\mu_o}{4\pi}\left\{\sin\theta\left[\frac{1}{cR}\frac{\partial}{\partial t} i(z', t-\frac{R}{c}) + \frac{1}{R^2} i(z', t-\frac{R}{c})\right]\right.$$

$$\left. + \sin\theta_m\left[\frac{1}{cR_m}\frac{\partial}{\partial t} i(z', t-\frac{R_m}{c}) + \frac{1}{R_m^2} i(z', t-\frac{R_m}{c})\right]\right\}\hat{a}_\phi dz' \qquad (5.13)$$

Let r be the vertical distance of point P from the channel (Fig 5.1). Values of R, R_m, $\sin\theta$ and $\sin\theta_m$ are given by

$$R = \left[r^2+(z-z')^2\right]^{1/2} \qquad (5.14)$$

$$R_m = \left[r^2+(z+z')^2\right]^{1/2} \qquad (5.15)$$

$$\text{Sin}\theta = \frac{r}{R} = \left[r \quad r^2+(z-z')^2 \right]^{-\frac{1}{2}} \tag{5.16}$$

$$\text{Sin}\theta_m = \frac{r}{R_m} = r\left[r^2+(z+z')^2 \right]^{-\frac{1}{2}} \tag{5.17}$$

where z is the vertical height of the point P.

Substitution of these values in equation (5.13) yields

$$d\bar{B}_{total} = \frac{\mu_o}{4\pi}\left\{ \frac{r}{\left[r^2+(z-z')^2\right]c} \frac{\partial}{\partial t} i\left(z', t - \frac{\left[r^2+(z-z')^2\right]^{\frac{1}{2}}}{c}\right) \right.$$

$$+ \frac{r}{\left[r^2+(z-z')^2\right]^{3/2}} i\left(z', t - \frac{\left[r^2+(z-z')^2\right]^{\frac{1}{2}}}{c}\right)$$

$$+ \frac{r}{c\left[r^2+(z+z')^2\right]} \frac{\partial}{\partial t} \left(z', t - \frac{\left[r^2+(z+z')^2\right]^{\frac{1}{2}}}{c}\right)$$

$$\left. + \frac{r}{\left[r^2+(z-z')^2\right]^{3/2}} i\left(z', t - \frac{\left[r^2+(z+z')^2\right]^{\frac{1}{2}}}{c}\right) \right\} \hat{a}_\phi \, dz' \tag{5.18}$$

The total magnetic field due to the channel current length l(t), which is a function of time and is given by equation (3.9), is found by integrating equation (5.27) from zero to $i(\tau)$. Therefore,

$$\bar{B}(r,\phi,z,t) = \frac{\mu_o}{4\pi}\int_o^{l(\tau)} \left\{ \frac{r}{\left[r^2+(z-z')^2\right]} \frac{\partial}{\partial t} i\left(z', t - \right.\right.$$

$$\left.\left. \frac{\left[r^2+(z-z')^2\right]^{\frac{1}{2}}}{c} \right) + \frac{r}{\left[r^2+(z-z')^2\right]^{3/2}} i\left(z', t - \frac{\left[r^2+(z-z')^2\right]^2}{c}\right)$$

$$+ \frac{r}{\left[r^2+(z+z')^2\right]} \frac{\partial}{\partial t} \; i\left(z', t-\frac{\left[r^2+(z+z')^2\right]}{c}\right)$$

$$+ \frac{r}{\left[r^2+(z-z')^2\right]^{3/2}} i\left(z', t-\frac{\left[r^2+(z\ z')^2\right]}{c}\right) \Bigg\} dz' \; \hat{a}_\phi \quad (5.19)$$

where

$$\tau = t - \frac{R}{c}$$

To find the electric field due to an infinitesimal current dipole dz' at a height z' along the channel, equations (5.3) and (5.4) are used. From equation (5.3)

$$d\bar{E} + \frac{\partial}{\partial t} d\bar{A} = - \nabla d\phi \quad (5.20)$$

and from equation (5.4)

$$d\phi = -c^2 \int_o^t \nabla . \; d\bar{A} \; dt \quad (5.21)$$

In polar coordinates the divergency of $\bar{A}$ is

$$\nabla . \; \bar{A} = \frac{1}{r^2} \frac{\partial}{\partial r} (r^2 A_{\hat{r}}) + \frac{1}{r \mathrm{Sin}\theta} \left[\frac{\partial}{\partial \theta} (A_\theta \; \mathrm{Sin}\theta) + \frac{\partial A\phi}{\partial \phi}\right] \quad (5.22)$$

Determining the divergence of equation (5.8) yields

$$\nabla . d\bar{A} = \frac{\mu o \mathrm{Cos}\theta}{4\pi R^2} \left[\frac{\partial}{\partial R} \left\{\left(R \; i\left(z', t-\frac{R}{c}\right)\right\}\right] dz' -$$

$$\frac{\mu o}{4\pi R^2 \, \mathrm{Sin}\theta} i(z', t-\frac{R}{c}) \, \frac{\partial}{\partial \theta}(\mathrm{Sin}^2\theta) \, dz'$$

$$= - \frac{\mu o \mathrm{Cos}\theta}{4\pi R^2} \, \mathrm{Cos}\theta \, i(z', t-\frac{R}{c}) dz' - \frac{\mu o \mathrm{Cos}\theta}{4\pi R c}$$

$$i(z, t-\frac{R}{c}) \, dz' \qquad (5.23)$$

Substitution of equation (5.23) in equation (5.21) yields

$$d\Phi = \frac{\mathrm{Cos}\theta}{4\pi\epsilon_o} \left[\frac{1}{R^2} \int_o^t i(z', \tau - \frac{R}{c}) \, d\tau + \frac{1}{cR} \right.$$

$$\left. i(z', t-\frac{R}{c}) \right] dz' \qquad (5.24)$$

because $c^2 = 1/\mu_o\epsilon_o$.

The negative gradient of equation (5.24) gives the result

$$- \nabla d\Phi = \left\{ \frac{\mathrm{Cos}\theta}{4\pi\epsilon_o} \left[\frac{2}{cR^2} i(z', t-\frac{R}{c}) + \frac{2}{R^3} \int_o^t i(z', \tau-\frac{R}{c}) d\tau \right. \right.$$

$$\left. + \frac{1}{c^2 R} \, \frac{\partial}{\partial t} i(z', t-\frac{R}{c}) \right] \hat{a}_R$$

$$+ \frac{\mathrm{Sin}\theta}{4\pi\epsilon_o R} \left[\frac{1}{R^2} \int_o^t i(z', \tau-\frac{R}{c}) d\tau \right.$$

$$\left. \left. + \frac{1}{cR} i(z', t-\frac{R}{c}) \right] \hat{a}_\theta \right\} dz' \qquad (5.25)$$

To find $\frac{\partial}{\partial t} d\bar{A}$, take the derivative of equation (5.8). The result is

$$\frac{\partial}{\partial t} d\bar{A} = \frac{\mu o}{4\pi} \left\{ \left[\frac{\text{Cos}\theta}{R} \frac{\partial}{\partial t} i(z', t-\frac{R}{c}) \right] \hat{a}_R + \left[\frac{\text{Sin}\theta}{R} \frac{\partial}{\partial t} i(z', t-\frac{R}{c}) \right] \hat{a}_\theta \right\} dz' \qquad (5.26)$$

Substitution of equations (5.25) and (5.26) in equation (5.20) gives

$$d\bar{E} = \frac{1}{4\pi\varepsilon o} \left\{ \text{Cos}\theta \left[\frac{2}{R^3} \int_o^t i(z', \tau-\frac{R}{c}) d\tau + \frac{2}{cR^2} i(z', t-\frac{R}{c}) \right] \hat{a}_R + \text{Sin}\theta \left[\frac{1}{R^3} \int_o^t i(z', \tau-\frac{R}{c}) d\tau + \frac{1}{cR^2} i(z', t-\frac{R}{c}) + \frac{1}{c^2 R} \frac{\partial}{\partial t} i(z', t-\frac{R}{c}) \right] \hat{a}_\theta \right\} dz' \qquad (5.27)$$

The field due to an infinitesimal imaginary element at a distance R_m from the observation point P (Fig 5.1) can be found from equation (5.27) by replacing R with R_m, θ with θ_m, $\hat{a}_r$ with $\hat{a}_{rm}$ and $\hat{a}_\theta$ with $\hat{a}_{\theta m}$.

Therefore, the electric field $d\bar{E}_m$ is

$$d\bar{E}_m = \frac{1}{4\pi\varepsilon_o} \left\{ \text{Cos}\theta_m \left[\frac{2}{R_m^3} \int_o^t i(z', \tau-\frac{R_m}{c}) d\tau + \frac{2}{cR_m^2} i(z', t-\frac{R_m}{c}) \right] \hat{a}_{Rm} \right.$$

$$+ \text{Sin}\theta_m \left[\frac{2}{R_m^3} \int_o^t i(z', \tau - \frac{R_m}{c})\, d\tau + \frac{1}{cR_m^2}\, i(z', t - \frac{R_m}{c}) \right.$$

$$\left. + \frac{1}{c^2 R_m} \frac{\partial}{\partial t}\, i(z', t - \frac{R_m}{c}) \right] \hat{a}_{\theta m} \Bigg\}\, dz' \qquad (5.28)$$

Before finding the total electric field by adding equations (5.27) and (5.28) it is convenient to convert the differential fields to cylindrical coordinates. From Fig 5.1 it can be found that

$$\hat{a}_R = \text{Sin}\theta\, \hat{a}_r + \text{Cos}\theta\, \hat{a}_z \qquad (5.29)$$

$$\hat{a}_\theta = \text{Cos}\theta\, \hat{a}_r - \text{Sin}\theta\, \hat{a}_z \qquad (5.30)$$

$$\hat{a}_{R_m} = \text{Cos}\theta_m\, \hat{a}_r + \text{Cos}\theta_m\, \hat{a}_z \qquad (5.31)$$

$$\hat{a}_{\theta_m} = \text{Cos}\theta_m\, \hat{a}_r - \text{Sin}\theta_m\, \hat{a}_z \qquad (5.32)$$

Substitution of these values in equations (5.27) and (5.28) results in

$$d\bar{E} = \frac{dz'}{4\pi\epsilon_o} \left\{ \left[\frac{(2\text{Cos}^2\theta - \text{Sin}^2\theta)}{R^3} \int_o^t i(z', \tau - \frac{R}{c}) d\tau \right.\right.$$

$$+ \frac{2\text{Cos}^2\theta - \text{Sin}^2\theta}{cR^2}\, i(z', t - \frac{R}{c})$$

$$\left. - \frac{\text{Sin}^2\theta}{c^2 R} \frac{\partial}{\partial t}\, i(z', t - \frac{R}{c}) \right] \hat{a}_z + \frac{3\text{Cos}\theta\text{Sin}\theta}{R^3} \int_o^t i(z' \tau - \frac{R}{c}) d\tau$$

$$+ \frac{3\text{Cos}\theta\text{Sin}\theta}{cR^2} i(z', t - \frac{R}{c}$$

$$+ \frac{\text{Cos}\theta\text{Sin}\theta}{c^2R} \frac{\partial}{\partial t} i(z', t - \frac{R}{c})\Big] \hat{a}_r \Bigg\} \qquad (5.33)$$

A similar equation for $d\bar{E}_m$ can be determined except that θ and R are replaced by θ_m and R_m, respectively. Similarly to equations (5.16) and (5.17) the values of Cos and $\text{Cos}\theta_m$ are defined as

$$\text{Cos}\theta = \frac{z - z'}{R} \qquad (5.34)$$

$$\text{Cos}\theta_m = \frac{z + z'}{R_m} \qquad (5.35)$$

Using equations (5.16), (5.17), (5.34) and (5.35), the resultant field at point P is

$$dE_{total} = d\bar{E} + d\bar{E}_m$$

$$= \frac{dz'}{r\pi\epsilon_o} \Bigg\{ \Bigg[\frac{2(z-z')^2 - r^2}{R^5} \int_o^t i(z', \tau - \frac{R}{c}) d\tau$$

$$+ \frac{2(z-z')^2 - r^2}{CR^4} i(z', t - \frac{R}{c})$$

$$- \frac{r^2}{c^2R^3} \frac{\partial}{\partial t} i(z', t - \frac{R}{c}) + \frac{2(z+z')^2 - r^2}{R_m^5} \int_o^t i(z', \tau - \frac{R_m}{c}) d\tau$$

$$+\frac{2(z+z')^2-r^2}{cR_m^4}\,i(z',t-\frac{R_m}{c})-\frac{r^2}{c^2R_m^3}\,\frac{\partial}{\partial t}\,i(z',t-\frac{R_m}{c})\Bigg]\hat{a}_z$$

$$+\Bigg[\frac{3(z-z')r}{R^5}\int_0^t i(z',\tau-\frac{R}{c})d\tau+\frac{3(z-z')r}{cR^4}\,i(z',t-\frac{R}{c})$$

$$+\frac{(z-z')r}{c^2R^3}\,\frac{\partial}{\partial t}\,i(z',t-\frac{R}{c})+\frac{3(z+z')}{R_m^5}\int_0^t i(z',\tau-\frac{R_m}{c})d\tau$$

$$+\frac{3(z+z')r}{cR_m^4}\,i(z',t-\frac{R_m}{c}+\frac{(z+z')r}{c^2R_m^3}\,\frac{\partial}{\partial t}\,i(z',t-\frac{R_m}{c}\Bigg]\hat{a}_r\Bigg\} \qquad (5.36)$$

The total electric field due to channel height 1 or 2 is obtained by integrating equation (5.36) and the result is

$$\bar{E} = \int_0^{l(t)} d\bar{E} \qquad (5.37)$$

Values of R and R_m in equation (5.36) have already been defined in equations (5.14) and (5.15). Equation (5.36) is exactly the same as Master et al. (1981) have used in their model without deriving it.

Note that the equation (5.36) depicts the total field comprising of radial and vertical components. However, the airborne measurements of the electric field is only in vertical $\hat{a}_z$ direction; whereas $\hat{a}_r$ component lies in the plane of the steady state aircraft, and its value is not recorded.

Equation (5.19) is the predicted value of magnetic field in $\hat{a}_\phi$ direction. In experimental data the value of $\bar{B}$ is recorded in two orthogonal components. These components

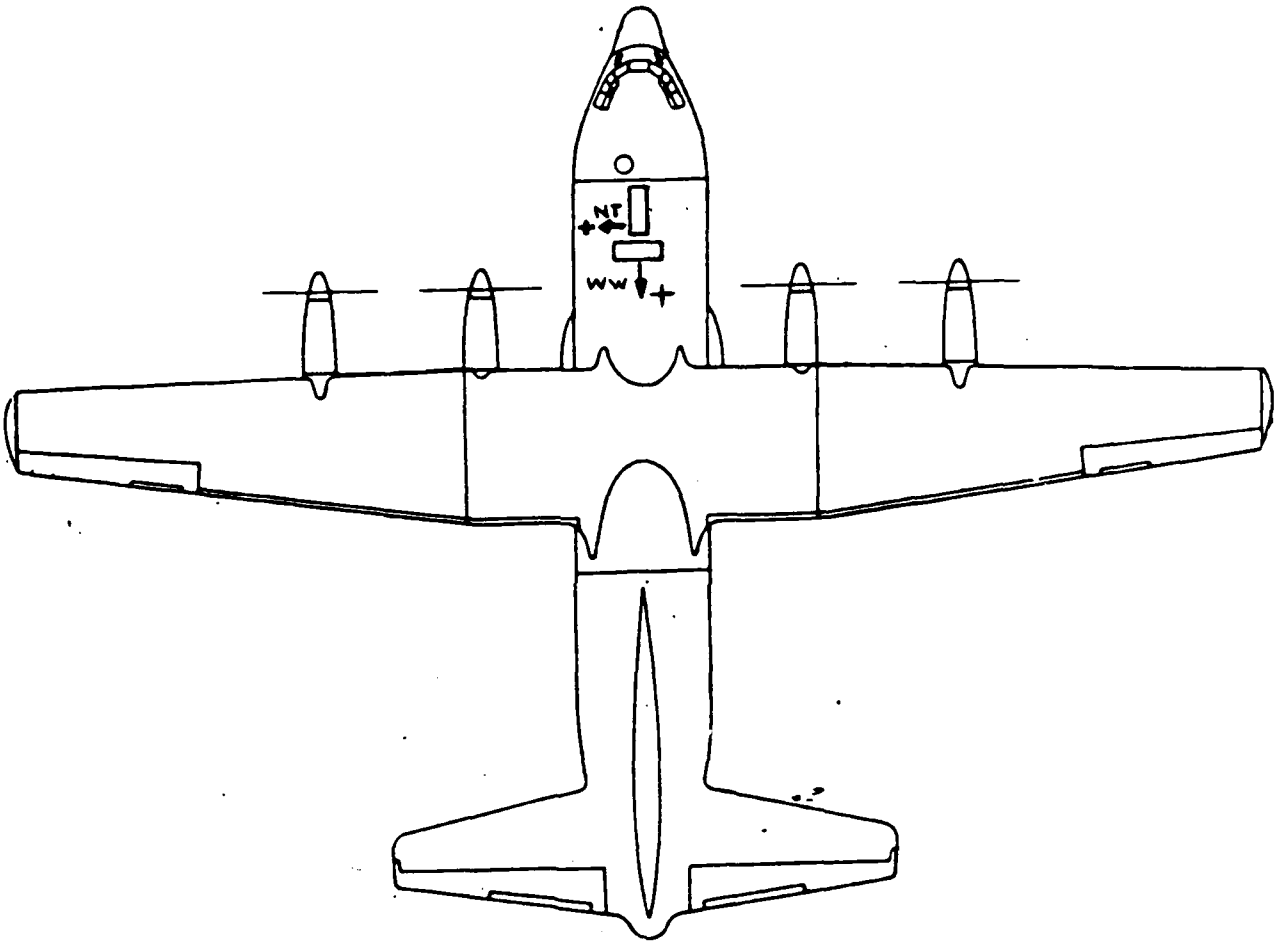

Fig 5.3 Direction of Measured Orthogonal Components of Magnetic Field B_ϕ.

are along the nose-to-tail and wing-to-wing direction as shown in Fig 5.3. These components, along with the aircraft bearing, are used to find the relative direction of the lightning return stroke. The detailed discussion on the validity of this data and direction finding will be discussed in one of the next chapters. However, it is apparent from equation (5.19) that in ideal conditions correct bearing of the lightning channel with respect to aircraft can be found.

VI. Master et al. Model (1981) And Modifications

Master et al. Model (1980)

This model is a modified version of the Lin et al. model (1980) and provides reasonable estimates of the return stroke fields in space. As suggested by the authors of this model, the EM fields computation was restricted to an altitude of 10 km and at ranges from 20 m to 10 km. However, Master et al. did not specify explicitly the reasons for restricting these ranges.

Similar to the Lin et al. model, the return stroke channel is like a vertical thin wire antenna of height H above a perfectly conducting ground. The geometry of the model is shown in Fig 5.1 and the mathematical expression that predicts the fields above ground level were derived in Chapter V and were given by equations (5.19) and (5.37). The current parameters of this model are due to subsequent return stroke rather than to a first return stroke. Subsequent return strokes were considered because they have fewer branches and relatively constant upward propagation velocity.

The modifications to the Lin et al. model (1980) are based on defining the current parameters. The Lin et al. model assumes that a short duration breakdown pulse current propagates upwards with constant amplitude and waveshape.

But, in this model the breakdown pulse is assumed to decrease with height because the subsequent stroke initial peak luminosity changes considerably with height (Jordan and Uman 1980). The attenuation in the breakdown pulse also removes the mirror image problem observed in the Lin et al. model. Mirror image is the field change of opposite polarity to that of the initial field when the breakdown pulse reaches the top of the channel and this effect is almost never observed in the subsequent return stroke (Lin et al. 1980).

The channel current waveform consists of three components called the uniform current, I_u, the corona current, i_c and the breakdown pulse current, i_p. Mathematically it can be represented as

$$i(z,t) = I_u + i_x + i_p \qquad (6.1)$$

A graphical comparison of the current waveforms in the Lin et al. model (1980) and Master et al. model (1981) are shown in Fig (6.1). It is obvious from Fig 6.1 that the minimum value of the corona and breakdown pulse are equal to the uniform current in the Lin et al. model; however, this value is considered as zero in Master et al. model (1981). Although not shown in Fig 6.1, the rise-to-peak of the breakdown pulse has also been modified from that of Lin et al. (1980) so as to make these parameters consistent with the results of Weidman and Krider (1978).

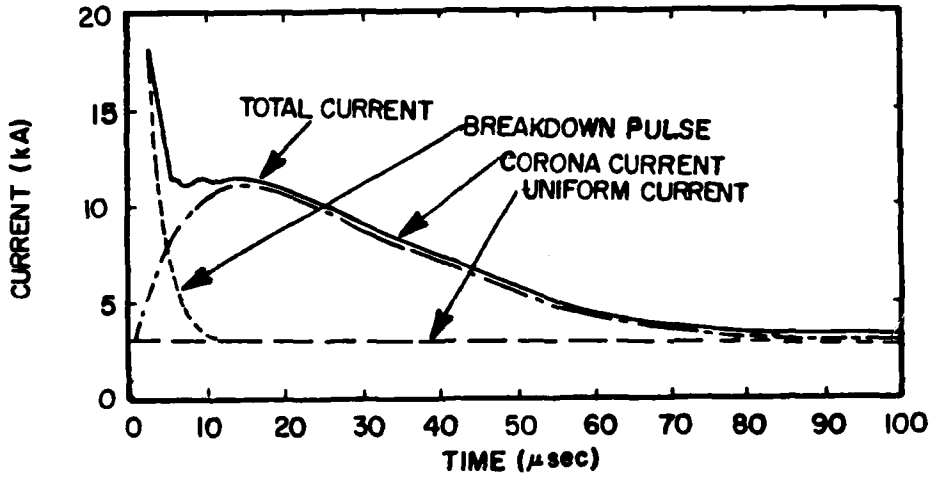

(a)

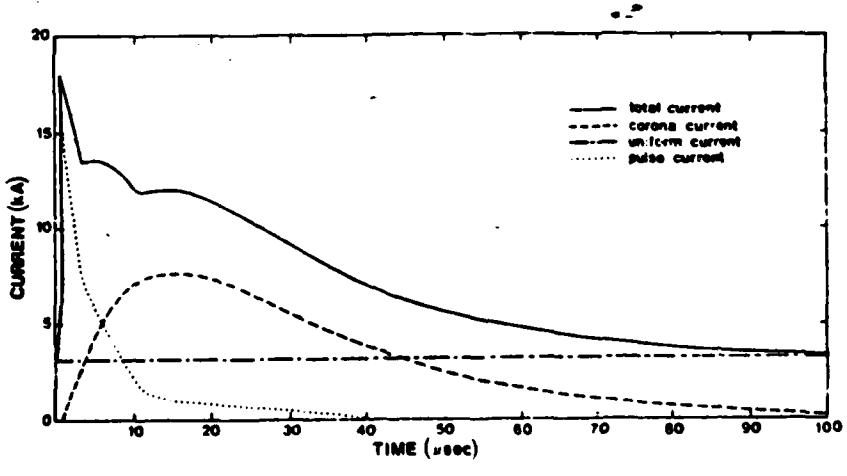

(b)

Fig 6-1 Graphical Comparison of Return Stroke Channel Current Waveforms (a) L et al. Model (1980) (b) Master et al. Model (1981)

Except for the modifications discussed above, the Master et al. model (1981) uses all the current parameter described in Lin et al. model (1980) in Chapter III. In Master et al. model the height dependent attenuation of the breakdown pulse current takes the form $i_p\ e^{-2'/\lambda}$ where λ = 1500 meters. Thus, the breakdown pulse decreases with height in exactly the same manner as does the corona current in Lin et al. model (1980).

Modifications

During this research only two modifications in Master et al. model were studied. These modifications are related to the variable propagation velocity and the wave-shape of the corona current. Master et al. model (1981) is in fact based on the statistical averages of various parameter in a return stroke. But the parameter chosen for modification are such that their statistical average will considerably effect the estimated value of the EM fields above the ground.

Lin et al. (1980) have mentioned that error in the measurement of propagation velocity could be as high as 30 to 60 percent. In fact, measured velocities depend on the height above the ground, at which the measurement was made. Also, Uman and McLain (1970) have proved that for distance D > 50 km

$$i(D,t) = \frac{2\pi cD}{\mu_o v}\ B(t+\frac{D}{c}) \qquad \text{for } 1 \leq H \qquad (6.2)$$

where l, H are the instantaneous and maximum length of the return stroke channel.

Equation (6.2) provides a simple relation between the channel current, velocity of current pulse propagation and the distant radiated magnetic field. Thus, if larger return stroke velocity is assumed, then the current peak value and the waveshape is altered. These arguments justify that variable velocity should be considered in modeling the current waveform.

Almost in all the nonlinear models the velocity of propagation is varying because of nonlinear parameters L and C. Braginskii (1958) has also considered the nonlinear velocity in an arc channel. Lin et al. (1980) has suggested that refinement in the model can be achieved by taking into consideration the decrease in velocity with height. Jordan and Uman (1980) have found that the peak luminosity of the subsequent strokes decreases to half the initial peak in less than one kilometer above ground. In recent studies Uman et al. (1982) report that average velocity for subsequent stroke is 1.2×10^8 m/sec and this velocity decreases with height.

The author has found out during these studies that if the attenuation factor of the current pulse in Master et al. model is not changed but the velocity of propagation is increased then the mirror image effect can be found.

It was also found by trial and error that the velocity variation between 1.5×10^8 m/sec and $.5 \times 10^8$ m/sec oculd be achieved. Since the change in velocity is considered height

dependent and there was no experimental data available with the author to put velocity in this form, $v_t = v_o\, e^{-z/H}$, for the first stroke, therefore, velocity variation was considered linear instead of exponential. Modification in subsequent stroke is not studied because experimental data for subsequent stroke was not made available. The modification made in Master et al. model is

$$v(z) = v_o(1-.33z/H) \qquad (6.3)$$

where v_o was taken as 1.5×10^8 m/sec and H = 5 km. This relation is satisfied for a return stroke travel time of 50 μsec, which is the same in the Master et al. model with constant velocity $v = 1\times10^8$ m/sec. Berger et al. (1975) have shown that average value of subsequent duration has exceeded 32 μsec for 50% of cases. If these values are taken into account, then the propagation velocity can still be increased. The results of this modification are shown in Fig 8.16 to 8.18.

The second modification made in the Master et al. model is in corona current waveshape. Bruce Golde (1941) suggested the double exponential decay waveform and in the later years most of the researchers were basing their models on this waveform. Uman (1969) and Lin (1978) made significant changes in the Bruce & Golde waveform. Uman (1969) suggested attenuation in the corona current waveform. Lin (1978) divided the channel current into three components as given by equation (6.1). Recent studies in current waveform were carried out by Berger et al. (1975), Garbanatti (1982), and Eriksson (1978). The typical return stroke

current measured by these authors is shown in Fig 6.2. According to these studies for the first and subsequent return strokes, current drops to 50% of peak value in almost 30 μsec. Fig 6.2(a) shows a large variation in the current waveform for the first return stroke. However, waveform A in Fig 6.2(a) indicates a fast decay in the current even after 30 μsec. The current parameters suggested by Uman et al. (1981) for the first return stroke of Master et al. model (1981) produce a current waveform much similar to this waveform. But the EM fields for first stroke predicted in space by Master et al. model (1981) and shown in Fig 8.13 to 8.15 are different from those of empirical data as shown in Fig 8.3 to 8.12. Because during this study empirical data only for the first return stroke was made available, therefore, a modification to the current waveform for the first return stroke is suggested. The modification in current waveform is also suggested because the current parameters in first stroke changes significantly with time. In Chapter VIII, it will be proved that combined effect of modified velocity and current waveform improve considerably the peak value of predicted fields.

For the current waveform modification values of α and β are varied with time so as to achieve maximum value of $\frac{dI}{dt}$ during 30 sec to 50 sec time and then minimum value of $\frac{dI}{dt}$ in the subseuqent 50 sec. It is assumed that total observation time is 100 sec. Since Master et

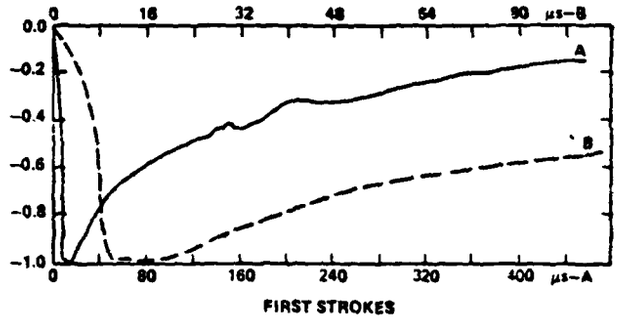

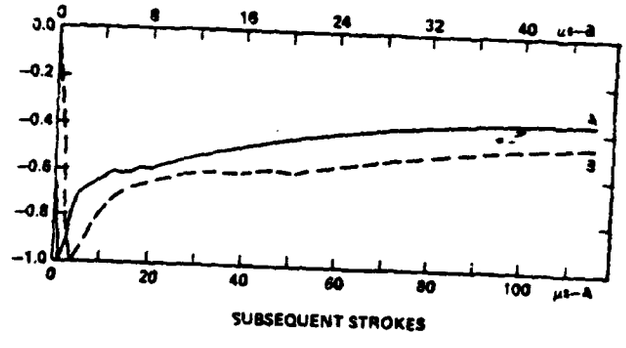

Fig 6.2 Average Return Stroke Currents Measured by Berger and His Coworkers (Uman et al., 1982)

al. model current waveform for first return stroke conforms with waveform A of Fig 6.2(a) up to 30 μsec, therefore, modification in the waveform was incorporated 30 μsec after the initiation of the return stroke. The value of α and β increases logrithmically as

$$\alpha = 1\times10^{5} \times \ln \frac{t}{20\times10^{-6}} + .6 \qquad + \geq 30 \text{ μsec} \quad (6.4)$$

$$\beta = 3\times10^{6} \times \ln \frac{t}{20\times10^{-6}} + .6 \qquad \pm \geq 30 \text{ μsec} \quad (6.5)$$

when 't' is in seconds.

The quantity .6 in the above equations is added to have numerical value 1 for the quantity within the brackets at 30 μsec. Between 30 to 30 μsec after the initiation of return stroke the values of α and β are increased to 1.5 times of its initial value and thus, rapid decay in the current occurs during 20 μsec period. However, in the subsequent 50 μsec only 1.47 times the values of α and β increases and thus, slow rate of change in current during this period. The results of this modification are shown in Fig 8.19 to Fig 8.21.

VII. Validity of Airborne Data

Measured values of electromagnetic fields and related parameters in lightning environments are vital for the testing of return stroke models and to ascertain the amount of electromagnetic coupling to the aircraft. The airborne measurements of fields have certain complexities which are comparable to the ground based measurements. Since in this thesis we are concerned mainly about the testing of the models, the problems associated with the acquired data which are used to justify the model will have to be discussed. The sources of error in the data are classified in four categories, namely,

1. Data collection
2. Direction finding
3. Range measurement
4. Channel height measurement

This classification is based on the system instrumentation and calibration used by the Flight Dynamics Laboratory for the collection of the airborne data during the years 1979 - 1981, and the data made available to the author for the comparison of the models presented in this thesis.

Data Collection Problems

The most serious problem in interpreting the airborne data is due to the conducting outer surface of the aircraft on

which the field's sensors are installed. The surface current on the aircraft caused by the incident electric field distort the electric field in the vicinity of the sensor and thus, the data recorded does not truly indicate the incident electric field. Additional uncertainties are added due to aircraft orientation with respect to the return stroke channel and the polarization of the incident E-field.

Perala et al. (1982) have provided an analytic treatment to this problem. Let $\bar{E}_i(\bar{r},t)$ and $\bar{H}_i(\bar{r},t)$ be the incident fields on the aircraft having surface area S and assume that initially the aircraft has no surface charges and surface currents. Then the incident field causes a surface current density J_s and charge σ. Due to this current and charge, the scattering fields $\bar{E}_s(\bar{r},t)$ and $\bar{H}_s(\bar{r},t)$ are then produced.

The total fields $\bar{E}_T$ and $\bar{H}_T$ in the vicinity of the aircraft are given by

$$\bar{E}_T(\bar{r},t) = \bar{E}_s(\bar{r},t) + \bar{E}_i(\bar{r},t) \tag{7.1}$$

$$\bar{H}_T(\bar{r},t) = \bar{H}_s(\bar{r}',t) + \bar{H}_i(\bar{r},t) \tag{7.2}$$

The current density J_s and σ are given by the equations

$$\bar{J}_s(\bar{r}_s,t) = \hat{n}x\bar{H}_T(\bar{r}_s,t) \tag{7.3}$$

$$\text{and } \sigma(\bar{r}_s,t) = \epsilon\hat{n}.\bar{E}_T(\bar{r}_s,t) \tag{7.4}$$

where the $\bar{r}_s$ vector is on the aircraft surface and $\hat{n}$ is the normal to the surface at that point.

It is obvious from equations (7.1) and (7.2) that the true value of the incident EM fields due to lightning are difficult to measure even using inverse-scattering techniques (Baum et al., 1982). Even with the same sensor, the fields measured at another aircraft under the similar conditons may have significant differences.

Another problem in airborne data collection is resonant effect of the aircraft. It has been observed that at certain frequencies the a/c body causes resonance in the EM fields. In fact, this is a multi-components damped sinusoidal behavior of the aircraft body which distorts the incident field and corrupts the measured data.

The EM fields, which are of interest in model testing comprise the vertical component of the $\bar{E}$ field in $\hat{a}_z$ direction and has two orthogonal components of H_ϕ, the magnetic field. The components of H_ϕ are measured with crossed magnetic loops and then used to find the angle of the lightning channel with respect to the aircraft bearing. In actual flight conditions the instantaneous banking and pitch angles of the aircraft reduces the perpendicular area of the sensing coil. The reduction in area is equal to cosine of the respective angles. Although the data were collected in level flights, angular errors can be caused due to air turbulence, etc. Crossed magnetic loops were installed along the nose-to-tail symmetry and wing-to-wing direction. A typical sensor location is

shown in Fig 5.3.

For electric field measurement, the flush plate dipole (FPD) were used. The disadvantage of this sensor is due to the attenuation caused by the added series resistance which increases the overall input impedance of the system (Baum et al., 1982). Calibration results of this sensor in the actual system were within 10% error from the theoretical value and a minimum sinusoidal signal of 50 μV amplitude could be detected. Thus, the electric field sensor could detect a minimum reading of less than 20 V/m which corresponds to a range of over 30 km. The magnetic field sensor consisted of one cylindrical moebius loop and the system response had error within 5%. The detailed theory about sensors and their performance is given by Rustan et al., 1982.

Direction Finding Problems

Crossed magnetic loops were used to find the relative bearing of the lightning channel with respect to the aircraft. It is assumed that the channel is vertical and its magnetic field is only in the $\hat{a}_\phi$ direction (in cylindrical coordinate). The voltages induced in the two magnetic field loops are proportional to $\sin\theta$ in one loop and $\cos\theta$ in the other loop. The relative bearing of the lightning channel is shown in Fig 7.1 and the two loops are supposed to be identical in shape and size. The ratio of the loop voltages gives the value $\tan\theta$ and thus, the value of θ defines the relative bearing of the channel. Since in actual measurements the magnetic field

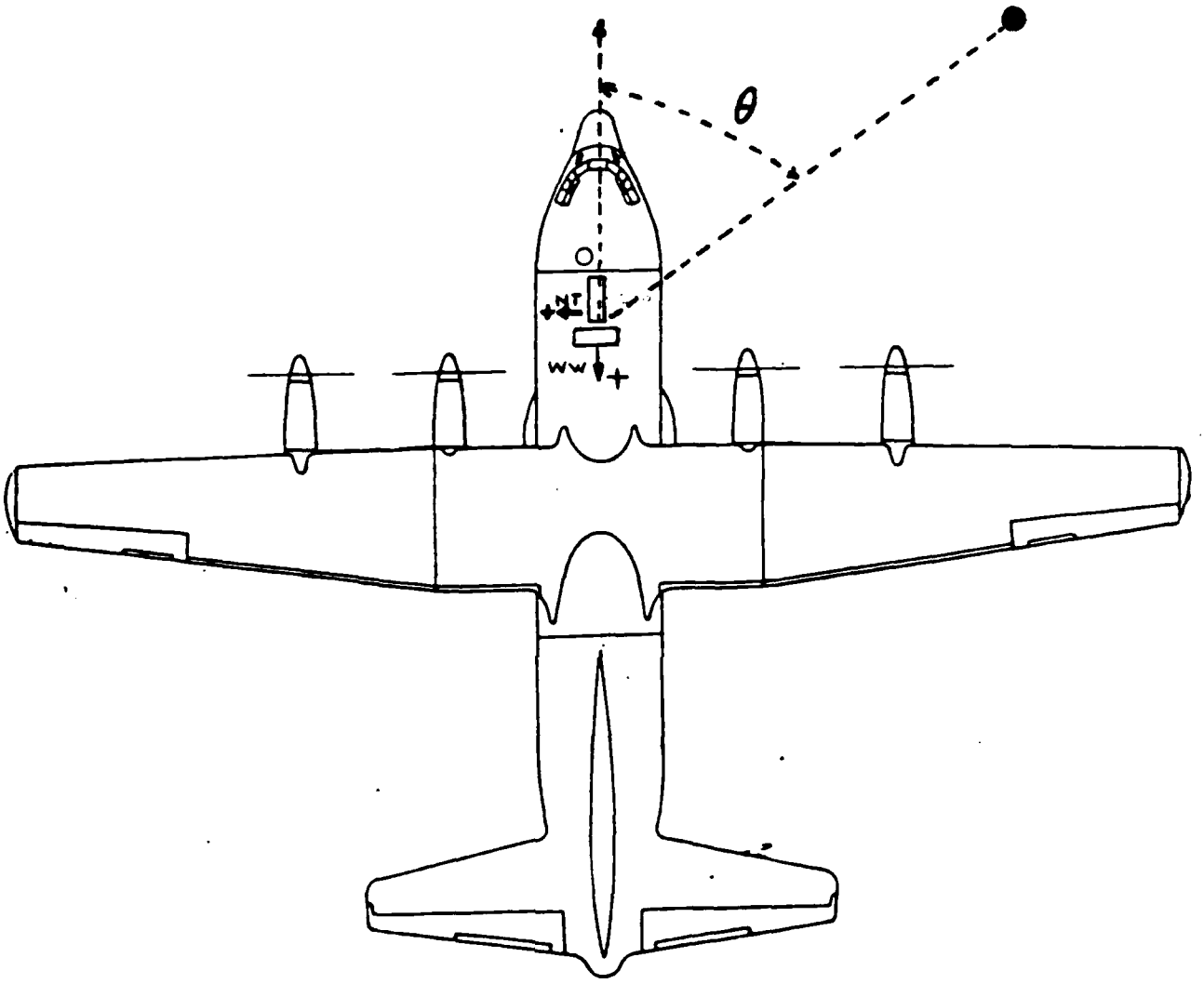

Fig 7.1 Relative Bearing of the Lightning Channel with Respect to Aircraft Axis.

components were used, the sign of the magnetic fields should determine the quadrant in which the channel was located. This scheme is shown in Fig 7.2. In this figure the wing-to-wing (ww) and nose-to-tail will indicate the perpendicular direction of the coil axis. The sign of the fields is also shown because these are not according to the usual coordinate axis.

As mentioned earlier in this chapter, the pitch and banking angles of the aircraft can cause error in direction finding. However, for most of the data collected during this experiment the aircraft was at steady flight where these types of errors are negligible.

Larger errors in direction finding are caused due to the reradiation of the incident magnetic field on the aircraft structure. Two sets of crossed magnetic loops installed on the top and bottom of the aircraft will yield different bearings. This is because the geometry of the aircraft differs in the upper and lower portions. A detailed description of this phenomena is given by Parker et al., (1982).

The third error in bearing detection is due to the nonlinear polarization of the incident field. Nonlinearity in polarization is caused due to nonhomogeneous atmospheric conditions and channel tortuosity. Bearing error due to tortuous channels near the aircraft can be large and no data are available on the amount of tortuosity in the channel. Parker et al. (1982) indicates that direction error in this case is given by

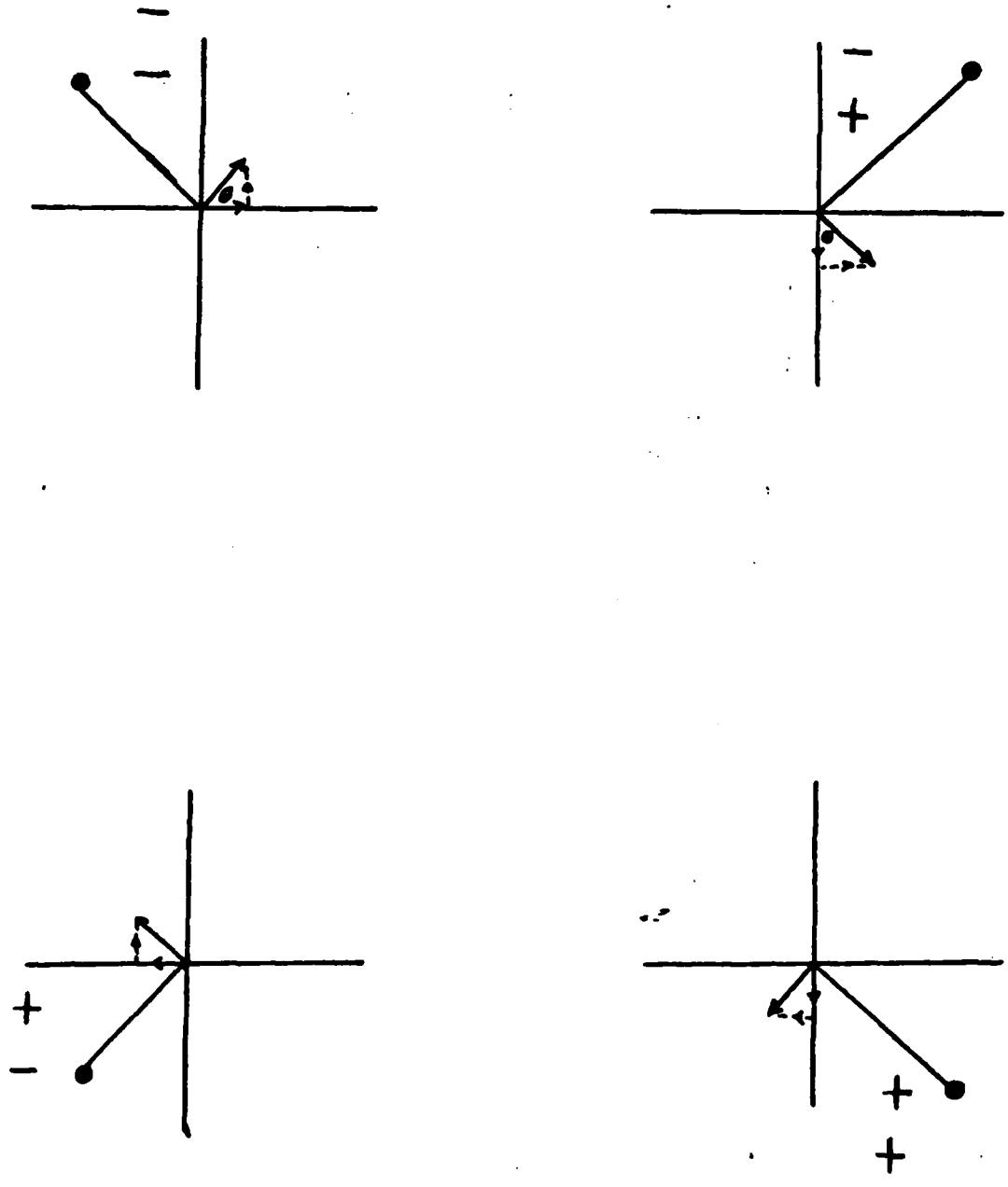

Fig 7.2 Location of Lightning Channel in a Quadrant and Corresponding of Magnetic Field Components

$$\text{Bearing error} = \tan^{-1}\left(\frac{GL_y/L_z}{1+GL_x/L_z}\right) \qquad (7.5)$$

where L_x, L_y and L_z are the components of tye lightning dipole in the x, y, and z direction and G is the geometrical factor

$$G = \frac{(Ez' + Qz)}{D} \qquad (7.6)$$

whre z' and z are the altitudes of the dipole and aircraft, respectively. D indicates the horizontal distance of the dipole from the sensors. Q is a factor dependent on geometry and the moment of the dipole.

The sky wave phonomena as discussed by Gradner (1980) also introduces bearing error but in our experiment this error is also of a negligible quantity.

The conclusion of this discussion is that even though crossed magnetic loops can be used to detect channel bearing, the results are not accurate. A rough estimate of the channel bearing, however, can be determined by this method.

Range Measurement

In this work tye electromagnetic fields predicted by a model are compared with experimental data at corresponding ranges. As calculated in Chapter V, (equations 5.19 and 5.3), the fields are highly dependent on the range from the observer to the lightning channel. Particularly in the near ranges EM fields are proportional to $\frac{1}{R3}$ and $\frac{1}{R2}$.

A small error in range detection, therefore, compounds the error in fields due to exponents in R. Consider, for example, the error in range R is δR. Then for the value of R^m we get

$$(R+\delta R)^m = R^m + mR^{m-1}\,\delta R$$

to first approximation and the error in R^m is $mR^{m-1}\,\delta R$. Thus when $m>1$ a small error δR in R is increased in R^m.

In actual data collection three methods were used to estimate the channel location with reference to the aircraft. The first method consists of finding the bearing of the channel as discussed above and then correlating this result with the isolated cloud source obtained from the aircraft radar. A typical radar picture of the clouds is shown in Fig 7.4. This method of estimating the range is not accurate and errors of 100% are possible for large cloud cells. The minimum diameter of the clouds in the airborne data is about 4 km.

The range calculated by this method was further compared with a stormscope display. The stormscope provides dots in a cathode-ray-tube screen display whenever a large discontinuity occurs in the field. From the crossed loops it calculates the azimuth to the flash and the range is determined by using the fact that the magnetic field is inversely proportional with distance. Under this assumption, $H = \frac{k}{r}$ where k is proportional to time derivative of channel current and considered to be constant. However, as has been discussed in the channel models, the currents are

highly variable. Thus, the range predicted by the stormscope technique may not be very accurate (Parker et al., 1982). From this description it is clear that the supporting information for range detection is not entirely accurate and that its correlation with the range from the first method does not reduce the error.

The third method, which could have provided a realistic range of the channel, consisted of the ground VHF network but this data have not been processed at this time. Thunder data was also recorded at the ground station by using a thunder microphone. However for most of the data, the lightning flash was located more than 20 km from the central ground station and thunder could not be heard.

Since all the three methods discussed here failed to provide a correct range for the channel, we considered the possibility of using J.A. Tiller's (1975) statistical data to estimate the ranges. Tiller has suggested that channel range can be estimated from the electric field measurements at the ground level. For close ranges his data is shown in Fig 7.3. However, when we checked his data it was found that the statistical averages were highly erratic. Table 7.1 compares the suggested fields and ranges calculated by Tiller (1975) with the author's estimates. Since these results were not consistent, this technique of estimating the range was abandoned. The ranges given for the experimental data represent the best engineering approximation possible based on

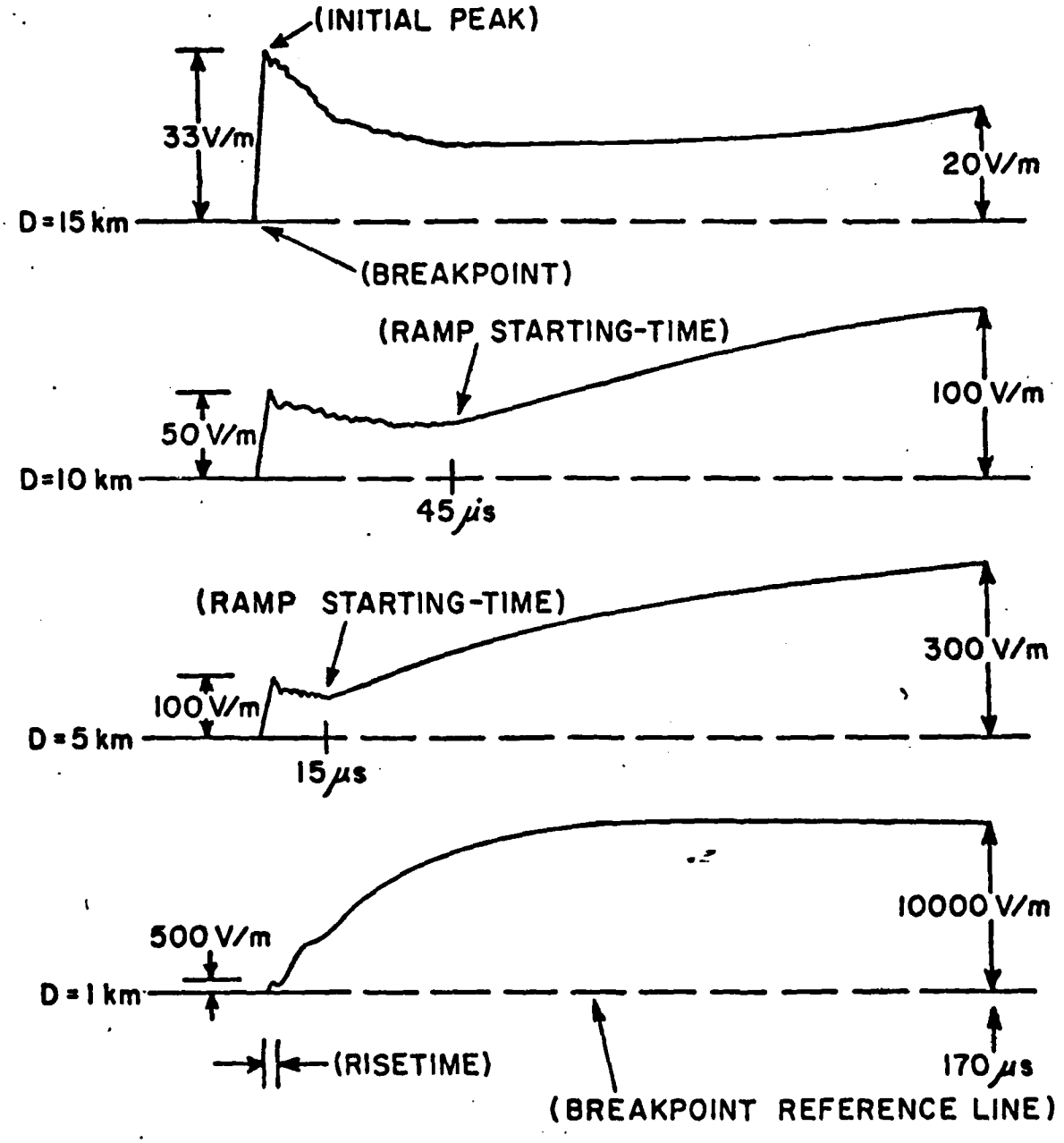

Fig 7.3 Range Approximation from Peak Electric Field Value (J.A. Tiller, 1975).

Table 7.1

ERROR IN J.A. TILLER (1975) DATA

D km	Tiller (1975) Estimated Peak E Field V/m	Author's Estimated Peak E Field V/m	Standard Deviation in Peak Field Due to Tiller Data
1	500	838	889
5	100	136.5	120.3
10	50	97	67
15	33	44.6	19

the airborne radar and the stormscope data.

Channel Height Problem

As is evident from equations (5.19) and (5.37), the field at any point depends upon the channel height H. Since no information was recorded about the channel height it is assumed that the channel height was about 5 km. This is the number used in the euqations to compare the measured data and the predicted data.

VIII. Comparison of Models

The linear and nonlinear mathematical lightning return stroke models presented in this thesis differ from each other in many aspects. Also, the predicted results from these models are nonidentical. To analyse models, we first consider the differences in their modeling procedure and then we will compare the results obtained from them. It is obvious from the description of the models that each model has a distinct level of sophistication which emerges from the approach taken to describe the lightning channel and the predicted EM fields. However, the models presented in this thesis are divided into three categories on the basis of the methods to describe the channel current.

The most simple and adequate approach in the modeling of the lightning process is to assume a temporal and spatial form of the channel current. The current wave form and its behavior in the assumed geometry of the channel is derived from the statistical data obtained from the natural lightning. Since it is difficult to measure the current parameters in space, therefore, most of the data is collected at the ground level and

from remote electromagnetic field measurements. The accuracy of the collected data depends on the technique and type of the equipment in use. Models presented by Bruce & Golde (1941), Dennis and Pierce (1964) and Lin et al. (1980) were evolved by following this technique. Lin et al. model (1980) has recently been improved by Master et al. (1981) and the newest model is assumed to provide more realistic fields above the ground level. The model proposed by Gardner (1980) is also of this type but differs in the approach to calculate EM fields. The channel geometry in the Gardner (1980) model is of generalized form and thus allows flexibility in calculating fields due to tortuous channels.

The second approach in the modeling of lightning channel is to consider the return stroke channel as an ordinary discharging RLC transmission line. The lumped elements, RLC, forming multilooped transmission line as shown in Fig 4.2 vary with height and time and as a result of this, the channel current becomes a function of height and time. The accuracy of this type of model depends on the number of segments describing the transmission line. Uman (1969) and Little (1978) have used this approach to model return strokes. However, Little (1978) has used constant RLC parameters in an unbranched lightning channel with the assumption that current pulse shape is identical at all points along the channel. Due to the last assumption, no corona charge can be removed

from the return stroke channel during the return stroke propagation time, charge being only transferred from the top to the bottom of the channel (Lin et al., 1980). Parameters of lightning current pulses deduced from this type of model are in rough agreement with the ground observation.

The third and the most sophisticated approach in return stroke modeling follows the theory of the development of an arc channel. Braginskii (1958) has described the physic of an arc channel. The arc channel model is explained on the basis of equations of conservation of mass, momentum and energy. Since the channel current and channel arc parameters interact with each other at all points along the channel, therefore, a detailed knowledge of parameters, such as ionization and recombination coefficients, electrical and thermal conductives in the channel, is necessary to describe the model. Strawe et al. (1980) has developed this type of lightning return stroke. The channel current is a function of environmental conditions and hence, it varies with time and height.

Comparison of Current Waveform

Channel current waveform in any return stroke model is of vital importance because the EM fields predicted by the models are strongly dependent on it. The

most important parameters in a current waveform are the risetime, falltime and the peak value of the current. As the physical conditions in a first return stroke and a subsequent return stroke are markedly different, therefore, the parameters which characterize the current waveform also differ in both kinds of return strokes. Fig 2.5 illustrates such differences as observed by different researchers. One of the earliest and most widely used empirical approximations to the return stroke current waveform at ground is due to Bruce and Golde (1941). The waveform is graphically shown in Fig 3.1, whereas, equation 3.3 represents it in mathematical form. The round peaked current waveform has average time to crest and to half value of about 5.6 μsec and 24 microseconds, respectively. The peak value of the current is 21 kA. In Bruce & Golde (1941) model, the current parameters in first and subsequent strokes are considered to be identical and this assumption is wrong because subsequent stroke current has a short risetime as illustrated in Fig 2.5. Due to equation 6.2, Lin (1978) has found that the return stroke velocity in the Bruce & Golde (1941) model is distant dependent and thus, the peak current in Bruce & Golde model (1941) increases sharply as the distance increases.

Another disadvantage in Bruce & Golde model is the infinite speed of information transformation. Apart from correcting this drawback in the Bruce & Golde model

(1941), Dennis & Pierce (1964) slightly modified the current waveform suggested in this model. Instead of having double exponent waveform, Dennis & Pierce (1964) suggested a triple exponent current waveform as in equation 2.3. The risetime, falltime to 50% of peak value and current peak value in the first stroke due to this waveform are 12.8 μsec, 52.9 μsec and 21 kA, respectively. But for the subsequent stroke, these values are 1.0 μsec, 50.1 μsec and 9.8 kA, respectively. The peak current values agree with the experimental data, whereas, the risetime in the waveform is excessive. It may be noted that the waveform suggested either by Bruce and Golde (1941) or Dennis & Pierce (1964) have poor representation of the initial rise-to-leak current when compared with the experimental data.

The current waveforms derived from the transmission line model of Little (1978) are shown in Fig 4.6a,b,&c. The current waveform near ground is sharply peaked and has a very short half value time. At the ground level, the current risetime varies from 1.3 μsec to 3.5 μsec without any significant frontal risetime and thus, exceeds the values found by Wiedman and Krider (1978). Due to the recent studies of Weidman and Krider (1978,1980), the sharp risetime in first and subsequent return strokes is identical and of the order of 90 ns. Also, the peak value of the current predicted by this model exceeds 50 kA and sometimes it is more than 90 kA; whereas, the measured

value of the peak current is of the order of 10 kA (Lin et al. (1980). In view of these current parameters, the predicted current waveform of the Little model (1978) is much different from the measured waveform.

Due to the discrepancies found in the current waveform suggested in the above mentioned models, Lin et al. (1980) suggested a new current waveform, which is compatable with the experimental data. As mentioned in Chapter III, the Line et al. model (1980) has suggested three components in the current waveform. In the Lin et al. (1980) improved model (Master et al. 1981), the breakdown pulse current in the first stroke increases from 0 to 15 kA in 5 μsec and then it rises abruptly to 30 kA in 1 μsec. The falltime to 50% value is approximately at 6.9 μsec. Thus, the sharp risetime of breakdown pulse is 100 ns. The corona current waveform is similar to Bruce & Golde (1941) waveform but, of course, with the changed value of α and β. Since breakdown pulse is responsible for the peak value and risetime, thus, it has removed the discrepancies in the current forms suggested in the earlier models. In Master et al. (1981) model, the value of peak current for the subsequent stroke is 17.9 kA. This includes the uniform current value, which is 3 kA. In the subseqeunt stroke, the breakdown pulse current increases from 0 to 3 kA in 1.0 μsec and then to a peak value of 14.9 kA at 1.1 μsec. It is apparent that

the fast risetimes in the first and subsequent return strokes are identical. This is exactly in accordance with the findings of Wiedman and Krider (1978,1980). However, the discrepancy in Lin et al. (1980) current waveform is an impulse like initial current peak. Such current peaks are not observed in actual waveforms. The direct measurements of current as shown in Fig 2.5 indicate a smooth curved wave shape near the peak values.

The curent waveform predicted by Strawe et al. model (1980) is shown in Fig 8.2. In case of first return stroke current waveform, there is a slow rising front of about 5 μsec duration and then the current reaches to its peak value of 24 kA.in a very short time (approximately 0.4 μsec). However, in the case of a subsequent stroke, there is no slow rising front and the current reaches to its peak value of 22.8 kA in about 1.6 μsec. The falltime to 50% of peak value is, however, very large in this case and this is contrary to the value found from experimental data. Except for the falltime in these predicted current waveforms, the parameters of risetime and current peak values are in good agreement with the experimental data.

The nonlinear model presented by Gardner (1980) does not specifically depend on a current waveform. However in the computation of the EM field, the current waveform of Dennis & Pierce (1964) given by equation 2.3 is used. Since this waveform has a slow risetime and does

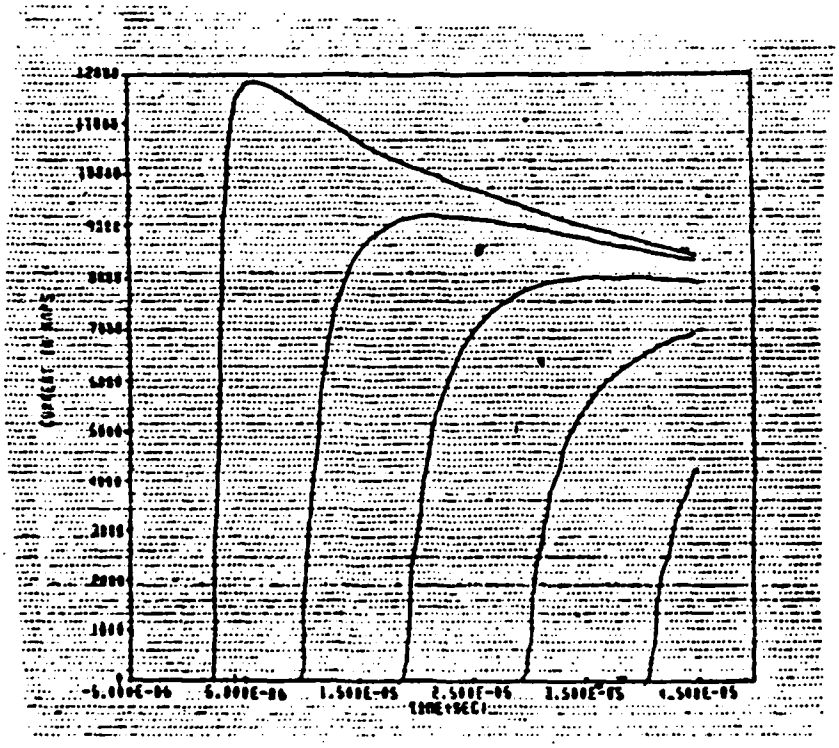

Fig 8.1 Current Waveforms in a Subsequent Stroke With Straight Verticle Channel. Waveforms are at 100, 600, 1000, 1400, 1800 Meters (Strawe et al., 1980)

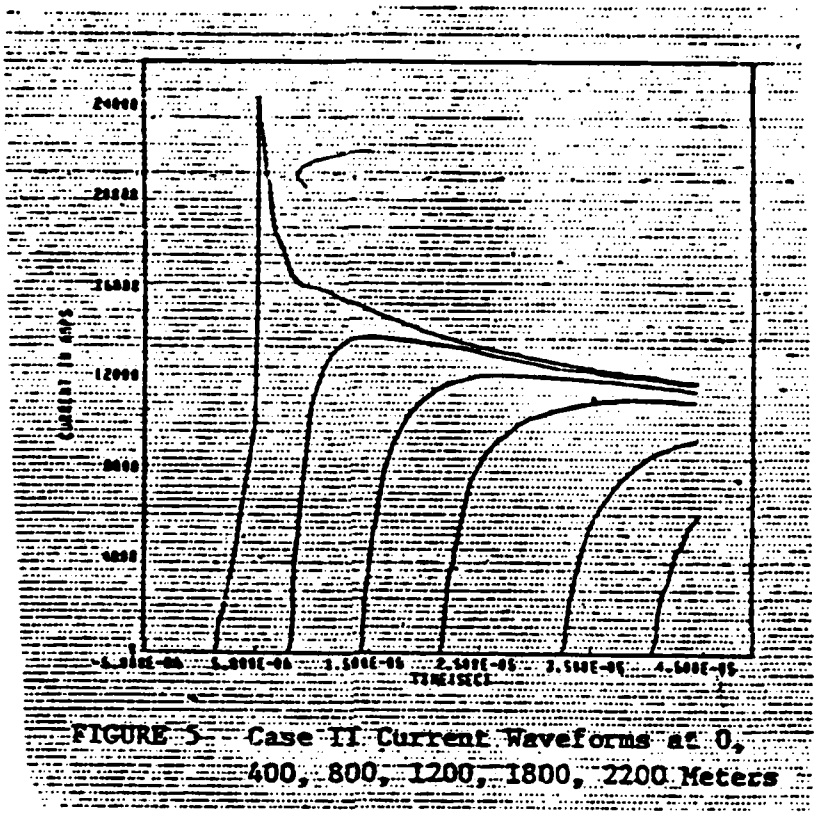

FIGURE 5 - Case II Current Waveforms at 0, 400, 800, 1200, 1800, 2200 Meters

Fig 8.2 Current Waveform in a First Stroke with Straight Verticle Channel. Waveforms are at 0, 400, 1200, 1800 and 2200 Meters (Strawe et al., 1980)

not account for the fast transition, therefore, the results dervied by Gardner (1980) on the basis of this inappropriate current waveform are inaccurate. The flexibility in the selection of current waveform in Gardner's model promises for the better results. Gardner's model, in fact, is more concerned about the finite conductivity of the earth's surface and the reflection of the radiation field from the ionosphere than the current waveform.

Table 8-1 shows a comparison of currents waveform parameters for the models presented in this thesis.

The behavior of the current pulse during its upwards propagation in the channel is also a point of interest in the return stroke modeling. Except for the models presented by Lin et al. (1980) and Master et al (1981), the velocity of porpagation of the current pulse decreases with height. The latest studies show that for the first-stroke the mean velocity within about 1 km near ground is 9.6×10^7 m/s, and the subsequent mean stroke velocity is 1.2×10^8 m/s (Uman et al., 1982). Since the mirror image effect as mentioned in Chapter VII is rarely observed in the first stroke and almost never in the subsequent stroke,therefore, it is believed that current peak amplitudes decreases with height. The current waveforms predicted by Strawe et al. (1980) model and shown in Fig 8.1 and 8.2 clearly substantiates this effect. In this model, the peak value of the current at ground due to a

first and subsequent stroke reduce to almost 33% value at the height of 1800 meters. However, the attenuation factor for current waveform in the Master et al. model (1981) is a function of height and its value differs for the first and the subsequent stroke. In Bruce and Golde model (1941), the current is uniform at any instant and thus the peak value of the current at any altitude is the same as is obvious from Fig 3.1. This discrepancy in the current waveform also exists in the model of Dennis & Pierce (1964). From Fig 8.1 it can be observed that peak value of current in Little model (1978) attenuates with the increasing channel height. In three kilometers trip of the return stroke, the peak value has reduced to 30% of the initial peak at ground level. This comparison shows that Bruce & Golde model (1941) and Dennis & Pierce model (1964) are of a primitive nature and lack in the basic definition of the current waveform. The current waveforms predicted by nonlinear models of Little (1978) and Strawe et al. (1980) are almost similar in shape but differ in magnitudes. The falltime to 50% peak value is better in Little's model (1978) than that of the Strawe's model (1980). However, the uniform current postulated in Lin et al. model (1980) is assumed to be flowing due to the leader current or it may start soon after the return stroke initiation. There is no evidence given in the Lin et al. model that shows it is different from the corona current.

Since Gardner (1980) has used the same current waveform as suggested by Dennis & Pierce (1964), therefore, it is needless to say that his model has made any significant contribution to improve the return stroke model.

Comparison of Predicted EM Fields

As the computer solution to the models, except for Master et al model (1981), were not available during this study, therefore, such models are compared theoretically for their predicted EM fields. The particular characteristics of these models has, however, already been discussed during the presentation of these models. The primary object of this section is, therefore, to determine the degree of correctness in their predicted fields.

Although Bruce & Golde model (1941) was modified by Dennis and Pierce (1964) to avoid the requirement of instantaneous transfer of charge, the fields predicted by these models are alike. This is because the basic structure of both the models is the same. Lin (1978) has tested Bruce & Golde model (1941) and according to his findings, the predicted fields at ground level for the distances less than 5 km matched the experimental data. However, for distances greater that 5 km there is a considerable mismatch in the predicted and experimental data. Since the Bruce & Golde

model (1941) and, for that matter, the Dennis & Pierce model (1964) has slow risetime in the current pulse, radiation term does not predominate in the first 20 μsec. Thus, inductive and electrostatic field components become stronger. Due to these reasons, the Bruce & Golde (1941) and Dennis & Pierce (1964) models perform well for short ranges but fail to perform well for distant observation points where radiated field is dominant. From the data of Table 8.1, it is evident that risetime for first return stroke in Dennis & Pierce model (1964) is larger than that of Bruce and Golde model (1964). Thus, for unbranched first return stroke, the performance of Bruce & Golde model (1964) is comparatively better than that of Dennis & Pierce model (1964).

Little's model (1978) has comparatively sharp risetime in the current pulse. Therefore, on the basis of above arguments, its performance is better for long distances and predicted data will not match the experimental data for short distances. Also, as seen in Fig 8.1, the decay time of the current pulse increases with the height and thus, magnetic field does not decay for a considerable time. This is probably true because ten samples of experimental data shown in Fig 8.3 to 8.12 indicate considerable amount of magnetic field up to 200 μsec.

In the model presented by Gardner (1980), the current waveform is due to Dennis & Pierce (1964) and hence, even if the earth is considered as perfect conductor and no ionosphere reflections occur, the fields predicted are those for the Dennis & Pierce model. Since the ionosphere reflection does not affect the data for lower ranges, therefore, Gardner's model is expected to work satisfactorily for low ranges. The effect of ionospheric reflection is dominant for frequencies more than 10 KHz. High frequency components in radiated field gets attenuated for distances greater than the channel height and thus, overall field value drops. This conclusion is in harmony with the experimental data.

In Strawe's model the current pulse has a very short risetime as compared to other models and the radiated field is much more dominant as compared to any other model but the results produced by this model are not realistic (Uman et al., 1982).

The Masters' model (1981) computer program, which was made available to the author, was used to compute the electric and magnetic fields at the corresponding altitude and distances where experimental data were collected by the Air Force Flight Dynamics Laboratory. This data are presented in Figs 8.3 to 8.10. In the empirical data the vertical component of electric field (E_v) was recorded through two sensors. These

sensors were located at aft upper fuselage (AUF) and aft lower fuselage (ALF) of the aircraft. For the near ranges, that is, from 27 km to 11 km distances, the data is only available due to ALF sensor. The author was told that there is a ratio of 2.6 in ALF and AUF sensors data but in the available data no such relation exists. Due to this reason, only ALF sensor data are used for the analysis. In this data, electric field units are in volts/meter. Magnetic field data were recorded due to two orthogonal sensors as discussed in Chapter VII. However, the peak magnetic field is the square root of the sum of the squares of fields sensed by individual sensors. Risetime for magnetic field is calculated from the best available plot. The magnetic field is plotted in ampere/meters.

The predicted fields due to Master et al. model (1981) are shown in Fig 8.13 to 8.15. In these figures, the left side column is for the ranges 2.7 km, 7 km and 11 km where lowest range is on the top. The right side column corresponds to 4 km, 10.2 km and 30 km ranges with the lowest range on the top. The bottom plot is for 35 km range. This scheme of data presentation is common in Figs 8.13 to 8.21. The Figs 8.16 to 8.18 are computer plots for the Master et al. model with velocity variation as suggested in equation 6.3. Figus 8.19 to 8.21 are the results when current waveform in the Masters' model is modified. In predicted

data the electric field is in volt/meter, whereas, the magnetic field is shown in amperes/meter.

The comparison of empirical data and predicted data is based on three factors, which are, risetime, initial peak value of fields and the time at which the electric and magnetic fields cross the base line. Most of this study is restricted to first return stroke data because the empirical data for subsequent return strokes were not available.

The risetime in the data is considered for the portion where fast transition occurs. For the Master et al. model (1981), this transition time is fixed and equal to 0.1 μsec. In the empirical data as shown in Table 8.2, the fast transition period is slightly more than 1 μsec for the ranges less than 30 km. However, for the ranges of 30 and 35 km, the fast transition period is four times that predicted by Master et al. model. As the author's of Master et al. model (1981) claim that the model works up to 10 km ranges, the risetime in predicted data and in the empirical data are in excellent agreement. The excess value of risetime in empirical data can be attributed to measurement error. As the risetime in Master et al. model (1981) was not modified, therefore, the above result holds good for the modified models.

In empirical results electric field (E_v) never crosses the base line. Rather, it stays much above the initial value. However, the electric field predicted by Master et al. model crosses the base line for the ranges less than 7 km and greater than 11 km. Thus, the performance of this model is restricted to limited ranges in respect of base line crossing. In fact, as can be seen from equation 5.36, electric field can cross the base line when $\frac{di}{dt}$ changes its sign from +ve to -ve and electrostatic and induced fields are less dominant. Therefore, it seems that radiation field becomes more dominant in the low ranges as compared to the experimental data. Particularly this phenomena cocurs due to the fast decaying of the corona pulse. In Fig 8.13, the field due to corona current has crossed the base line for the range of 11 km, whereas, in Fig 8.16 it is seen that due to velocity variation, this tendancy of crossing the base line is reduced and the peak value of the field has increased. This fact of crossing the base line due to corona current was further amplified when the corona current shape in the Master et al. model (1981) was modified. The results of modified current waveform are shown in Fig 8.19 to 8.21. With the fast decaying corona current as shown in Fig 8.22. Although with this modification the tendancy of crossing the base line has increased but

the peak value of the electric field has increased and it is better than the value of electric field predicted by Master et al. model (1981). The data due to modified velocity and current waveform are shown in Tables 8.4 and 8.5. It can be inferred from these results that simultaneous implementation of these modifications will improve the peak field value and base line cross over problem. A comparison of data in Tables 8.2 and 8.3 indicates that the peak value of predicted fields by the Master et al. (1981) model is much less than the experimental data. Also, the value of $|\frac{dE}{dt}|$ is almost ten times less than that for the empirical data in the near ranges. However, as the range increases, the difference in the peak values of predicted and experimental decreases. Also, the time derivative of the electric field becomes almost identical to that of the empirical data.

Another difference in the data of Table 8.2 and 8.3 is that peak value of $|E_{max}|$ in Table 8.3 increases from 2.7 km range to 7 km range, and then it starts decreasing. This behavior of $|E_{max}|$ is contrary to the results from Table 8.2. It is not understood clearly why this phonomena occurs in Master et al. model (1981). Most probably this is because of the image current and channel height. Since after 5 km the distances from the channel image start becoming comparable with the direct distances from the channel and, therefore, E-field starts reducing with the distance.

TABLE 8.1
COMPARISON OF CURRENT WAVEFORM PARAMETERS
IN VARIOUS MODELS

Model Presented by	First Return Stroke			Subsequent Return Stroke		
	t_r μsec	t_f μsec	i_p kA	t_r μsec	t_f μsec	i_p kA
Bruce & Golde (1941)	5.6	24	21	-	-	-
Dennis & Pierce (1964)	12.8	52.9	21	1.0	50.1	9.8
Master et al. (1981)	5.1	6.9	35	1.1	3.8	17.9
Little (1978)	1.3-3.5	40.0	50-90	1	-	-
Gardner (1980)	Same as for Dennis & Pierce (1964)					
Strawe et al. (1980)	1.6	>100	24	5.4	>100	11.8

t_r = risetime

t_f = fall time to 50% of peak value

i_p = peak value of the channel current

TABLE 8.2

EMPIRICAL DATA

Reference No.	Return Stroke Type	D km	Z km	t_{re} sec	t_{rb} sec	$\lvert E_{max} \rvert$ V/m	$\lvert B_{max} \rvert$ A/m	$\lvert \frac{dE}{dt} \rvert$ B/m-sec	$\lvert \frac{dB}{dt} \rvert$ A/m-sec
238D 4.5	First	2.7	5.1	0.51	0.399	1003.85	.906	1.27×10^{9}	2.79×10^{5}
238D 4.73	First	4.0	5.1	0.122	.1632	2799	.233	1.71×10^{11}	1.143×10^{3}
238D 4.144	Subseq	7.0	5.1	0.1442	.2346	6.384×10^{3}	.293	$.383 \times 10^{8}$	7.69×10^{5}
238D 4.101	First	10.2	5.1	0.139	.275	1024	.229	4.4×10^{9}	4.4×10^{5}
238D 4.8	First	11.0	5.1	0.123	.253	189-42AUF 620.0ALF	.30	3.414×10^{9}	1.48×10^{5}
237B 4.13	First	30.0	4.0	.448	.448	15.0AUF 54.0 ALF	.086	0.1×10^{9}	1.48×10^{5}
237B 4.16	First	30.0	4.0	.408	.448	18.8AUF 77.5ALF	.13	0.13×10^{9}	1.56×10^{5}
237B 4.23	First	30.0	4.0	.287	.369	17.6AUF 73.6AUF	.135	$.178 \times 10^{9}$	2.11×10^{5}
237B 4.14	First	35.0	4.0	.289	.41	8.2AUF 57.57ALF	.052	$.07 \times 10^{9}$	$.075 \times 10^{5}$
237B 4.20	First	35.0	4.0	.41	.41	9.5AUF 40.65 ALF	.065	$.078 \times 10^{9}$	1.5×10^{5}

TABLE 8.3

DATA FROM THE FIRST RETURN STROKE

(Master et al. Model, 1981)

D km	E km	t_{re}&t_{rb} μsec	$\lvert E_{max} \rvert$ V/m	$\lvert B_{max} \rvert$ A/m	$\frac{dE}{dt}$ V/m-sec	$\lvert \frac{dB}{dt} \rvert$ A/m-sec
2.7	5.1	0.1	13.7	.142	1.17×10^8	0.69×10^5
4.0	5.1	0.1	31.74	.16	1.8×10^8	0.97×10^5
7.0	5.1	0.1	45.2	.15	2.39×10^8	0.68×10^5
10.2	5.1	0.1	42.0	.12	2.15×10^8	0.55×10^5
11.0	5.1	0.1	40.12	.073	2.1×10^8	0.244×10^5
30.0	4.0	0.1	17.24	.0447	0.81×10^8	0.225×10^5
35.0	4.0	0.1	14.3	.0397	0.74×10^8	0.202×10^5

Symbols are same as in Table 8.2

TABLE 8-4

DATA FOR FIRST RETURN STROKE WITH

MODIFIED PROPAGATION VELOCITY

D km	Z km	t_{re}&t_{rb} μsec	$\lvert E_{max} \rvert$ V/M	$\lvert B_{max} \rvert$ A/M	$\lvert \frac{dE}{dt} \rvert$ V/M-sec	$\lvert \frac{db}{dt} \rvert$ A/m-sec
2,7	5.1	0.1	25	0.216	2.5×10^8	10.4×10^5
4.0	5.1	0.1	44.4	0.23	2.5×10^8	12.2×10^5
7.0	5.1	0.1	63.5	0.216	3.3×10^8	11.8×10^5
10.2	5.1	0.1	50.8	0.176	2.3×10^8	9.5×10^5
11.0	5.1	0.1	56.3	0.167	3.1×10^8	9.07×10^5
30.0	4.0	0.1	24.56	0.064	1.31×10^8	3.33×10^5
35.0	4.0	0.1	21.05	0.056	1.14×10^8	3.08×10^5

Symbols are the same as in Table 8-2

TABLE 8-5

DATA FOR FIRST RETURN STROKE WITH
MODIFIED CURRENT PULSE WAVEFORM

D km	Z km	t_{re}&t_{rb} μsec	$\lvert E_{max} \rvert$ V/m	$\lvert B_{max} \rvert$ A/m	$\lvert \frac{dE}{dt} \rvert$ V/m-sec	$\lvert \frac{dB}{dt} \rvert$ A/m-sec
2.7	5.1	0.1	41.22	.35	3.42×10^8	18.15×10^5
4.0	5.1	0.1	69.84	.38	3.49×10^8	21.5×10^5
7.0	5.1	0.1	88.88	.307	4.76×10^8	16.75×10^5
10.2	5.1	0.1	86.792	.237	4.9×10^8	13.26×10^5
11.0	5.1	0.1	78.07	.244	4.2×10^8	12.24×10^5
30.0	4.0	0.1	33.04	.086	1.7×10^8	3.91×10^5
35.0	4.0	0.1	28.94	.073	1.6×10^8	1.03×10^5

Symbols have the same meaning as in Table 8-2

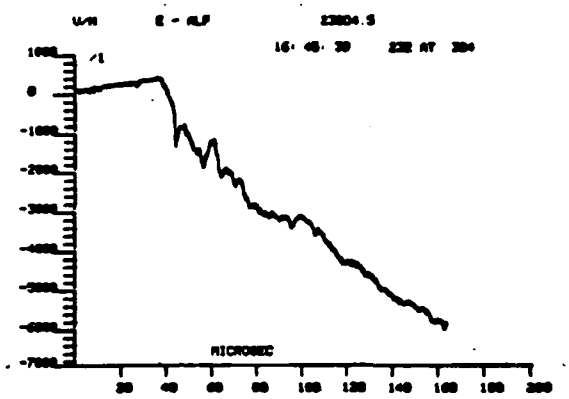

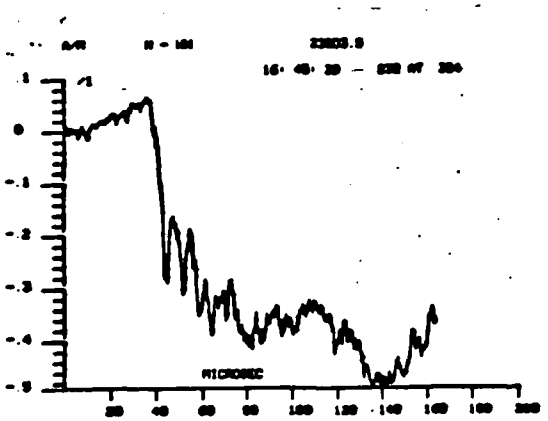

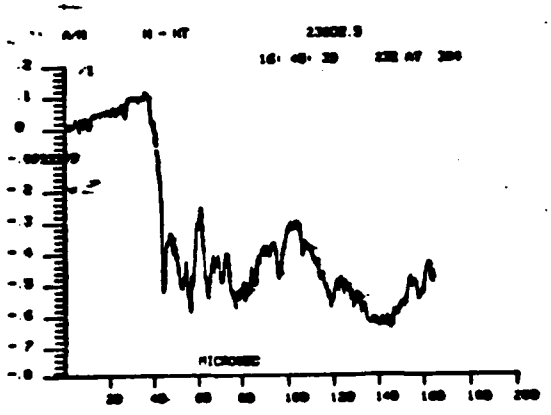

Fig 8.3 Electric and Magnetic Fields for a First Stroke At a Distance of 2.7 km and Altitude 5.1 km.

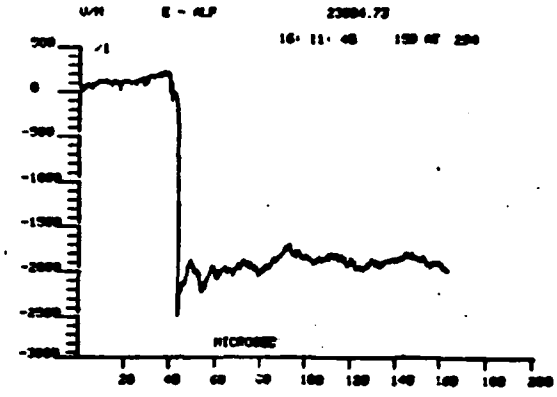

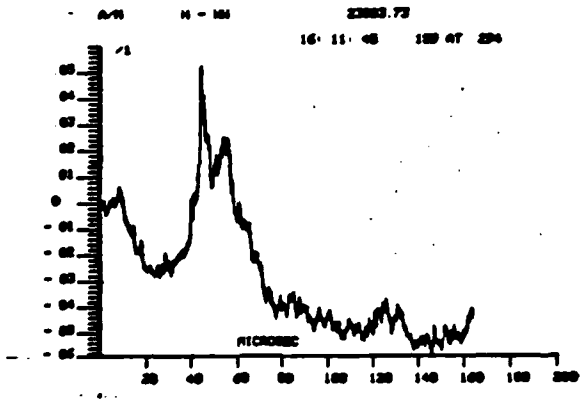

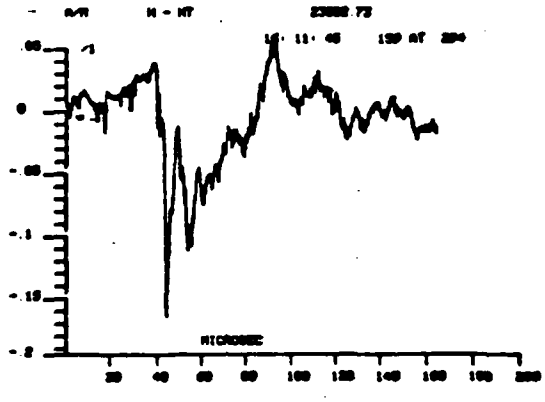

Fig 8.4 Electric and Magnetic Fields for the First Stroke at a Distance of 4 km and Altitude 5.1 km

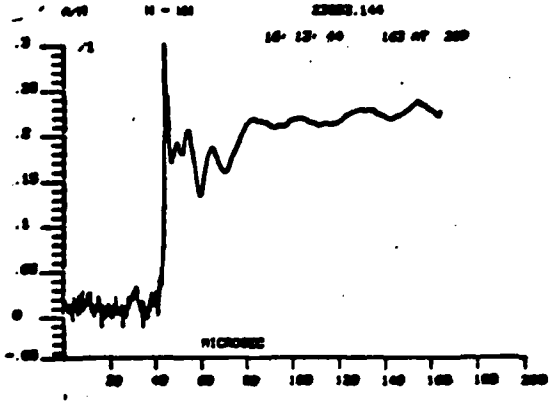

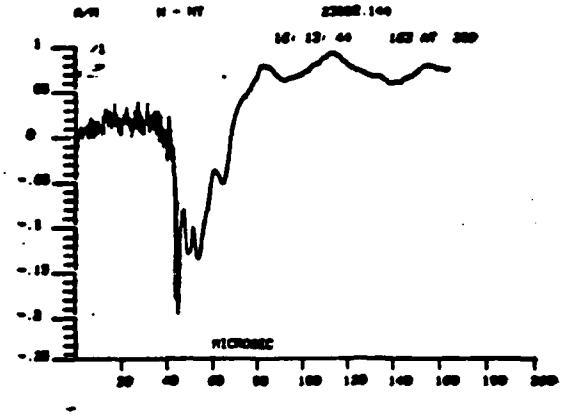

Fig 8.5 Electric and Magnetic Fields for a Subsequent Stroke at a Distance of 7 km and Altitude 5.1 km

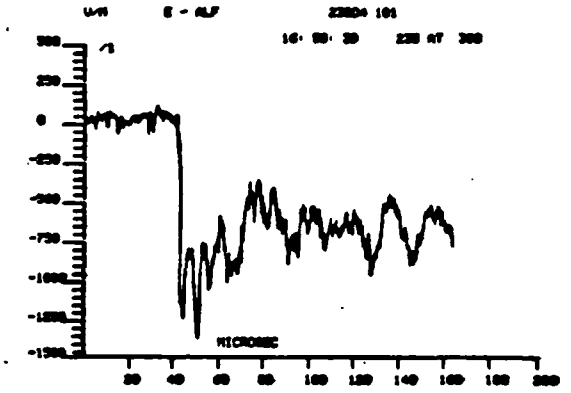

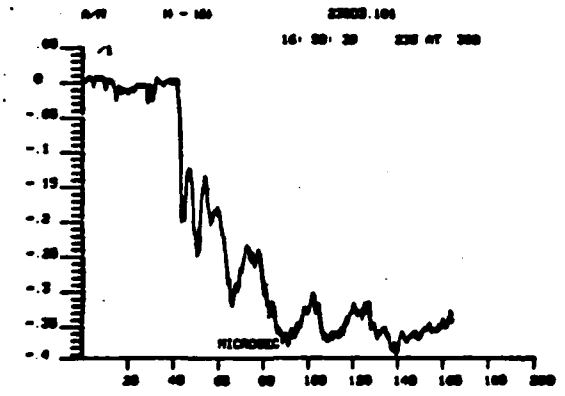

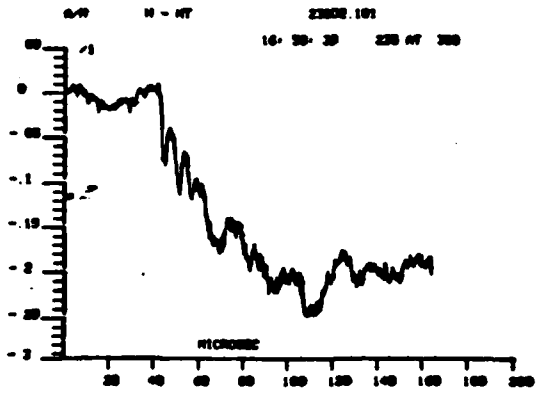

Fig 8.6 Electric and Magnetic Fields for the First Return Stroke at a Distance of 10.2 km and Altitude 5.1 km

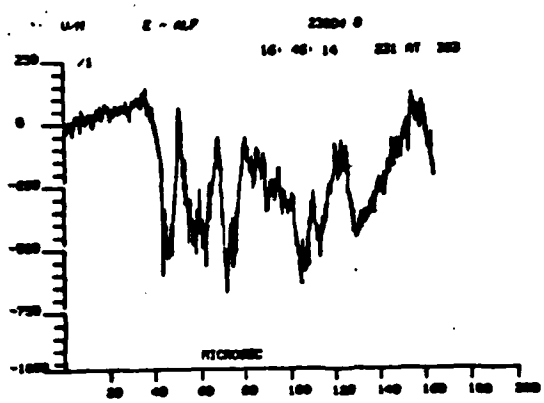

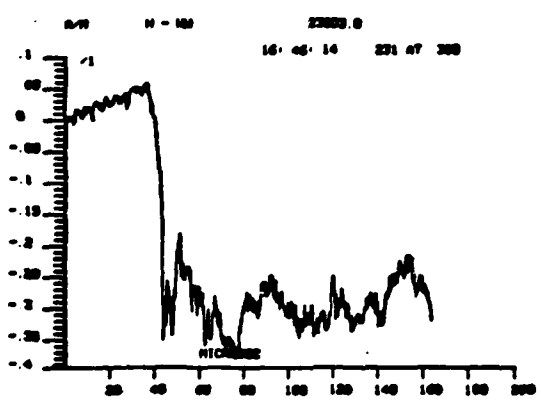

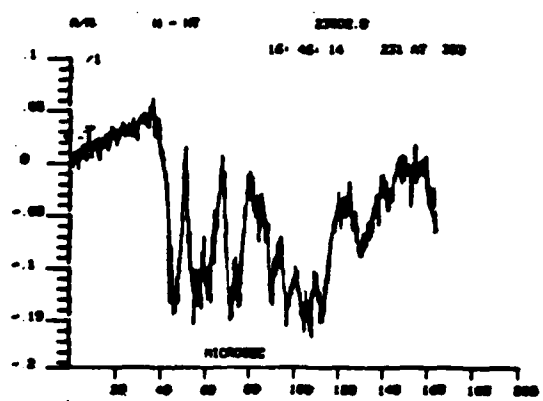

Fig 8.7 Electric and Magnetic fields for a First Stroke at a Distance of 11 km and Altitude 5.1 km

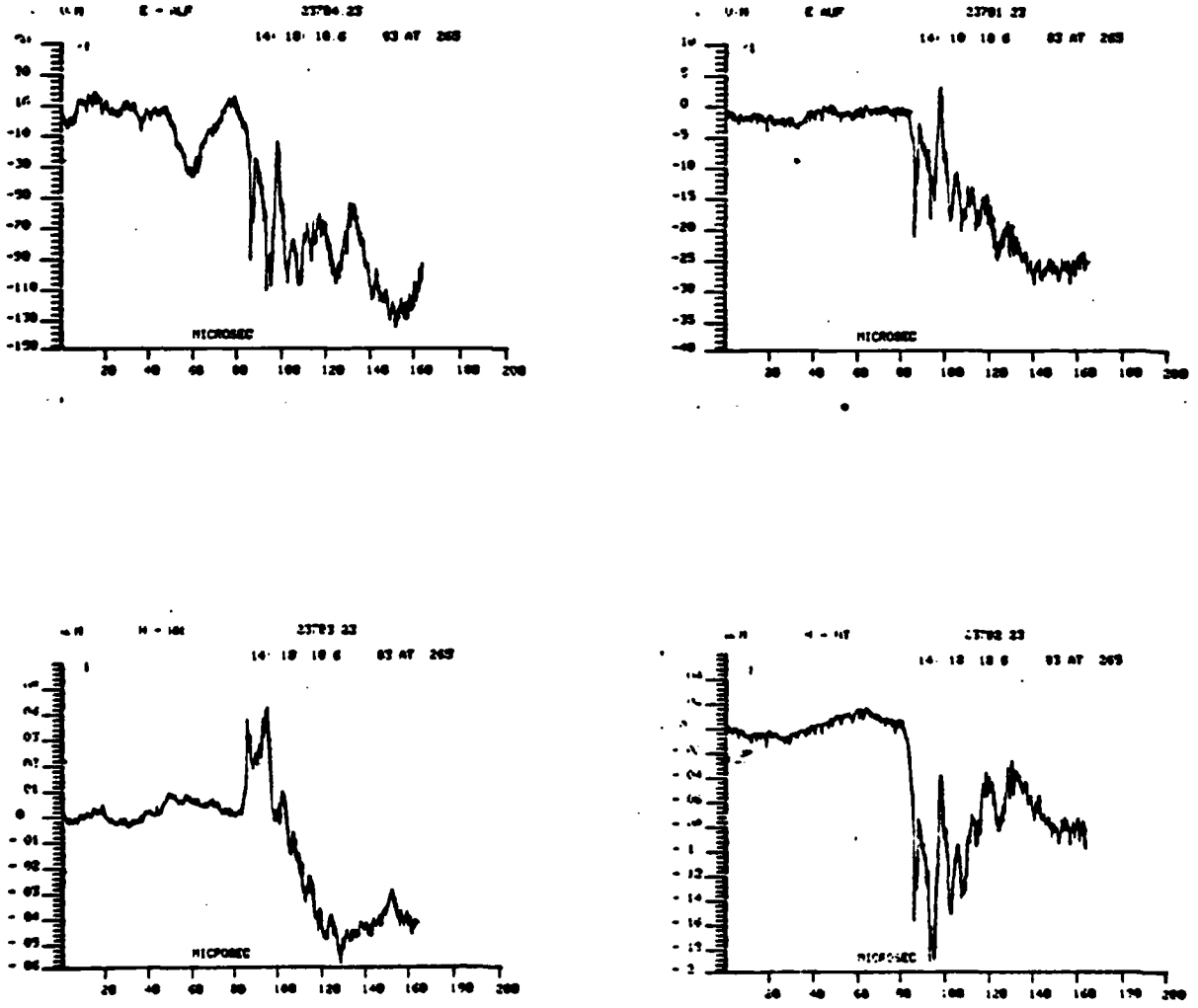

Fig 8.8 Electric and Magnetic Fields for a First Stroke at a Distance of 30 km and Altitude 4 km.

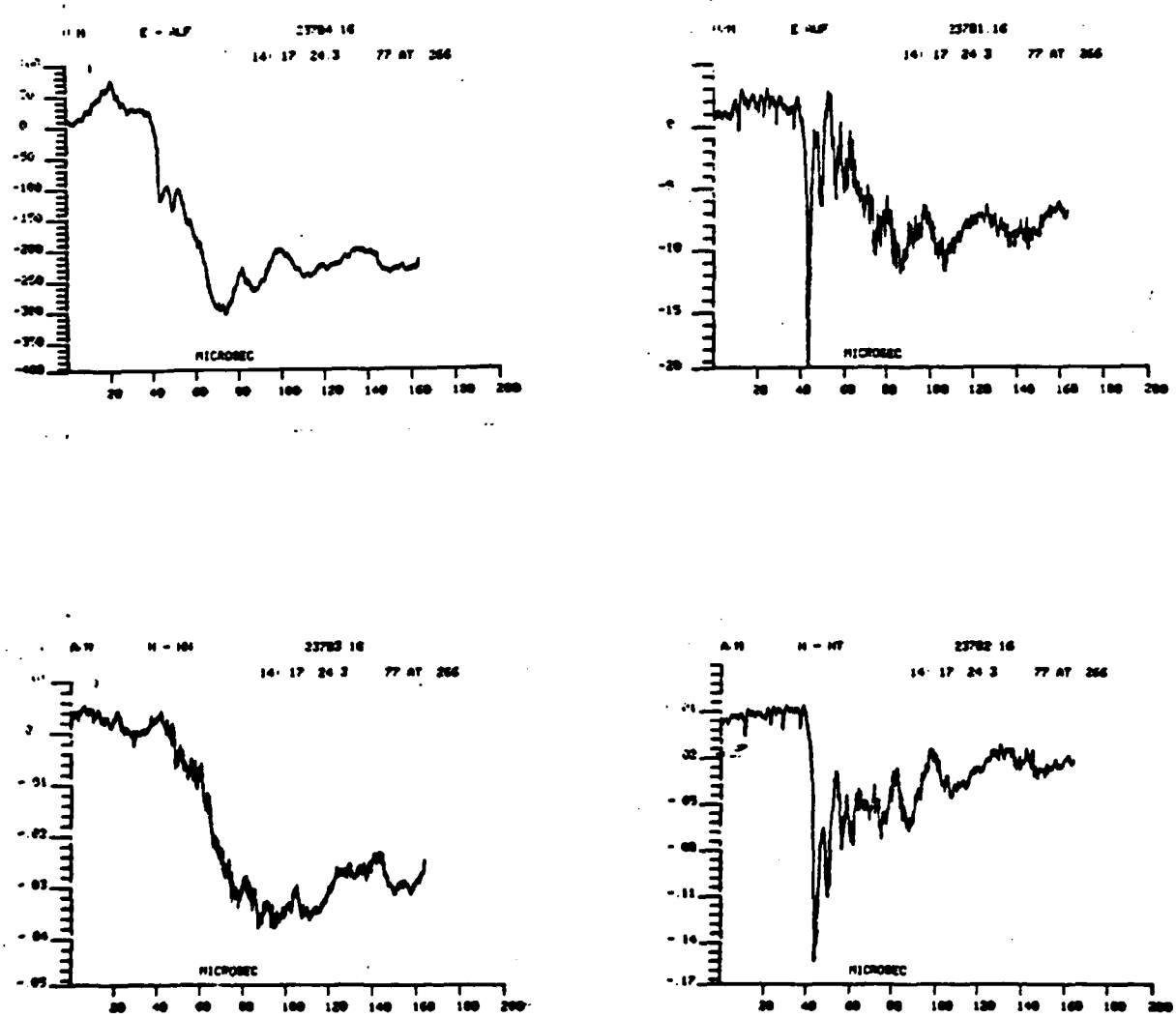

Fig 8.9 Electric and Magnetic Fields for a First Return Stroke at a Distance of 30 km and Altitude 4 km.

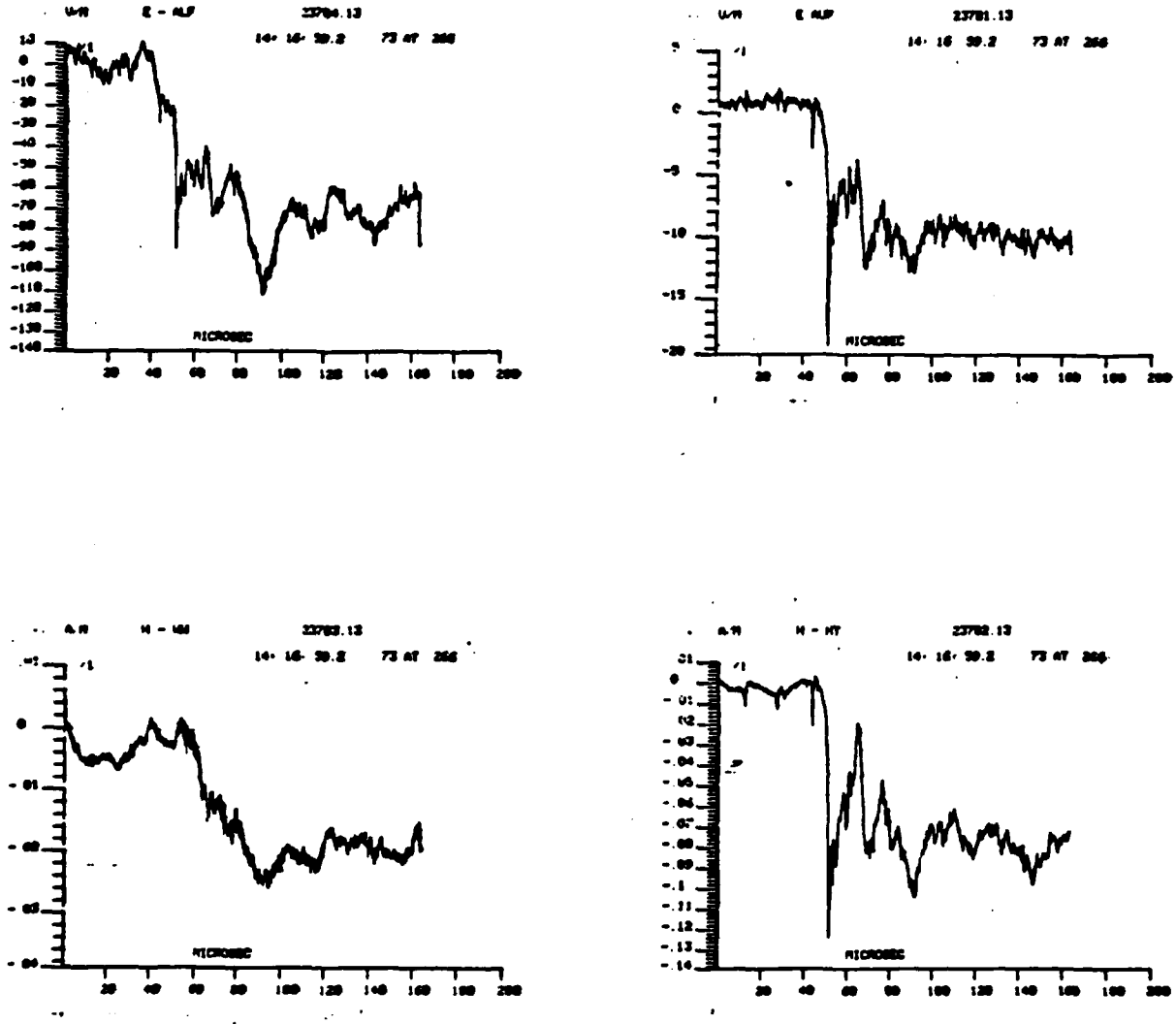

Fig 8.10 Electric and Magnetic Fields for a First Stroke at a Distance of 30 km and Altitude 4 km.

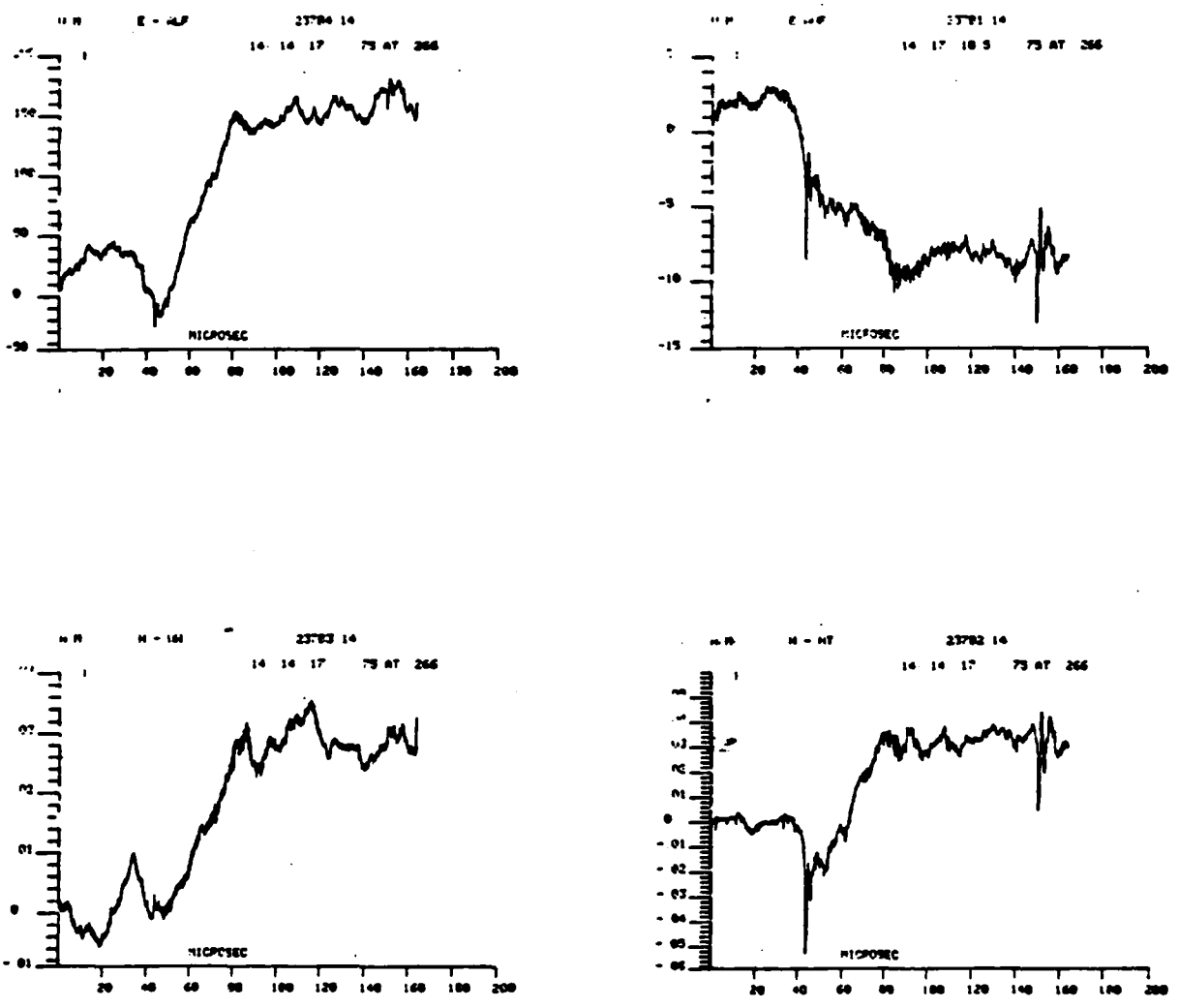

Fig 8.11 Electric and Magnetic Fields for a First Stroke at a Distance of 35 km and Altitude 40 km.

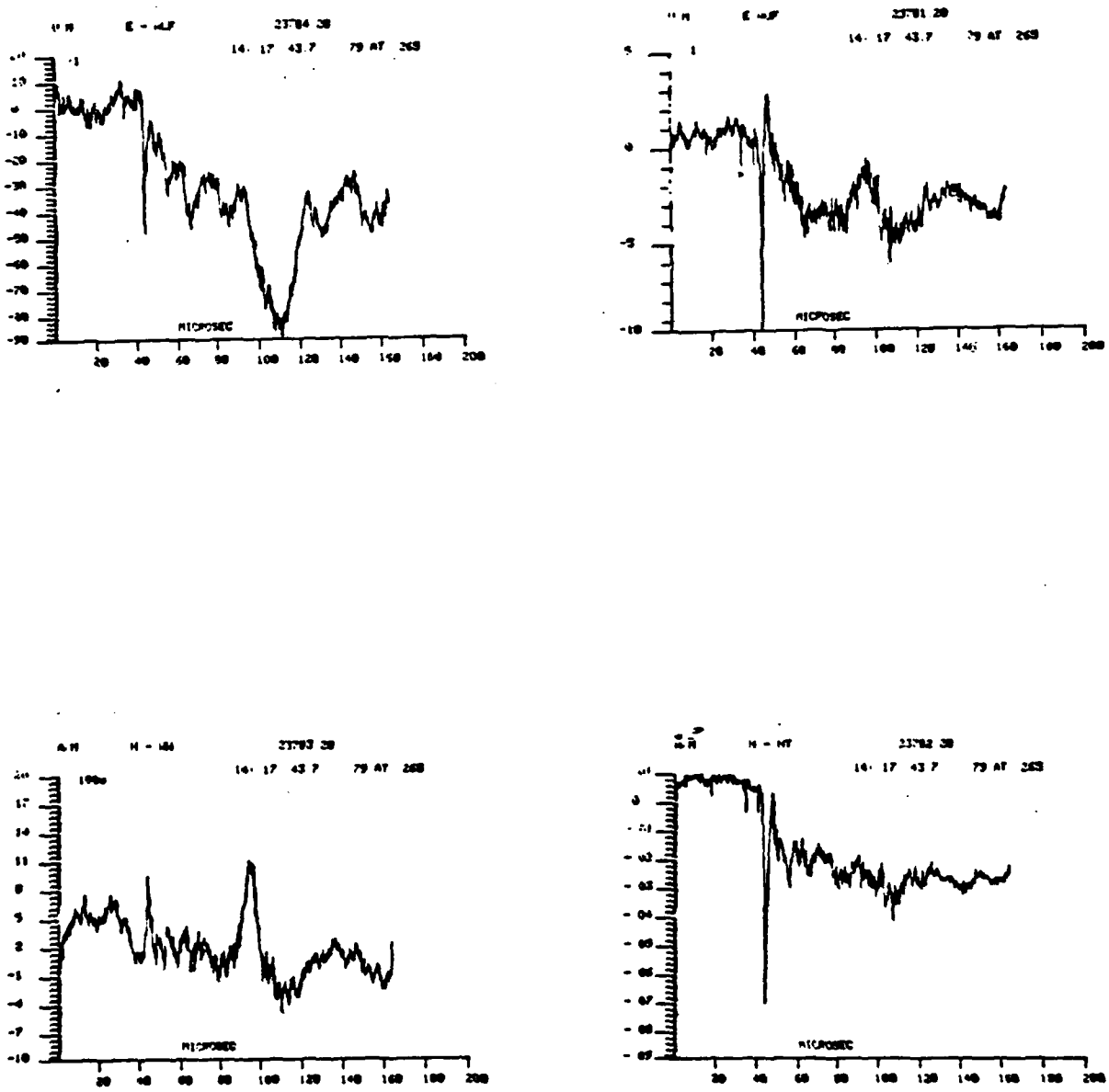

Fig 8.12 Electric and Magnetic Fields for a First Stroke at a Distance of 35 km and Altitude 4 km.

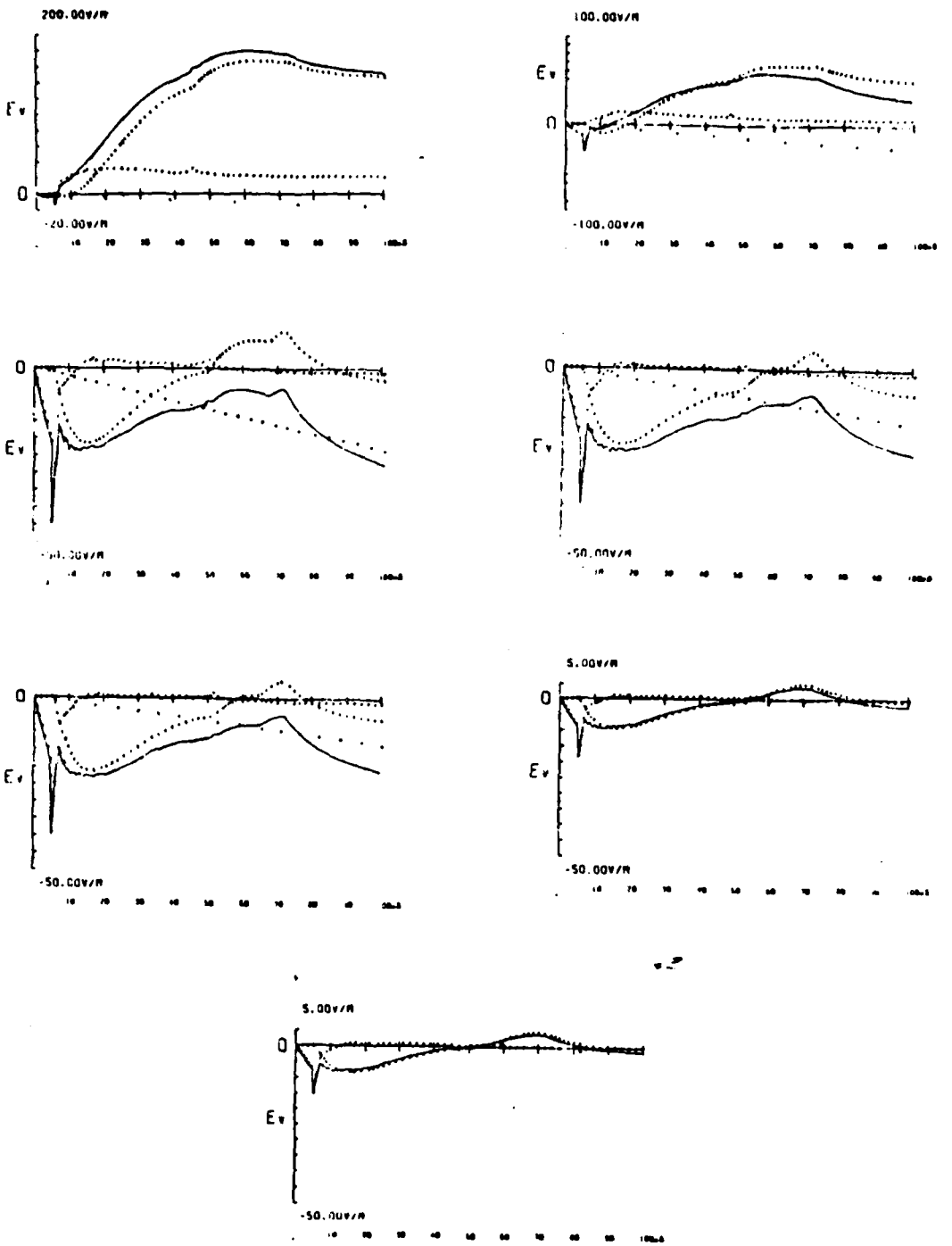

Fig 8.13 Verticle E-Field due to Master et al. Model (1981). Range (km); (a) 2.7; (b) 4.0; (c) 7.0 (d) 10.2; (e) 11.0; (f) 30.0; (g) 35. Altitude (km): 5 for a-e, 4 for g-h.

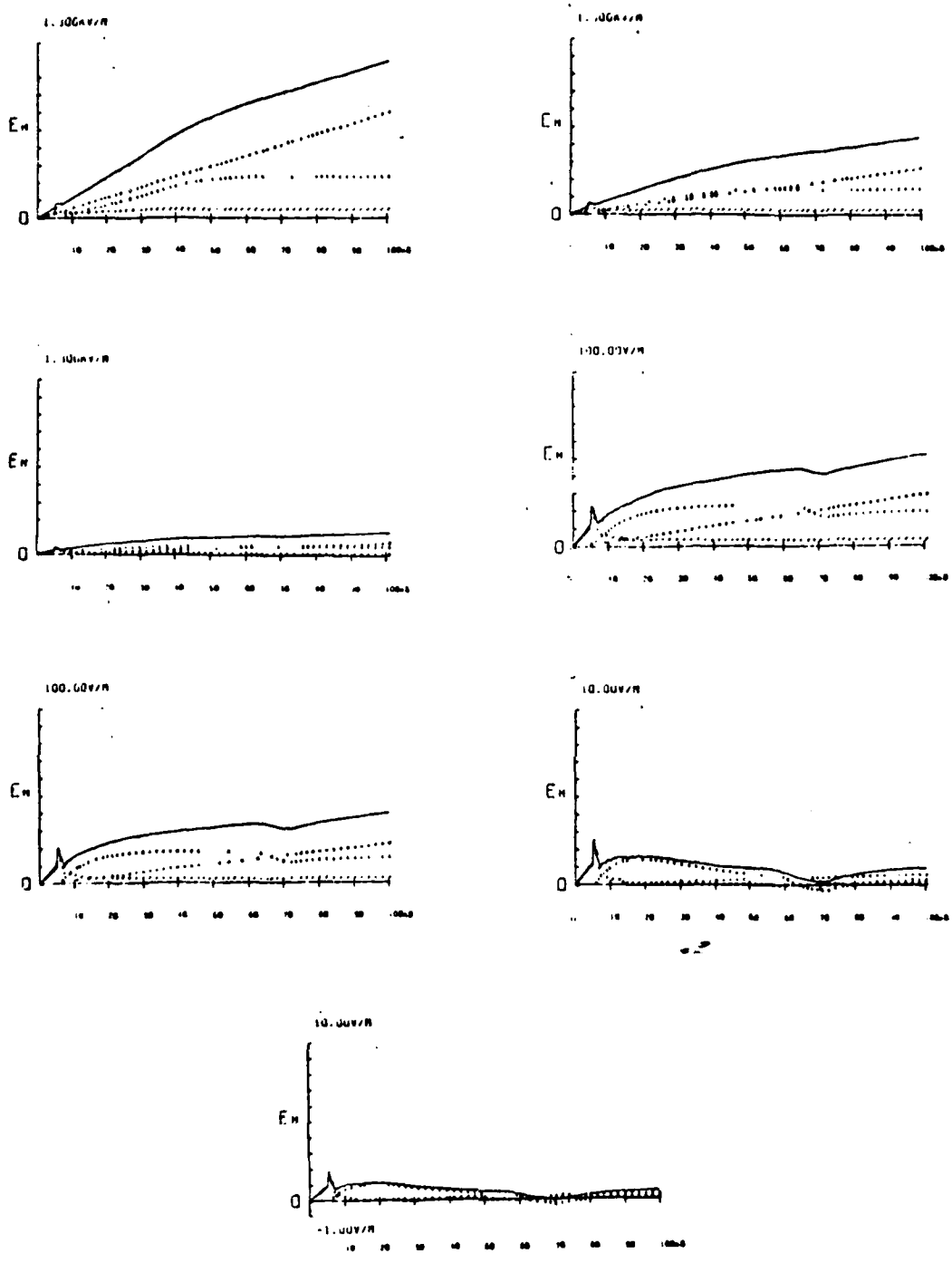

Fig 8.14 Horizontal E-Field due to Master et al. Model (1981). Ranges and Altitudes as in Fig 8.13.

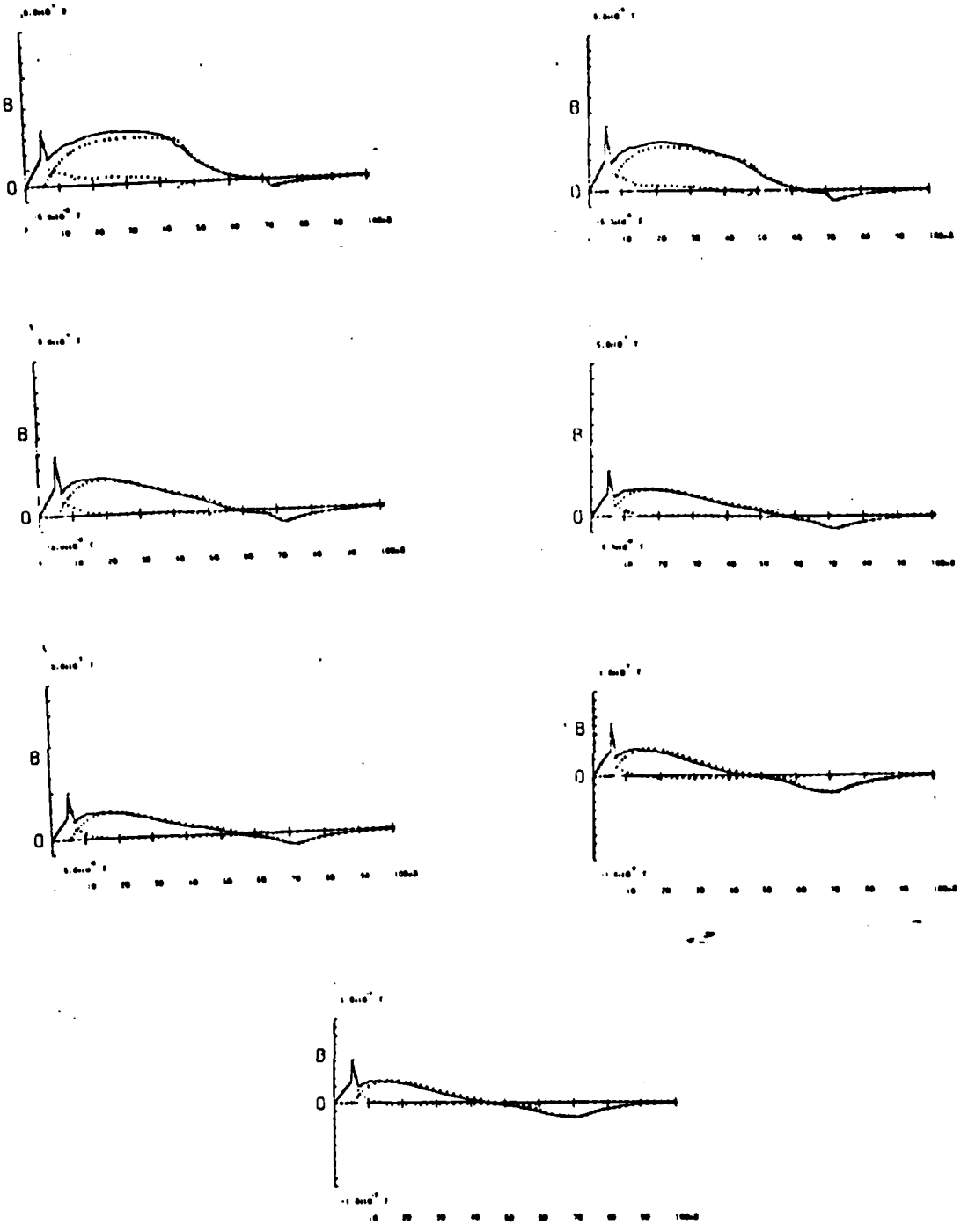

Fig 8.15 Magnetic Field due to Master et al. Model (1981). Ranges and Altitudes as in Fig 8.13.

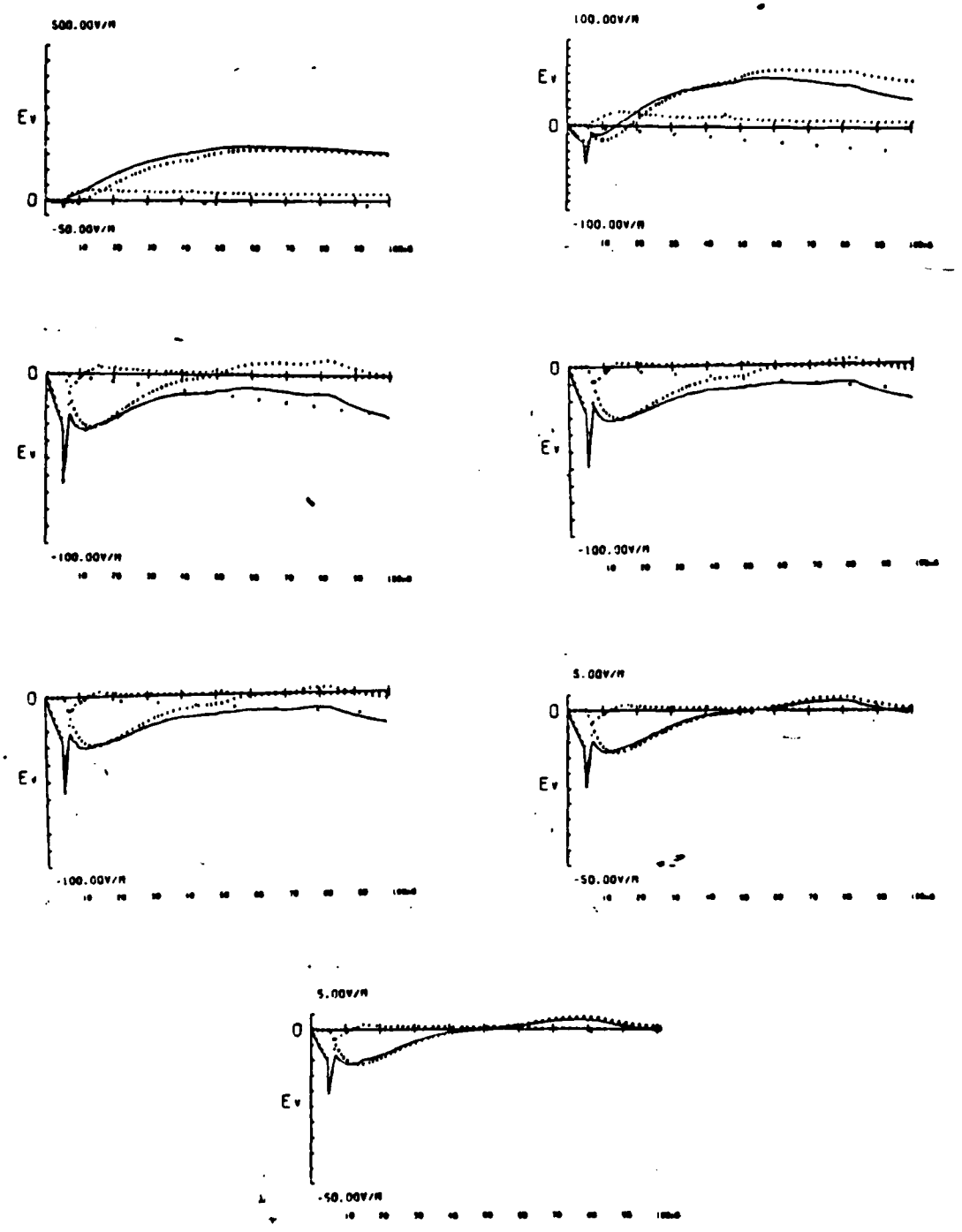

Fig 8.16 Verticle E-Field with Current Pulse Propagation Velocity Varying with Height. Ranges and Altitudes as in Fig 8.13.

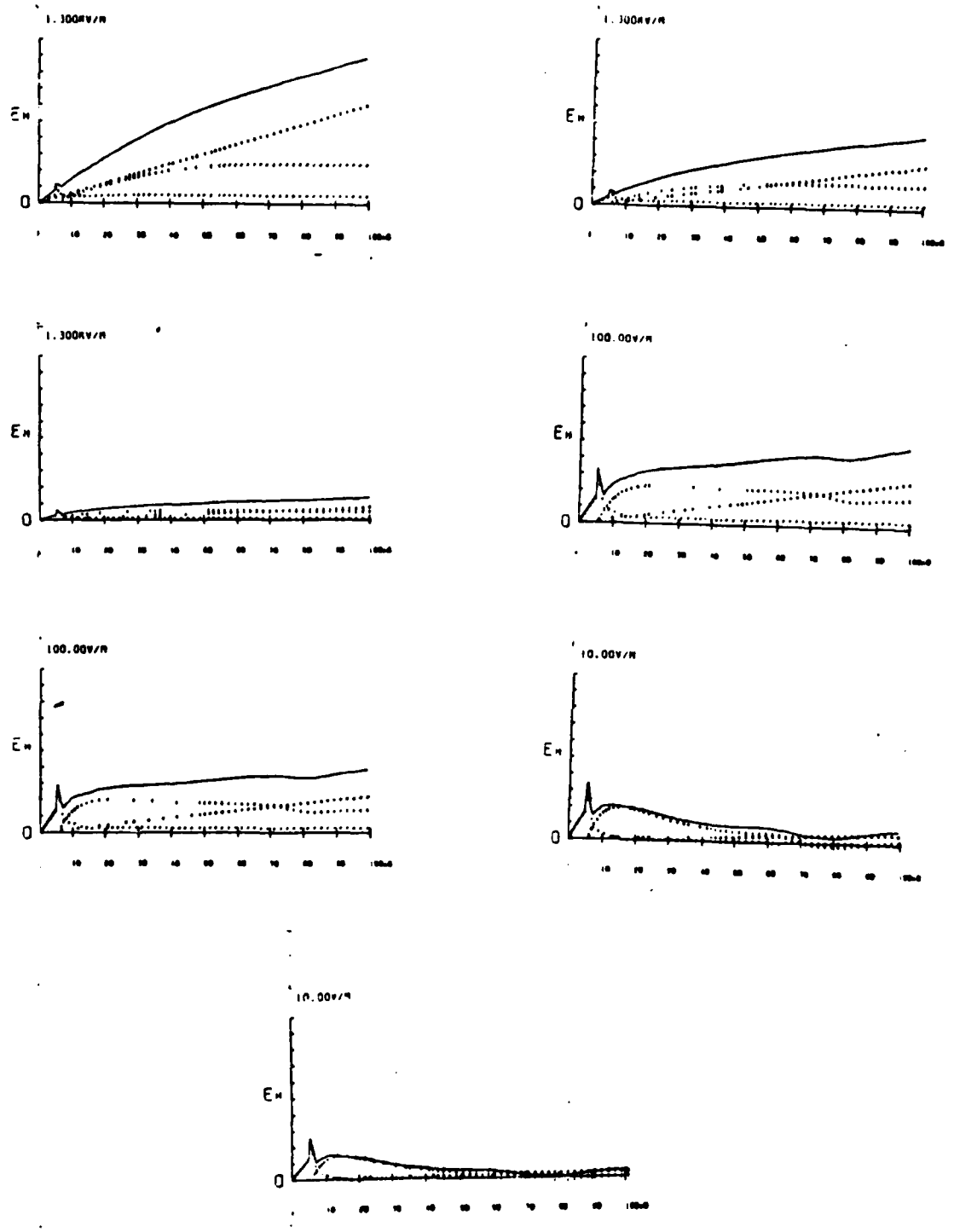

Fig 8.17 Horizontal E-Field with Current Pulse Propagation Velocity Varying With Height. Ranges and Altitudes as in Fig 8.13.

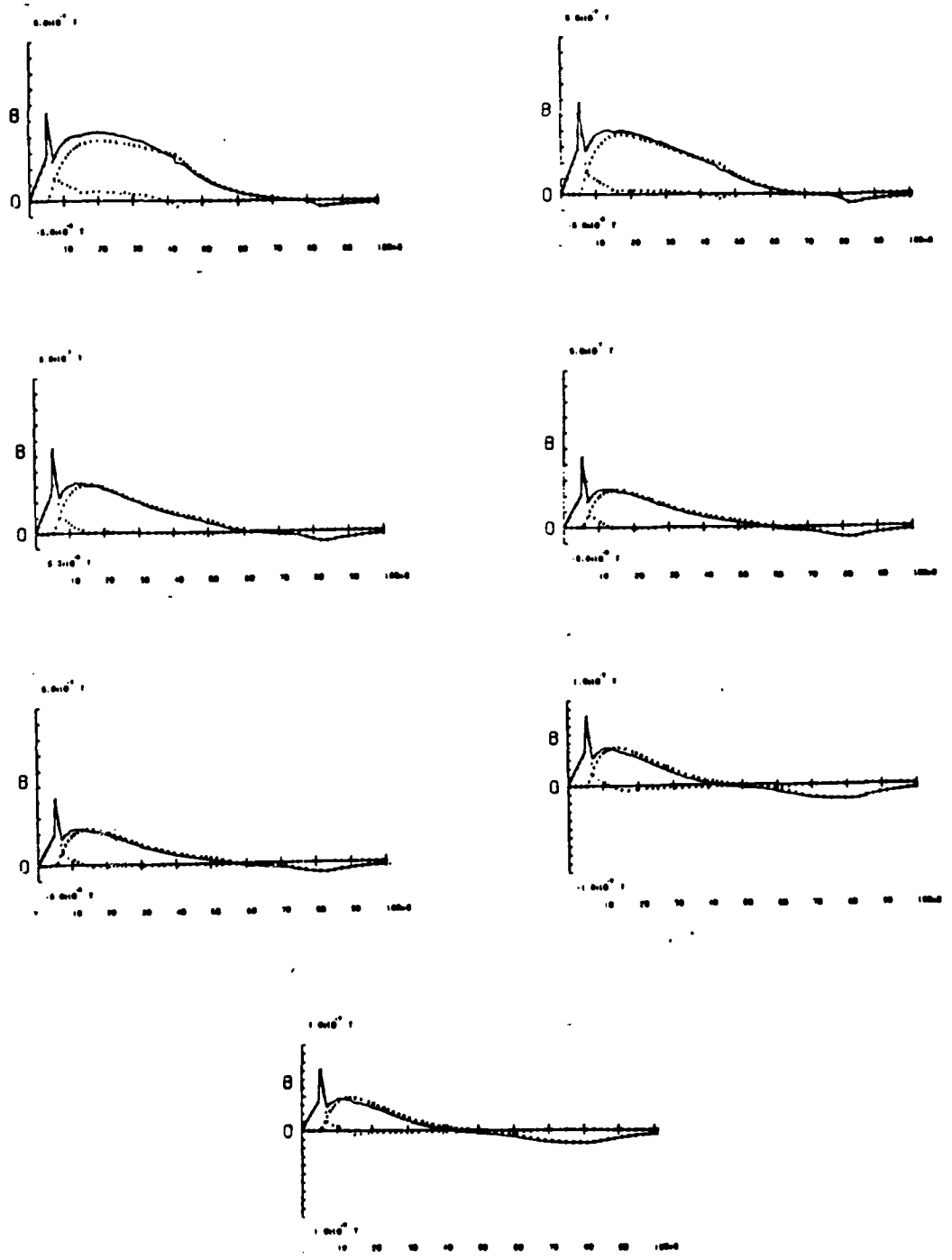

Fig 8.18 Magnetic Field with Current Pulse Propagation Velocity Varying with Height. Ranges and Altitudes as in Fig 8.13.

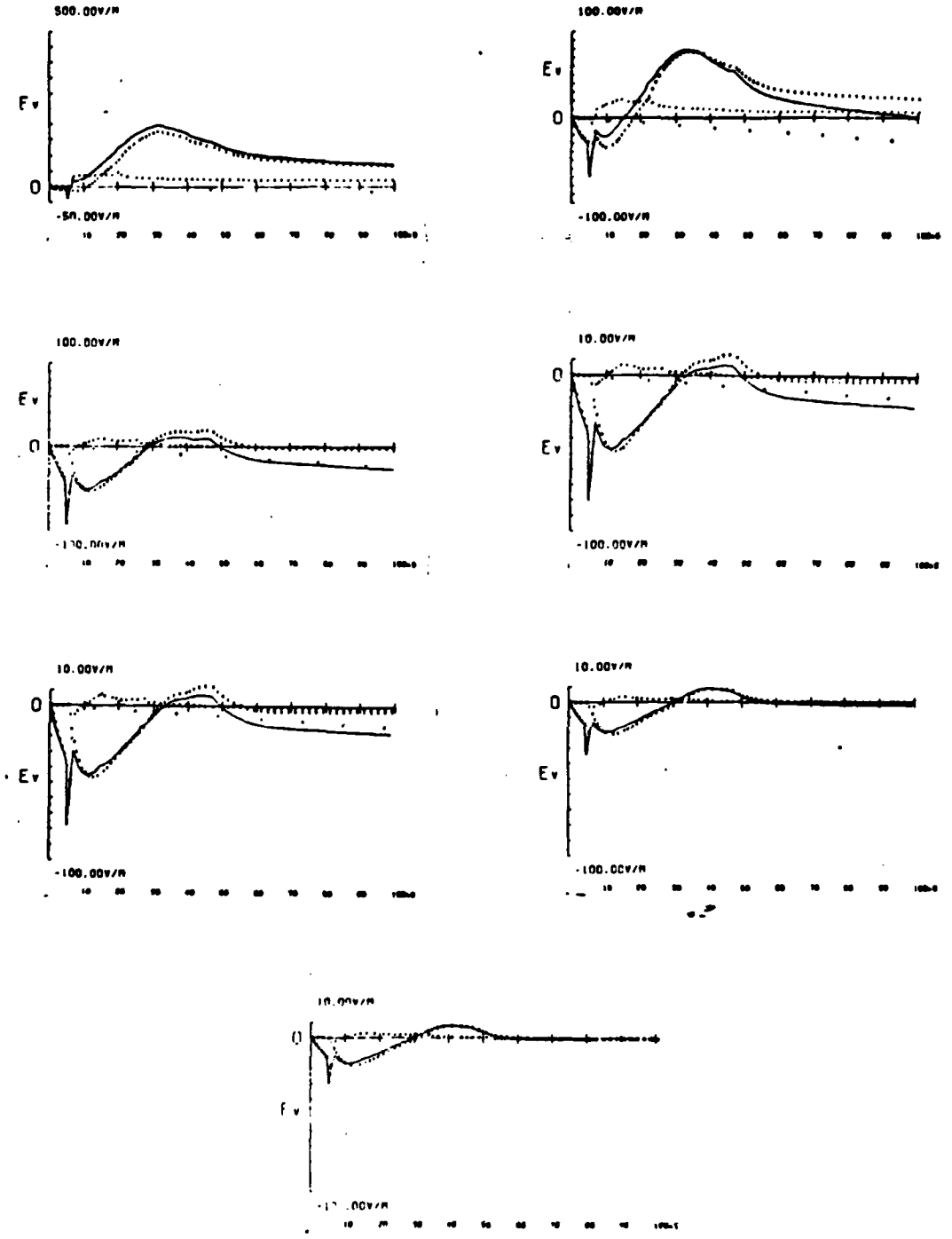

Fig 8.19 Verticle E-Field Due to Modified Current Waveform of Equations 6.4 and 6.5. Ranges and Altitudes as in Fig 8.13.

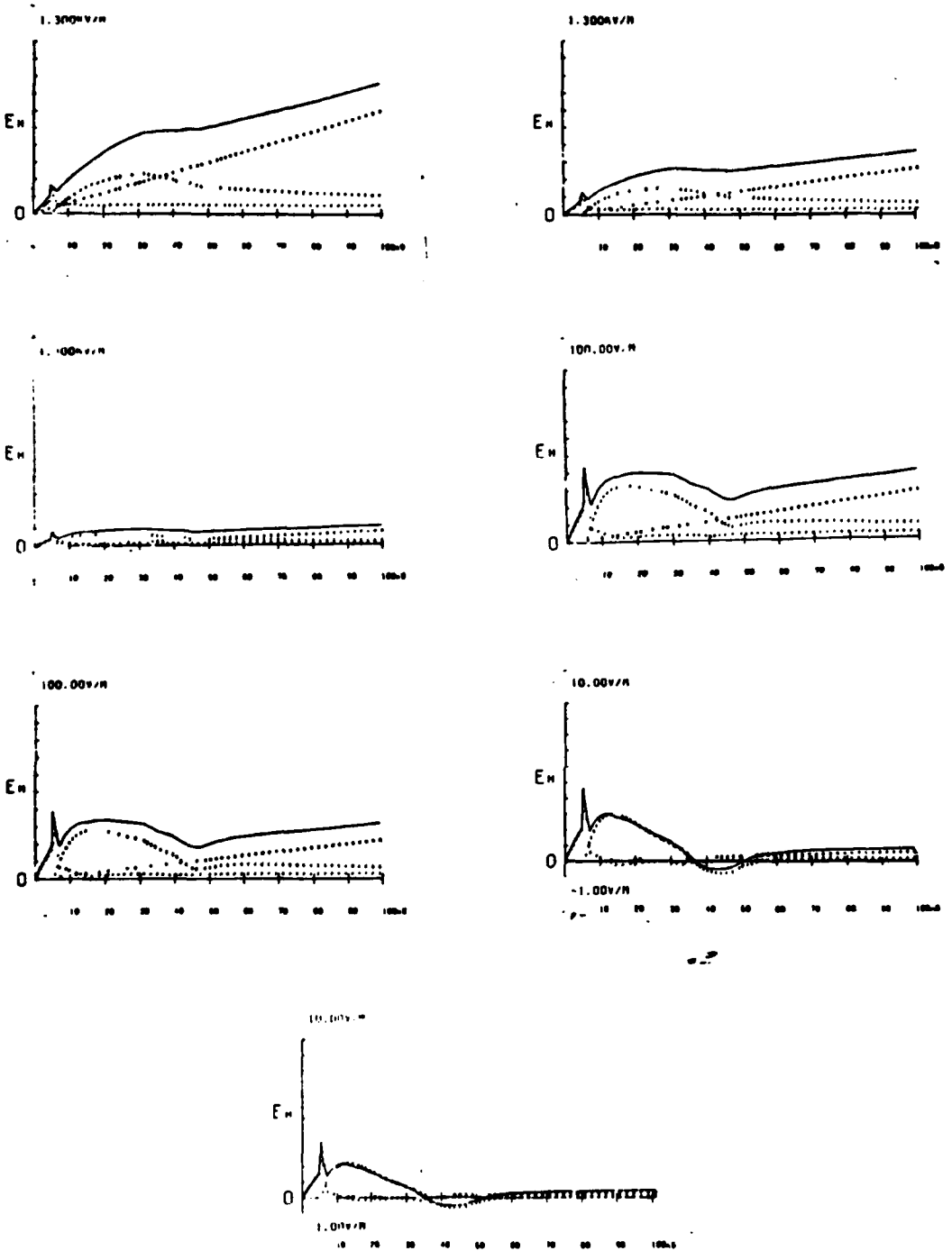

Fig 8.20 Horizontal E-Field Due to Modified Current Waveform of Equation 6.4 and 6.5. Ranges and Altitudes as in Fig 8.13.

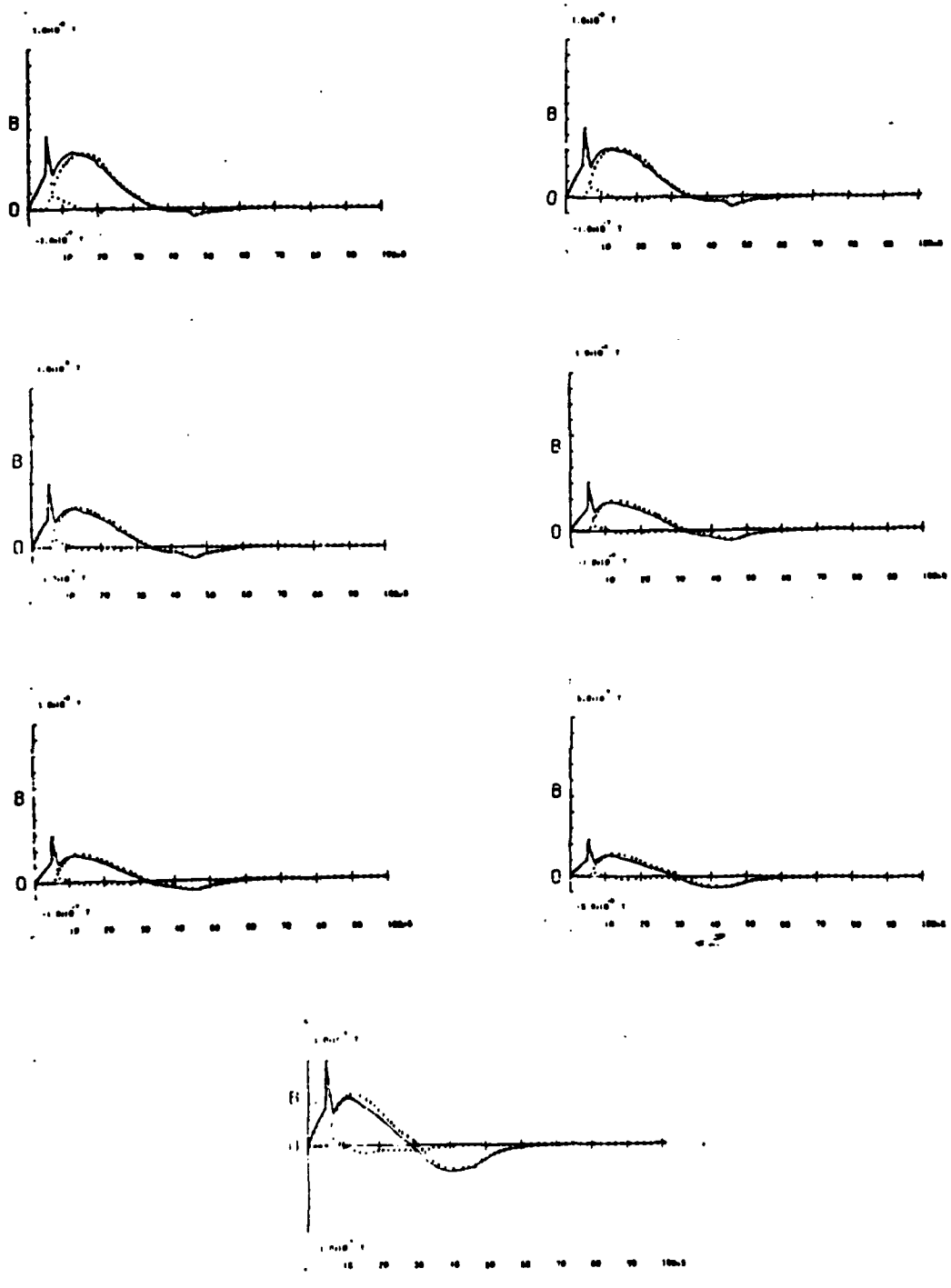

Fig 8.21 Magnetic field due to Modified Current Waveform of Equations 6.4 and 6.5. Ranges and Altitudes as in Fig 8.13.

IX. Conclusions and Recommendations

Conclusions

Master et al. model (1981) presented in this thesis predicts fast risetime correctly. However, the peak value of EM field is much less than empirical value. EM field in actual data never crosses the base line but the fields predicted by Master et al. model (1981) very often cross the base line. The modified velocity for current pulse propagation has significantly reduced the tendency of crossing the base line. With this modified velocity, the peak value of the EM fields has also improved.

Modified current waveform has increased the peak value of EM fields very much but with this the tendency of crossing the base line has been advanced in time scale. It is hoped that the combined effect of modified velocity and current waveform will improve the predicted values of EM field.

Since no significant amount of empirical data for subsequent strokes was available, therefore, this aspect of Master et al. model (1981) could not be studied. Velocity variation in subsequent strokes is very nominal. However, from the comparison of different models and waveforms measured by different researchers, it is felt

that current waveform modification in Master et al. model is necessary. Particularly, the peak value of EM fields predicted by Master's model (1981) are significantly low in space.

Strawe's model (1979) has very good risetime in its predicted current waveforms. Also, as the current waveform in this model varies with time, therefore, this model has great potential to provide realistic results. At present, this model needs to be refined. Gardner model (1980) presently does not propose a better solution for the problems in existing models. The concept presented in this model can be used only for the finer details in a successful model.

Recommendations

In the detailed study of Master et al. model more data samples should be collected and compared to the predicted results. Since this model is primarily meant for subsequent strokes, empirical data for subsequent strikes is required to correctly assess the performance of this model. For the first return stroke, current waveform is required to be modified in order to improve the peak EM fields and also to reduce the base line cross over tendency.

Strawe et al. model (1980) computer program should be modified for the channel diameter. The channel dia-

meter reduces with time but it can be considered as a function of height as well. Thus, this dual variation in channel diameter with height and time is hoped to produce better results or at least it will provide an opportunity to assess the behavior of predicted EM field with channel diameter variation.

Gardner's model may be tested with current waveform of Master et al. model. The predicted result once compared with experimental data will allow the future researchers to assess the credibility of this model.

Bibliography

1. Baum, R.K. "Airborne Lightning Characterization, Lightning Technology." Proceedings of a Technical Symposium Held at NASA Langley Research Center, Hampton, VA, April, 1980. Supplement to NASA Conference Publication 2128, FAA-RD-80-30, pp 1-19.

2. Baum, C.E. et al. "Measurement of Electromagnetic Properties of Lightning with 10 nano Second Resolution in Lightning Technology," NASA Conf Publ. 2128, FAA-RD-80-30, pp 39-82 (1980).

3. Baum et al. "The Measurement of Lightning Environmental Parameters Related to Interaction Electronic System," IEEE Trans. Vol EMC-24 (1982).

4. Berger et al. "Parameters of Lightning Flashes," Electra Vol. 80, pp 23-37 (1975).

5. Boyle, J.S. and R.E. Orville. "Return Stroke Velocity Measurements in Multi Stroke Lightning Flash." J. Geophysics. Res. 81, 4461-4466 (1976).

6. Braginiskii, S.I. "Theory of Development of Spark Channel," Soviet Phys. JETP Vol. 34(7), pp 1068-1074, (1954).

7. Bruce, C.E.R. and R.H. Golde. "The Lightning Discharge," The Journal of the Institute of Electrical Engineers, Vol. 88 Par II (Dec. 1941).

8. Corbin, J.C. "Protection/hardening of Aircraft Electronic Systems Against the Indirect Effect of Lightning," Ref FAA-RD-79-6, 97-103 Fed. Aviat. Admin., Washington DC (1979).

9. Corbin, J.C. et al. "Assessment of Aircraft Susceptibility/Vulnerabilities to Lightning and Development of Lightning Protection Design Criteria," IEEE Transactions on Electromagnetic Compatibility, Vol. EMC-24,225-237 (May 1982).

10. Dennis, A.S. and E.T. Pierce,. "The Return Stroke of the Lightning Flash to Earth as a Source of VLF Atomspheric," Radio Sci., J. Res. Vol 68D, pp 777-794 (1964).

11. Gardner, R.L. "A Model of Lightning Return Stroke, "PhD Thesis University of Colorado (1980).

12. Lin, Y.T. "Lightning Return Stroke Models" PhD Thesis, University of Florida (1978).

13. Lin, Y.T. et al. "Lightning Return Stroke Model." JGR Vol 85:1571-1583 (March, 1980).

14. Little, P.F. "Transmission Line Representation of a Lightning Return Stroke," J. Phys. D Applied Physics Vol II, pp 1983-1910 (1978).

15. Master, M.J. et al. "Calculations of Lighting Return Storkes Electric and Magnetic Fields Above Ground." JGR, Vol 86:12127,12132 (Dec. 1981).

16. McCann, G.D. "The Measurement of Lightning Current in Direct Strokes." Trans. AIEEE, 63, 1157-1164, 1944.

17. Parker et al. "Airborne Warning System for Natural and Aircraft Initial Lightning." IEEE Trans. Vol EMC-24, pp 137-158 (1982).

18. Perala et al. "Electromagnetic Interaction Lightning with Aircraft". IEEE Trans. Vol. EMC-24, pp 173-203 (1982).

19. Plonsey R. and E.C. Collin. "Principles and Applications at Electromagnetic Fields." McGraw-Hill, Inc. New York (1961).

20. Plumer, J.A. et al. "The Direct Effect of Lightning on Aircraft" IEEE Transactions on Electromagnetic Compatibility, Vo, EMC-24, pp 158-172 (May, 1982).

21. Price, G.H. and E.T. Pierce. "The Modeling of Lightning Current in the Lightning Return Stroke," Radio Sci. 12, pp 381-388 (1977).

22. Rustan et al. "Airborne Lightning Characterization Technical Report," (In process of Publication).

23. Strawe, D.F. "Nonlinear Modeling of Lightning Return Stroke," in Proc. Fed. Aviation Admin/Florida Inst. Tech. Wrokshop Grounding Lightning Tech., March 6-9, 1979, Melbourne, Florida, Rep. FAA-RD-79-6, pp 9-15.

24. Szpor, S. "Comparison of Polish to American Lightning Records," IEEE Trans. Power App. Syst. PAS-88, pp. 646-652 (1969).

25. Thomson, E.M. "The Dependance of Lightning Return Stroke Characteristics on Latitude." J. Geo. Physics Res. Vol 85, pp 1050-1056 (1980).

26. Uman, M.A. & D.K. McLam. "Magnetic Field of Lightning Return Stroke," JGR Vol 74, pp 6899-6909 (1969).

27. Uman, M.A. Lightning, McGraw-Hill, Inc., New York, 1969.

28. Uman et al. "A Review of Natural Lightning: Experimental Data and Modeling," IEEE Trans Electromagnetic Compatibility, Vol. EMC-24, pp 79-112 (May 1982).

29. Wait, J.R. "Terrestrial Propagation of Very-Low-Frequency Radio Waves," A Theoretical Investigation, J. Res N.B.S.-D Radio Propagation 64D, pp 153-204 (1960).

Vita

Shad M. Hanif was born on 20 April 1942 at Lahore, Pakistan. He obtained his M.A. degree in Mathematics from the University of Punjab in 1965. From Dec 1966 to June 1969, he was a lecturer in Mathematics in the Hussain Shaheed Government College Rawalakote, Azad Kashmir. After a year long training in electronics at PAF cCollege of Aeronautical Engineering, he was commissioned in January 1976 in the Signals Branch of Pakistan Air Force. He attended the School of Electronics at PAF Base Korangi Creek, Karachi from April 1970 to October 1970 and obtained a diploma in Radar Engineering. From November 1970 to August 1973, he served as Electronics Maintenance Officer in a Radar Squadron of Pakistan Air Force. In September 1973, he was assigned to the college of Aeronautical Engineering and from there he obtained the Bachelor of Engineering (Avionics) degree in January 1976. After serving for five years as Maintenance Engineer, he was assigned in May 1981 to the U.S. Air Force Institute of Technology, Wright-patterson Air Force Base, Ohio to complete a Master's Degree in Electrical Engineering.

Permanent Address: 2-Nanak Street
Mujahidabad, Mughalpura
Lahore-Pakistan

Unclassified
SECURITY CLASSIFICATION OF THIS PAGE (When Data Entered)

REPORT DOCUMENTATION PAGE

READ INSTRUCTIONS BEFORE COMPLETING FORM

1. REPORT NUMBER: AFIT/GE/EE/82D-61	2. GOVT ACCESSION NO. A124 680
3. RECIPIENT'S CATALOG NUMBER	
4. TITLE (and Subtitle): A REVIEW AND COMPARISON OF LIGHTNING RETURN STROKE MODELS USING EXPERIMENTAL DATA	5. TYPE OF REPORT & PERIOD COVERED: MS Thesis
	6. PERFORMING ORG. REPORT NUMBER
7. AUTHOR(s): Shad M. Hanif, Sqn Ldr PAF	8. CONTRACT OR GRANT NUMBER(s)
9. PERFORMING ORGANIZATION NAME AND ADDRESS: Air Force Institute of Technology (AFIT/EN) Wright-Patterson AFB OH 45433	10. PROGRAM ELEMENT, PROJECT, TASK AREA & WORK UNIT NUMBERS
11. CONTROLLING OFFICE NAME AND ADDRESS: Air Force Wright-Aeronautical Laboratory/ FIESL Wright-Patterson AFB, Ohio 45433	12. REPORT DATE: December 1982 13. NUMBER OF PAGES
14. MONITORING AGENCY NAME & ADDRESS (if different from Controlling Office)	15. SECURITY CLASS. (of this report): Unclassified 15a. DECLASSIFICATION/ DOWNGRADING SCHEDULE

16. DISTRIBUTION STATEMENT (of this Report)

Approved for public release; distribution unlimited

17. DISTRIBUTION STATEMENT (of the abstract entered in Block 20, if different from Report)

18. SUPPLEMENTARY NOTES

Approved for public release: IAW AFR 190-17.

LYNN E. WOLAVER
Dean for Research and Professional Development
Air Force Institute of Technology (AFIT)
Wright-Patterson AFB OH 45433

19 JAN 1983

19. KEY WORDS (Continue on reverse side if necessary and identify by block number)

Lightning models
Electromagnetic fields
Analysis and comparison at altitudes

20. ABSTRACT (Continue on reverse side if necessary and identify by block number)

A detailed review of the seven lightning return stroke models is presented. These models were proposed by Bruce and Golde (1964), Dennis and Pierce (1964), Little (1978), Y.T. Lin et al. (1980), and Master et al. (1981). For the better understanding of the subject a review of lightning return stroke process is also included. The equations to compute the electric and magnetic fields in space due to a vertical channel are also derived. The last part of the thesis is related to the compari-

DD FORM 1 JAN 73 1473 EDITION OF 1 NOV 65 IS OBSOLETE

Unclassified
SECURITY CLASSIFICATION OF THIS PAGE (When Data Entered)

son of these models. The predicted fields due to Master et al, were plotted and compared with the emprical results. Also, Master et al. model (1981) was modified for the channel current wave form. The polots due to these modifications are included and compared with the experimental data.